Master's thesis

NTNU
Norwegian University of Science and Technology
Faculty of Natural Sciences
Department of Physics

Jacob Benestad

Electron-magnon coupling and magnon-induced superconductivity in hybrid structures of metals and magnets with non-collinear ground states

Master's thesis in Applied Physics and Mathematics
Supervisor: Asle Sudbø
June 2022

NTNU
Norwegian University of
Science and Technology

Jacob Benestad

Electron-magnon coupling and magnon-induced superconductivity in hybrid structures of metals and magnets with non-collinear ground states

Master's thesis in Applied Physics and Mathematics
Supervisor: Asle Sudbø
June 2022

Norwegian University of Science and Technology
Faculty of Natural Sciences
Department of Physics

NTNU
Norwegian University of
Science and Technology

Summary

Electron-magnon interactions in a bilayer of monoatomic metal and a non-collinear spiral phase ferromagnetic insulator are studied on a triangular lattice, motivated by recent interest in similar systems with simpler collinear magnetic layers. To this intent, a framework for treating coupling between electrons and non-collinear spins is presented by modifying existing theory in the case of collinear spin structures based on a canonical transformation to an effective Hamiltonian. This is achieved using Fishman and Haraldsen's general rotation model for non-collinear spin structures. The system's properties as an unconventional magnon-mediated superconductor are investigated, with an analysis of how magnon squeezing from the chosen spin structure affects the BCS pairing strength and what type of symmetries one could expect to find for the superconducting state. With the spiral phase ferromagnetic insulator, the bilayer is found to in theory host p-wave superconductivity, although evidence suggests the BCS pairing strength will be weaker than in the case of a collinear ferromagnetic insulator. The linearised gap equation was solved close to the Fermi surface using an approximated potential, and an analysis across the whole first Brillouin zone was attempted but the k-space resolution was deemed insufficient. However, an interesting observation is the appearance of interaction terms in the Hamiltonian that could facilitate electron pair scattering without a spin flip as a result of the non-collinear structure, giving rise to $S_z = \pm 1$ spin polarised Cooper pairs. Such spin polarised Cooper pairs have interesting applications in spintronics, and while unpolarised terms seem to dominate in the example studied in this thesis there could exist other non-collinear magnetic structures where the polarised pairs play an important role. The ideas of the framework presented here can with a bit of effort be extended in order to perform an analysis of more complicated 3D magnetic structures.

Sammendrag

Elektron-magnon interaksjoner i et dobbeltlag av monoatomisk metall og en ferromagnetisk isolator med ikke-kolineær spiralfase er studert på et triangulært gitter, motivert av nylig interesse i liknende systemer med enklere kolineære magnetiske lag. Med dette formål presenteres et rammeverk for å beregne kobling mellom elektroner og ikke-kolineære spin, som er en modifisering av eksisterende teori for kolineære spinstrukturer basert på en kanonisk transformasjon til en effektiv Hamilton-operator. Dette er gjort ved å ta i bruk Fishman og Haraldsen sin generelle rotasjonsmodell for ikke-kolineære spinstrukturer. Systemets egenskaper som en ukonvensjonell magnon-formidlet superleder er undersøkt, med en analyse av hvordan "squeezing" av magnonene fra den valgte spinstrukturen påvirker styrken av BCS par-dannelse og hva slags type symmetrier man kan forvente å finne for den superledende tilstanden. Dobbeltlaget som har en en ferromagnetisk isolator med ikke-kolineær spiralfase finner vi at kan ha p-bølge superledning i teorien, men forventer at styrken på BCS interaksjonen blir mindre enn for tilfellet med en kolineær ferromagnetisk isolator. Den lineæriserte gaplikningen ble løst nær Fermiflaten for et approksimert potensial, og en analyse ble forsøkt for en fullstendig beregning over hele første Brillouinsone, men oppløsningen i k-rom ble for lav. Derimot var det interessant å observere at det dukker opp interaksjons-termer i Hamilton-operatoren for spredning av elektronpar uten spinflip som et resultat av den ikke-kolineære strukturen, hvilket kan gi opphav til $S_z = \pm 1$ polariserte Cooper par. Slike polariserte Cooper par har interessante bruksområder i spintronikk, og selv om de upolariserte parene dominerer for eksempelet studert i denne masteroppgaven kunne man tenke seg at det finnes andre strukturer der de polariserte parene spiller en viktigere rolle. Ideene fra rammeverket presentert i denne oppgaven kan med litt arbeid generaliseres for å studere mer kompliserte 3D spinstrukturer.

Preface

This Master's thesis presents the work carried out during the last semester of the five-year integrated Master's degree programme in Applied Physics and Mathematics at the Norwegian University of Science and Technology (NTNU). Some of the work presented was done as part of my specialisation project *Magnon-spectra in quantum magnets with non-collinear ground states* in the penultimate semester. The subject of the thesis is research in the field of theoretical condensed matter physics. I would like to thank my supervisor Professor Asle Sudbø, who has given plenty of his time and expertise in supervising this project. Also, I must thank Kristian Mæland, Niels Henrik Aase, Eirik Erlandsen and Even Thingstad for rewarding discussions and their great insight regarding some of the different topics that appear in this thesis. Additionally I would like to thank QuSpin, and especially my fellow Master students at QuSpin, for providing an excellent working environment. I also give thanks to my family and friends for their support.

Jacob D. Benestad

Jacob D. Benestad
Trondheim, Norway
June 2022

Table of Contents

List of Tables

List of Figures

Abbreviations

Irrep	=	Irreducible representation
FMI	=	Ferromagnetic insulator
AFMI	=	Anti-ferromagnetic insulator
SPFMI	=	Spiral phase ferromagnetic insulator
NM	=	Normal metal
DOS	=	Density of states
HP	=	Holstein-Primakoff
BCS	=	Bardeen-Cooper-Schrieffer
BZ	=	Brillouin zone

Chapter 1

Introduction

1.1 Background

Since the first experimental discovery of superconductivity by Heike Kamerlingh Onnes in 1911 [1] the exploration and science of superconducting materials has reigned as one of the big fields of research within condensed matter physics. It would take almost forty years until Ginzburg and Landau developed a phenomenological theory of superconductivity in 1950 [2]; only a few years later Bardeen, Cooper and Schrieffer would present a microscopic description in 1957 [3]. A solid theoretical groundwork had been laid. In modern times, research has focused mainly on high-temperature superconductivity. However, with the advent of spintronics there has been an increasing interest in materials with tunable superconducting properties and generating spin-polarised triplet super-currents at material interfaces [4]. Combined with investigation of unconventional pairing mechanisms for superconductivity, this has fueled plenty of recent research into magnon-mediated superconductivity in material bilayers and trilayers. These studies include experimental findings of time-reversal symmetry-breaking superconductivity in bismuth/nickel bilayers [5] and theoretical studies of superconductivity in bilayers and trilayers of metals and topological insulators together with ferromagnetic insulators (FMI) and antiferromagnetic insulators (AFMI) [6]–[10]. Consequently one of the new avenues to explore would be magnon-mediated superconductivity in a bilayer where the ferromagnetic/antiferromagnetic insulator is replaced by a non-collinear spin structure to see how this would influence the superconductivity of the bilayer system.

Non-collinear magnetic structures are interesting in their own right, for instance in the realm of topologically protected spin structures such as skyrmions, which could have applications in novel magnetic storage devices. In fact non-collinear magnetic structures have already been studied in another context of superconductivity, suggested as a mechanism for spin mixing in a magnet/superconductor junction [4]. It is not unreasonable to think that this idea of spin mixing can also be applied in the case of magnon-mediated superconductivity. Much of the litterature on non-collinear magnets builds on foundational

works by Dzyaloshinskii and Moriya; the former showing that the relativistic spin lattice and magnetic moment interactions result in spin canting [11], while the latter identified that the underlying microscopic mechanism is spin-orbit coupling [12]. This so-called Dzyaloshinskii-Moryia interaction (DMI), which favours a canting of the spins, allows for a plethora of different (and sometimes quite exotic) spin structures as it competes with other interactions on different lattice symmetries.

1.2 Scope

The aim of this thesis is to study a metal/magnet bilayer where the magnetic part has a non-collinear spin structure and is electrically insulating. Specifically we investigate how the magnon squeezing coefficients in this case will influence the enhancement of the BCS potential, motivated by the example of massive enhancement in the case of the fully uncompensated antiferromagnetic bilayer [7]–[10]. We also look into what kind of symmetries the superconducting state should have, and how the non-collinearity could give rise to interactions allowing for spin-polarised triplet pairing through spin mixing. This thesis is a continuation of work carried out in the author's project thesis from the previous semester, where the magnon properties of a certain non-collinear magnet was studied. Thus it is this particular magnetic structure we limit the bilayer to.

1.3 Thesis structure

The thesis can be divided into roughly two parts; the first part in Chapters 1-3 presenting some existing theory in order to lay a groundwork for the second part in Chapters 4-6 where the novel work of this thesis is presented. It begins with a discussion of some preliminary concepts and mathematical methods in Chapter 2 that will be central for calculations and analysis in the remaining chapters. Chapter 3 presents the specific model that will be studied in this thesis. For the sake of the thesis being self contained, the section about the magnetic part of the bilayer is a reiteration of parts of the author's unpublished project thesis, since the same type of non-collinear magnet will be used in our bilayer here. The same applies for the first part of Section 2.3 in Chapter 2. In Chapter 4, which is the main part of this thesis, the magnon-mediated interaction for electron pairing is derived. The last section of this chapter presents some numerical results for the electron pair interaction. Chapter 5 discusses the generalised BCS theory, what type of symmetries one can expect from the superconducting order parameter, and presents some numerical results for an approximation of the linearised gap function in addition to a numerical calculation of the Eliashberg spectral function. In Chapter 6 we recap the findings of the thesis, and briefly present some suggestions for future research.

1.4 Conventions and notation

We follow a common convention in condensed matter physics literature by setting the reduced Planck's constant $\hbar = 1$. In several instances it becomes necessary to use notation with a lot of indices in subscript and/or superscript. In order to avoid confusion about what

denotes a vector or matrix element and what denotes the position on the crystal lattice, carthesian vector and matrix elements are denoted by subscripts x, y and z with their position in the lattice denoted as a superscript. In the case of fermion and boson operators all indices are in general written in subscript. The use of $\langle i, j \rangle$ under a sum denotes a sum over lattice sites i and their nearest neighbours j. Vectors are denoted in bold font (e.g $\boldsymbol{x}$), no special notation is given for operators or matrices. It should be clear from the context of an equation what quantities are operators and matrices. For matrices and vectors we denote the transpose as A^T, the complex conjugate as A^*, while $A^\dagger \equiv (A^*)^T$ denotes the complex conjugate transpose. We use $\Re$ as notation for the real magnitude of a complex number, and $\Im$ as notation for the imaginary magnitude. In some instances we may use the full phrase of an existing abbreviation for the sake of making the text more verbose.

Chapter 2

Preliminaries

2.1 Linear spin wave theory

The concept of a particle's spin is inherently a quantum phenomenon, and while a semi-classical treatment of spin waves can be performed by considering precession of microscopic magnets [13], a fully quantum mechanical description turns out to be more suited in the case of this thesis. Spin waves in a magnetic insulator are in this case regarded as quantised excitations of the localised spins [14], [15]. Such long-lived excitations are called magnons, named for their analogy to photons and phonons that represent excitations of the electromagnetic field and lattice vibrations respectively. However while photons and phonons are bosons of spin 0, magnons carry a quantum spin of 1 as the excitation of an electron spin requires a spin flip from $-1/2$ to $1/2$. Quantum magnets can be modeled in terms of spin operators using the Heisenberg model, where each spin is described by a vector operator $\boldsymbol{S}_i$ living on the Bloch sphere. The textbook example is that of a FMI, described by the Heisenberg model

$$\mathcal{H}_{\text{FMI}} = -|J| \sum_{\langle i,j \rangle} \boldsymbol{S}_i \cdot \boldsymbol{S}_j. \tag{2.1}$$

Since spin waves here are defined as magnetic excitations the magnons are described by second-quantisation operators for bosons, representing the creation/destruction of such excitations. In order to study spin waves in a Heisenberg model it is therefore necessary to perform a mapping from the spin operators to bosonic creation and destruction operators.

2.1.1 Holstein-Primakoff transformation

The Holstein-Primakoff (HP) transformation [16] is one possible way to map spin operators onto bosonic operators. The idea is that the creation and destruction of a magnon corresponds to ladder-operators on the Dicke states $|s, m_s\rangle$, which are eigenstates of the spin operators

$$\boldsymbol{S}^2 |s, m_s\rangle = \hbar^2 s(s+1) |s, m_s\rangle , \tag{2.2}$$

$$S_z \left|s, m_s\right\rangle = \hbar m_s \left|s, m_s\right\rangle . \tag{2.3}$$

Furthermore the spin ladder-operators are defined from

$$S_\pm \left|s, m_s\right\rangle = \hbar\sqrt{s(s+1) - m_s(m_s \pm 1)}\left|s, m_s \pm 1\right\rangle . \tag{2.4}$$

We define the top Dicke state $|s, s\rangle$ to be the spin ground state (spin "up"), which is equivalent to the vacuum state of spin fluctuations. Note that we could just as well have chosen the bottom Dicke state to be the magnon vacuum state so that spin "down" would be the ground state of the magnet. The magnon creation and destruction operators are then defined as

$$a^\dagger \left|n\right\rangle = a^\dagger \left|s, s-n\right\rangle = \sqrt{n+1}\left|s, s-n-1\right\rangle , \tag{2.5}$$

$$a \left|n\right\rangle = a \left|s, s-n\right\rangle = \sqrt{n}\left|s, s-n+1\right\rangle , \tag{2.6}$$

$$a^\dagger a \left|n\right\rangle = a^\dagger a \left|s, s-n\right\rangle = n \left|s, s-n\right\rangle . \tag{2.7}$$

Setting $m_s = s - n$ in Eqs. (2.3) an (2.4) we can relate the boson operators to the spin operators. Let us demonstrate for the S_+ operator

$$\begin{aligned}
S_+ \left|s, s-n\right\rangle &= \hbar\sqrt{s(s+1) - (s-n)(s-n+1)}\left|s, s-n+1\right\rangle \\
&= \hbar\sqrt{2sn}\sqrt{1 + \frac{1-n}{2s}}\left|s, s-n+1\right\rangle \\
&= \hbar\sqrt{2s}\sqrt{n}\sum_{k=0}^{\infty}\frac{(-1)^{k-1}(2k)!}{4^k(k!)^2(2k-1)}\left(\frac{1-n}{2s}\right)^k\left|s, s-n+1\right\rangle \\
&= \hbar\sqrt{2s}\underbrace{\sum_{k=0}^{\infty}\frac{(-1)^{k-1}(2k)!}{4^k(k!)^2(2k-1)}\left(-\frac{a^\dagger a}{2s}\right)^k}_{=\sqrt{1-\frac{a^\dagger a}{2s}}}\underbrace{\sqrt{n}\left|s, s-n+1\right\rangle}_{=a\left|s, s-n\right\rangle} \\
&= \hbar\sqrt{2s}\sqrt{1 - \frac{a^\dagger a}{2s}}a\left|s, s-n\right\rangle .
\end{aligned}$$

A similar derivation can be performed for S_-, while the relation between the S_z operator and boson number operator is easily seen. The HP transformations are thus given by

$$S_+ = \hbar\sqrt{2s}\sqrt{1 - \frac{a^\dagger a}{2s}}a, \tag{2.8}$$

$$S_- = \hbar\sqrt{2s}a^\dagger\sqrt{1 - \frac{a^\dagger a}{2s}}, \tag{2.9}$$

$$S_z = \hbar(s - a^\dagger a). \tag{2.10}$$

The transformations for $S\pm$ are obviously very nonlinear in bosonic operators, however in linear spin wave theory only terms up to quadratic order are considered. Therefore the HP transformations in linear spin wave theory simplify to

$$S_+ \approx \hbar\sqrt{2s}a, \qquad S_- \approx \hbar\sqrt{2s}a^\dagger, \qquad S_z = \hbar(s - a^\dagger a). \tag{2.11}$$

What we have essentially done is to approximate the magnons as excitations of harmonic oscillators. Assuming the Bloch sphere is oriented such that the ground state lies along the z-axis of the spin coordinate system, then the HP transformation can be seen as a projection down onto the xy-plane (which is the phase space of the harmonic oscillator). The nonlinear terms we discarded would account for the curvature of the Bloch sphere. It is obvious that such a projection works well for a system with many Dicke state levels that is close to the ground state, where the Bloch sphere is essentially flat. However since the localised electron spins are two-level systems it seems at first glance that a linearisation of the HP-transformation would be a bad approximation. Luckily it turns out that linear spin wave theory actually is a reasonably good approximation as long as the system is restricted to low temperatures, since the average number of spin excitations per lattice site then becomes very small so that the number-operator term in Eqs. (2.8) and (2.9) can safely be ignored [17].

2.2 Schrieffer-Wolff transformation

Models that include two-particle interactions appear frequently within the field of condensed matter physics, manifested as four-operator interaction terms in the language of second quantisation. Famously, the microscopic theory of superconductivity by Bardeen, Cooper and Schrieffer (BCS) uses a Hamiltonian with an attractive four-operator term as its starting point [3]. As will be seen in later chapters, the BCS theory Hamiltonian is actually what motivates the use of the Schrieffer-Wolff transformation in this thesis. In any case, there are situations where one starts out with a Hamiltonian with fermion operator terms of quadratic order that one wishes to map onto a four-operator model. Indeed the original application of the Schrieffer-Wolff transformation was to relate the Anderson model (quadratic in fermionic creation/destruction operators) to the Kondo model (which has a four-operator interaction term) [18]. Let us now assume we have a very simple model for coupling between bosonic and fermionic fields denoted by $\varphi_{\boldsymbol{q}}$ and $c_{\boldsymbol{k}}$ respectively

$$\mathcal{H} = \sum_{\boldsymbol{k}} \epsilon_{\boldsymbol{k}} c^\dagger_{\boldsymbol{k}} c_{\boldsymbol{k}} + \sum_{\boldsymbol{q}} \omega_{\boldsymbol{q}} \varphi^\dagger_{\boldsymbol{q}} \varphi_{\boldsymbol{q}} + g \sum_{\boldsymbol{k},\boldsymbol{q}} \left(\varphi_{\boldsymbol{q}} c^\dagger_{\boldsymbol{k}} c_{\boldsymbol{k}} + \text{h.c} \right). \tag{2.12}$$

We want to map this model onto a four-operator theory and get rid of the bosonic operators because the four-operator model has a better developed framework for computing interesting quantities, so the idea is to perform a canonical transformation of this Hamiltonian to a new effective Hamiltonian

$$\mathcal{H}_{\text{eff}} = e^{\eta S} \mathcal{H} e^{-\eta S}, \tag{2.13}$$

where η is a smallness parameter. The idea is now to choose a generator ηS so that the canonical transformation results in an effective Hamiltonian where the terms that are quadratic in fermion operators vanish. To achieve this let us first write the boson-fermion interaction as a perturbation term in the original Hamiltonian

$$\mathcal{H} = \mathcal{H}_0 + \eta \mathcal{H}_1, \tag{2.14}$$

so that in this case

$$\mathcal{H}_0 \equiv \sum_{\boldsymbol{k}} \epsilon_{\boldsymbol{k}} c^\dagger_{\boldsymbol{k}} c_{\boldsymbol{k}} + \sum_{\boldsymbol{q}} \omega_{\boldsymbol{q}} \varphi^\dagger_{\boldsymbol{q}} \varphi_{\boldsymbol{q}}, \qquad \eta \mathcal{H}_1 \equiv g \sum_{\boldsymbol{k},\boldsymbol{q}} \left(\varphi_{\boldsymbol{q}} c^\dagger_{\boldsymbol{k}} c_{\boldsymbol{k}} + \text{h.c} \right). \tag{2.15}$$

Next we use the Baker–Campbell–Hausdorff expansion to write the canonical transformation as a perturbation series

$$\mathcal{H}_{\text{eff}} = \mathcal{H}_0 + \eta\mathcal{H}_1 + \eta[S,\mathcal{H}_0] + \eta^2[S,\mathcal{H}_1] + \frac{1}{2}\eta^2[S,[S,\mathcal{H}_0]] + \frac{1}{2}\eta^3[S,[S,\mathcal{H}_1]] + \ldots \quad (2.16)$$

Having assumed that the parameter η is small, we ignore all terms of order $O(\eta^3)$ and are left with

$$\mathcal{H}_{\text{eff}} \approx \mathcal{H}_0 + \eta\mathcal{H}_1 + \eta[S,\mathcal{H}_0] + \eta^2[S,\mathcal{H}_1] + \frac{1}{2}\eta^2[S,[S,\mathcal{H}_0]]. \quad (2.17)$$

To get rid of the linear bosonic operator terms in the effective Hamiltonian the first order terms in η should vanish. This means that the generator ηS should take a form such that

$$\eta\mathcal{H}_1 + \eta[S,\mathcal{H}_0] = 0. \quad (2.18)$$

This constraint tells us that the generator has a similar form to the interaction term $\eta\mathcal{H}_1$. By inserting the resulting expression for $\eta[S,\mathcal{H}_0]$ into Eq. (2.17) we find that the effective Hamiltonian can be written as

$$\mathcal{H}_{\text{eff}} \approx \mathcal{H}_0 + \frac{1}{2}[\eta S,\eta\mathcal{H}_1] = \mathcal{H}_0 - \frac{1}{2}[\eta\mathcal{H}_1,\eta S]. \quad (2.19)$$

Since both $\eta\mathcal{H}_1$ and ηS are quadratic in fermion operators the resulting term will indeed consist of four fermionic operators. The boson-fermion interaction has thus been rewritten as a two-particle fermion-fermion interaction. The same principle can be applied for more complicated systems including spinful particles with several boson modes.

2.3 Bosonic diagonalisation theory

The model that will be discussed in this thesis includes a magnetic layer that is somewhat more complicated than collinear FMIs and AFMIs. For a treatment of magnons in such lattices with several different directions of magnetisation it is therefore necessary to consider diagonalisation of more than just one or two bosonic modes, where the diagonalisation has the constraint that the new operators must still represent bosons. This motivates the use of a Bogoliuabov transformation that is generalised to an arbitrary number of modes [19]–[22]. In fact, as the amount increases beyond two or three modes the task of finding an analytical expression for the transformation that diagonalises the system becomes very cumbersome, and so one must turn to a numerical treatment instead. The theory presented in the first part of this section was part of the author's project thesis [23]. Let us consider a system where there are m bosonic modes. The Hamiltonian for such a system will in general require a Hilbert space of dimension $4m$, since the bosonic operator basis consists of creation and destruction operators for both positive and negative momenta for each of the m modes. However the Hamiltonians we encounter in condensed matter physics can often be written in the form of a Bogoliuabov Hamiltonian

$$\mathcal{H}_{\text{Bog}} = \sum_{i,j=1}^{m} \left[M_1^{ij} a^\dagger_{\boldsymbol{q},i} a_{\boldsymbol{q},j} + M_2^{ij} a^\dagger_{\boldsymbol{q},i} a^\dagger_{-\boldsymbol{q},j} + M_3^{ij} a_{-\boldsymbol{q},i} a_{\boldsymbol{q},j} + M_4^{ij} a_{-\boldsymbol{q},i} a^\dagger_{-\boldsymbol{q},j} \right], \quad (2.20)$$

which means that the diagonalisation can be described by a $2m$ basis (thus half the size of the general case) as suggested by Colpa [20]. The coefficients in Eq. (2.20) are elements of matrices $M_1, M_2, M_3, M_4 \in \mathbb{C}^{m\times m}$. The Hamiltonian describing the system is therefore reduced from a $4m \times 4m$ matrix equation to a $2m \times 2m$ in the smaller basis, reducing the problem size by a factor 4. In matrix notation the Bogoliuabov Hamiltonian takes the form

$$\mathcal{H}_{\text{Bog}} = \boldsymbol{\alpha}^\dagger M \boldsymbol{\alpha}, \tag{2.21}$$

with

$$M = \begin{bmatrix} M_1 & M_2 \\ M_3 & M_4 \end{bmatrix}, \qquad \boldsymbol{\alpha}^\dagger = \begin{bmatrix} \boldsymbol{a}_{\boldsymbol{q}}^\dagger & \boldsymbol{a}_{-\boldsymbol{q}} \end{bmatrix}, \qquad \boldsymbol{\alpha} = \begin{bmatrix} \boldsymbol{a}_{\boldsymbol{q}} \\ \boldsymbol{a}_{-\boldsymbol{q}}^\dagger \end{bmatrix}. \tag{2.22}$$

The matrix M is sometimes referred to as the grand-dynamical matrix. As mentioned briefly in the start of this section, the task is to find a transformation T of the operators $\boldsymbol{\alpha}$, $\boldsymbol{\alpha}^\dagger$ that diagonalises the Hamiltonian. What this means is that

$$\mathcal{H}_{\text{Bog}} = \boldsymbol{\alpha}^\dagger M \boldsymbol{\alpha} = \boldsymbol{\alpha}^\dagger T^\dagger (T^\dagger)^{-1} M T^{-1} T \boldsymbol{\alpha} = \boldsymbol{\mathcal{A}}^\dagger D \boldsymbol{\mathcal{A}}, \tag{2.23}$$

so that the matrix

$$D \equiv (T^\dagger)^{-1} M T^{-1} = \text{diag}(\omega_1, \omega_2, ..., \omega_{2m}), \tag{2.24}$$

is diagonal. The elements of D are different bands in the bosonic energy spectrum. Physically, the basis for the diagonalised system represents long-lived bosonic excitations; and so naturally they must also satisfy bosonic commutation relations. This gives us an additional constraint on the diagonalisation, where in matrix form the transformed vectors $\boldsymbol{\mathcal{A}}$, $\boldsymbol{\mathcal{A}}^\dagger$ must satisfy

$$\boldsymbol{\mathcal{A}}\boldsymbol{\mathcal{A}}^\dagger - \left((\boldsymbol{\mathcal{A}}^\dagger)^T (\boldsymbol{\mathcal{A}})^T \right)^T = \sigma_3. \tag{2.25}$$

Here σ_3 is the "para unit matrix"

$$\sigma_3 = \text{diag}(1, 1, ..., 1, -1, ..., -1), \tag{2.26}$$

which has a similar form to the Pauli z-matrix generalised to an arbitrary dimension and therefore motivates the chosen notation for this matrix. Equation (2.25) may be rewritten in the form

$$T^\dagger \sigma_3 = \sigma_3 T^{-1}. \tag{2.27}$$

Together with the diagonalisation in equation (2.24) this gives

$$M T^{-1} = T^\dagger D = \sigma_3 T^{-1} \sigma_3 D. \tag{2.28}$$

Defining $\sigma_3 D \equiv \text{diag}(\lambda_1, \lambda_2, ..., \lambda_{2m})$, we consider equation (2.28) for each column $\boldsymbol{w}_\rho$ of T^{-1}. Then the problem of determining the energy bands $\omega_1, ..., \omega_{2m}$ and finding the corresponding Bogoliubov transformation T essentially boils down to solving $2m$ eigenproblems

$$\sigma_3 M \boldsymbol{w}_\rho = \lambda_\rho \boldsymbol{w}_\rho, \qquad \rho = 1, 2, ..., 2m. \tag{2.29}$$

Colpa presents quite an elegant algorithm for finding the Bogoliubov transformation T for systems of many bosonic modes. This thesis will only deal with problem sizes limited to

a two-digit amount of bosonic modes, which is too large for an analytic treatment but also small enough that solving (2.29) directly is not much slower than using Colpa's algorithm. As we will discuss in the next chapter, finding normalised eigenvectors of (2.29) using an eigensolver gives us a simple way to keep track of the energy band ordering. However, the fact that numerical eigensolvers often only give us the normalised eigenvectors means that we must enforce the bosonic commutation also after solving the eigensystem. Because while the columns of the inverse transformation matrix T^{-1} now have the right shape, the normalisation from the eigensolver means that they in general have the wrong magnitude. Luckily this can easily be fixed; we write the correct columns of T^{-1} as the normalised eigenvectors times some factor

$$\boldsymbol{w}_\rho = C_\rho \hat{\boldsymbol{w}}_\rho. \tag{2.30}$$

We can use Eq. (2.27) to determine the correct factors C_ρ

$$\sigma_3 = \begin{pmatrix} C_1^2 \boldsymbol{w}_1^\dagger \sigma_3 \boldsymbol{w}_1 & & & \\ & C_2^2 \boldsymbol{w}_2^\dagger \sigma_3 \boldsymbol{w}_2 & & \\ & & \ddots & \\ & & & C_{2m}^2 \boldsymbol{w}_{2m}^\dagger \sigma_3 \boldsymbol{w}_{2m} \end{pmatrix}. \tag{2.31}$$

The eigenvectors of correct magnitude are given by the factors C_ρ that satisfy this equation.

2.3.1 Sorting of numerically simulated energy bands

One of the problems we encounter when treating the diagonalisation of a Hamiltonian numerically over the 1st Brillouin zone (BZ) is that the eigenpairs may not necessarily follow the same ordering at different points in the BZ. We are in some sense at the mercy of the eigensolver that only takes some local input and does not know there is some global band structure that should determine the ordering. Figure 2.1 illustrates this problem and desired result. For the case where all bands are isolated the solution is trivial, one needs only to order the eigenpairs according to the magnitude of the eigenvalues. In fact most eigensolvers will already provide such a sorting. In the case of band crossings things get more complicated, as it becomes necessary to determine if the bands cross or not.

There is a quite elegant way of dealing with the non-isolated band sorting problem based on continuity of the eigenvectors [24], [25]. Continuity of the eigenvector tells us that two eigenvectors belonging to the same band should be approximately equal if located sufficiently close to one another on the BZ, with their inner product being approximately 1 since we consider them to be normalised (which is the case if we have not yet re-enforced the bosonic commutation relation). In the case where the two eigenvectors do not belong to the same band the magnitude of the inner product will be somewhere between 0 and 1, and our assumption is that this magnitude will be less than if they had belonged to the same band. The task of sorting the bands correctly therefore becomes an assignment problem where we order the adjacent eigenvectors in a way that maximises their overlap. This type of problem is otherwise known as weighted bipartite perfect matching. Let $|\psi_i(\boldsymbol{q})\rangle$ be the i'th normalised eigenvector at point $\boldsymbol{q}$ and $|\psi_j(\boldsymbol{q}+\delta\boldsymbol{q})\rangle$ be the j'th normalised eigenvector some adjacent point, where we in general let the ordering at the two points be different. We define the matrix

$$W_{ij} \equiv -\big|\, \langle \psi_i(\boldsymbol{q}) | \psi_j(\boldsymbol{q}+\delta\boldsymbol{q}) \rangle \,\big|^2. \tag{2.32}$$

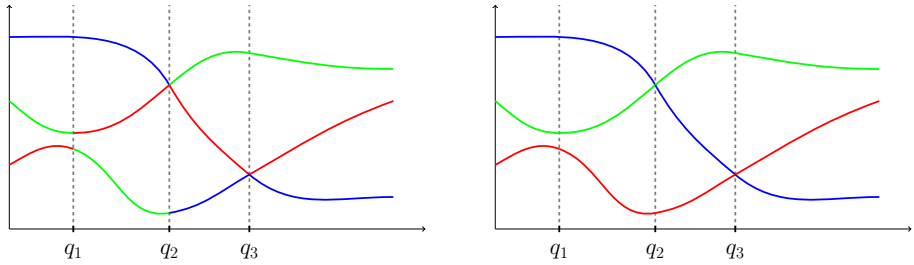

Figure 2.1: Illustration of the band sorting problem in a numerically calculated spectrum. Such a calculation involves solving an eigensystem at each point in the 1st BZ, and in general the eigenpair ordering can differ at two different points. Figure 2.1a shows an example where the eigenvalues of different bands (denoted by separate colours) have been mixed. Figure 2.1b shows the correctly sorted bands.

The task is to find a permutation matrix P of same dimension as W that gives the minimal "cost", ie.

$$\underset{P\in\mathbb{R}^{m\times m}}{\arg\min} \sum_{ij} W_{ij}P_{ij}. \tag{2.33}$$

For a numerical treatment in Python this can be achieved by using Scipy's function `scipy.optimize.linear_sum_assignment`, which uses the Hungarian algorithm [26].

2.3.2 Phase-differences in the Bogoliubov transformation eigenvectors

Assuming that the Bogoliubov transformation matrix $T_{\boldsymbol{q}}$ is correctly sorted, there is still one other problem we encounter when diagonalising numerically rather than analytically. Although most eigensolvers provide a solution where the eigenvectors are normalised, the overall phase can still be arbitrary since multiplying the entire eigenvector with f.ex -1 still gives a normalised eigenvector corresponding to that same eigenvalue. In other words, the eigenvectors are not unique [21]. Suppose that we have a continuous wavefunction in $\boldsymbol{q}$ for the r'th band is denoted by $|\psi_r(\boldsymbol{q})\rangle$, yet our eigensolver gives us

$$|\tilde{\psi}_r(\boldsymbol{q})\rangle = e^{i\theta_r(\boldsymbol{q})}\,|\psi_r(\boldsymbol{q})\rangle\,, \tag{2.34}$$

with some arbitrary $\theta_r(\boldsymbol{q})$ in each point $\boldsymbol{q}$. In many applications this is not a problem we care about. However since we are dealing with wavefunctions across the 1st BZ we must be a bit careful whenever elements of the magnon transformation matrix appear in an expression, so that no unphysical phase contributions arise.

2.4 Group theory for the triangular lattice

This section is in most part a reiteration of theory presented in some unpublished notes by Thingstad [27] and the Master's thesis of Otnes [28]. The model considered in this thesis

(which will later be described in detail) has triangular lattice symmetries. Symmetry discussions for different physical quantities require that we introduce the lattice harmonics for the given lattice symmetry. The lattice harmonics are basis functions that respect the symmetry of the lattice, and in the case of a triangular lattice these symmetries are described by the point group C_{6v}. There are 12 symmetry operations that form the elements of this group. These consist of 6 rotation operations (where we have included the identity operation) and 6 mirror operations. We list all 12 symmetry operations T in the E_1 irreducible representation (irrep):

$$\begin{aligned}
D^{(E_1)}(E) &= \begin{pmatrix} 1 & 0 \\ 0 & 1 \end{pmatrix} & D^{(E_1)}(C_2) &= \begin{pmatrix} -1 & 0 \\ 0 & -1 \end{pmatrix} \\
D^{(E_1)}(C_3) &= \begin{pmatrix} -1/2 & -\sqrt{3}/2 \\ \sqrt{3}/2 & -1/2 \end{pmatrix} & D^{(E_1)}(C_3^{-1}) &= \begin{pmatrix} -1/2 & \sqrt{3}/2 \\ -\sqrt{3}/2 & -1/2 \end{pmatrix} \\
D^{(E_1)}(C_6) &= \begin{pmatrix} 1/2 & -\sqrt{3}/2 \\ \sqrt{3}/2 & 1/2 \end{pmatrix} & D^{(E_1)}(C_6^{-1}) &= \begin{pmatrix} 1/2 & \sqrt{3}/2 \\ -\sqrt{3}/2 & 1/2 \end{pmatrix} \\
D^{(E_1)}(\sigma_{d1}) &= \begin{pmatrix} -1 & 0 \\ 0 & 1 \end{pmatrix} & D^{(E_1)}(\sigma_{v1}) &= \begin{pmatrix} 1 & 0 \\ 0 & -1 \end{pmatrix} \\
D^{(E_1)}(\sigma_{d2}) &= \begin{pmatrix} 1/2 & -\sqrt{3}/2 \\ -\sqrt{3}/2 & -1/2 \end{pmatrix} & D^{(E_1)}(\sigma_{v2}) &= \begin{pmatrix} -1/2 & \sqrt{3}/2 \\ \sqrt{3}/2 & 1/2 \end{pmatrix} \\
D^{(E_1)}(\sigma_{d3}) &= \begin{pmatrix} 1/2 & \sqrt{3}/2 \\ \sqrt{3}/2 & -1/2 \end{pmatrix} & D^{(E_1)}(\sigma_{v3}) &= \begin{pmatrix} -1/2 & -\sqrt{3}/2 \\ -\sqrt{3}/2 & 1/2 \end{pmatrix}
\end{aligned} \tag{2.35}$$

Here each operation takes the form $D^{(E_1)}(T)$. Let us define the projection operator

$$\mathcal{P}_\kappa^{(\eta)} = \frac{d_\eta}{g} \sum_T D_{\kappa\kappa}^{(\eta)}(T)^* T, \tag{2.36}$$

where η is an irrep of dimension d_η. Furthermore, $D_{\kappa\kappa}^{(\eta)}(T)$ is a diagonal matrix element of the operation T in irrep η and g is the number of elements in the group. In addition to the two-dimensional irrep E_1 for which we listed the group elements, there is another two-dimensional irrep E_2 and four one-dimensional irreps A_1, A_2, B_1 and B_2. The group elements $D^{(E_2)}(T)$ are listed in Table 2.1. For the one-dimensional irreps the label κ is redundant and $D_{\kappa\kappa}^{(\eta)}(T)$ is equivalent to the character of the operation (which is defined as the trace of the operation matrix). The different characters for all irreps and operations are listed in Table 2.2.

Now assume we have a function $f(\boldsymbol{k})$ that is periodic on the Brillouin zone of the triangular lattice, so that it may be written in terms of basis functions that respect the lattice symmetry. The idea is that this function can be written in terms of functions spanning the irreducible subspaces [29]

$$f(\boldsymbol{k}) = \sum_{\eta,\kappa} f_\kappa^{(\eta)}(\boldsymbol{k}). \tag{2.37}$$

Projecting this function onto one of the irreps we get

$$f_\kappa^{(\eta)}(\boldsymbol{k}) = \mathcal{P}_\kappa^{(\eta)} f(\boldsymbol{k}) = \frac{d_\eta}{g} \sum_T D_{\kappa\kappa}^{(\eta)}(T)^* T f(\boldsymbol{k}). \tag{2.38}$$

T	$D^{(E_2)}(T)$	T	$D^{(E_2)}(T)$
E	$D^{(E_2)}(E)$	C_2	$D^{(E_2)}(E)$
C_3	$D^{(E_2)}(C_3)$	C_3^{-1}	$D^{(E_2)}(C_3^{-1})$
C_6	$D^{(E_2)}(C_3^{-1})$	C_6^{-1}	$D^{(E_2)}(C_3)$
σ_{d1}	$D^{(E_2)}(\sigma_{d1})$	σ_{v1}	$D^{(E_2)}(\sigma_{d1})$
σ_{d2}	$D^{(E_2)}(\sigma_{d2})$	σ_{v2}	$D^{(E_2)}(\sigma_{d2})$
σ_{d3}	$D^{(E_2)}(\sigma_{d3})$	σ_{v3}	$D^{(E_2)}(\sigma_{d3})$

Table 2.1: Conversion of group elements to the E_2 irrep from the E_1 irrep elements listed in (2.35).

	E	C_2	$2C_3$	$2C_6$	$3\sigma_d$	$3\sigma_v$
A_1	1	1	1	1	1	1
A_2	1	1	1	1	-1	-1
B_1	1	-1	1	-1	1	-1
B_2	1	-1	1	-1	-1	1
E_1	2	-2	-1	1	0	0
E_2	2	-2	-1	-1	0	0

Table 2.2: Character Table for the C_{6v} group.

Note that we may write a symmetry operation on the function $f(\boldsymbol{k})$ as $Tf(\boldsymbol{k}) = f(T\boldsymbol{k})$. The periodicity of this function allows us to express the function as a Fourier series

$$f(\boldsymbol{k}) = \sum_{\boldsymbol{n}} f_{\boldsymbol{n}} e^{i\boldsymbol{R_n}\cdot\boldsymbol{k}}, \tag{2.39}$$

where $\boldsymbol{R_n} = n\boldsymbol{a}_1 + m\boldsymbol{a}_2$ are the real space lattice coordinates with $\boldsymbol{n} = (n, m)$. Thus we may write

$$f^{(\eta)}(\boldsymbol{k}) = \sum_{\boldsymbol{n}} \frac{d_\eta}{g} \sum_T D^{(\eta)}_{\kappa\kappa}(T)^* f_{\boldsymbol{n}} e^{i\boldsymbol{R_n}\cdot T\boldsymbol{k}}. \tag{2.40}$$

We consider only functions $f(\boldsymbol{k})$ that are real, meaning that we can express the projection in terms of cosines and sines. For the symmetry operation $T\boldsymbol{k}$ we consider generators in the E_1 irrep so that

$$f^{(\eta)}(\boldsymbol{k}) = \sum_{\boldsymbol{n}} f_{\boldsymbol{n}} \frac{d_\eta}{g} \sum_T D^{(\eta)}_{\kappa\kappa}(T)^* \left(\cos\left(\boldsymbol{R_n}\cdot D^{(E_1)}(T)\boldsymbol{k}\right) + \sin\left(\boldsymbol{R_n}\cdot D^{(E_1)}(T)\boldsymbol{k}\right)\right). \tag{2.41}$$

The function can then be written in terms of the lattice basis functions

$$f(\boldsymbol{k}) = \sum_{\eta,\kappa,\boldsymbol{n}} f_{\boldsymbol{n}} \tilde{B}^{\eta,\kappa}_{\boldsymbol{n}}(\boldsymbol{k}), \tag{2.42}$$

giving the following expression for the lattice harmonics

$$\tilde{B}^{\eta,\kappa}_{\boldsymbol{n}}(\boldsymbol{k}) = \frac{d_\eta}{g}\sum_T D^{(\eta)}_{\kappa\kappa}(T)^* \left(\cos\left(\boldsymbol{R_n}\cdot D^{(E_1)}(T)\boldsymbol{k}\right) + \sin\left(\boldsymbol{R_n}\cdot D^{(E_1)}(T)\boldsymbol{k}\right)\right). \tag{2.43}$$

These basis functions are orthogonal, but not necessarily normalised. We define the normalised basis functions as

$$B^{\eta,\kappa}_{\boldsymbol{n}}(\boldsymbol{k}) = \tilde{B}^{\eta,\kappa}_{\boldsymbol{n}}(\boldsymbol{k})/\mathcal{N}, \tag{2.44}$$

where the normalisation factor is determined from

$$\mathcal{N}^2 = \int_{1.\ \mathrm{BZ}} d\boldsymbol{k}\, \tilde{B}^{\eta,\kappa}_{\boldsymbol{n}}(\boldsymbol{k})^2. \tag{2.45}$$

We only consider the on-site and nearest neighbour harmonics, yielding a total of seven unique basis functions listed in Table 2.3. To get an idea of what these harmonics look like the basis functions have been plotted in Figure 2.2. We can gather the labels η, n, m and κ that describe unique lattice harmonics into a single label $\alpha \in \{s, 2s, p_x, p_y, d_{xy}, d_{x^2-y^2}, f\}$, where the basis functions satisfy both orthonormality and completeness relations

$$\int_{1.\ \mathrm{BZ}} d\boldsymbol{k}\, B_\alpha(\boldsymbol{k})B_\beta(\boldsymbol{k}) = \delta_{\alpha\beta}, \tag{2.46}$$

$$\sum_\alpha B_\alpha(\boldsymbol{k})B_\alpha(\boldsymbol{k'}) = \delta_{\boldsymbol{k}\boldsymbol{k'}}. \tag{2.47}$$

Symmetry	Irrep	(n,m)	κ	Normalised basis function
s	A_1	$(0,0)$	1	$\frac{1}{\sqrt{A_{\mathrm{BZ}}}}$
$2s$	A_1	$(0,1)$	1	$\sqrt{\frac{2}{3A_{\mathrm{BZ}}}}\left(\cos(k_x a) + 2\cos(\frac{k_x a}{2})\cos(\frac{k_y a\sqrt{3}}{2})\right)$
p_x	E_1	$(1,0)$	1	$\frac{2}{\sqrt{3A_{\mathrm{BZ}}}}\left(\sin(k_x a) + \sin(\frac{k_x a}{2})\cos(\frac{k_y a\sqrt{3}}{2})\right)$
p_y	E_1	$(0,1)$	2	$\frac{2}{\sqrt{A_{\mathrm{BZ}}}}\cos(\frac{k_x a}{2})\sin(\frac{k_y a\sqrt{3}}{2})$
d_{xy}	E_2	$(0,1)$	1	$\frac{-2}{\sqrt{A_{\mathrm{BZ}}}}\sin(\frac{k_x a}{2})\sin(\frac{k_y a\sqrt{3}}{2})$
$d_{x^2-y^2}$	E_2	$(1,0)$	2	$\frac{2}{\sqrt{3A_{\mathrm{BZ}}}}\left(\cos(k_x a) - \cos(\frac{k_x a}{2})\cos(\frac{k_y a\sqrt{3}}{2})\right)$
f	B_2	$(1,0)$	1	$\sqrt{\frac{2}{3A_{\mathrm{BZ}}}}\left(\sin(k_x a) - 2\sin(\frac{k_x a}{2})\cos(\frac{k_y a\sqrt{3}}{2})\right)$

Table 2.3: Normalised basis functions for the seven most relevant harmonics on a triangular lattice.

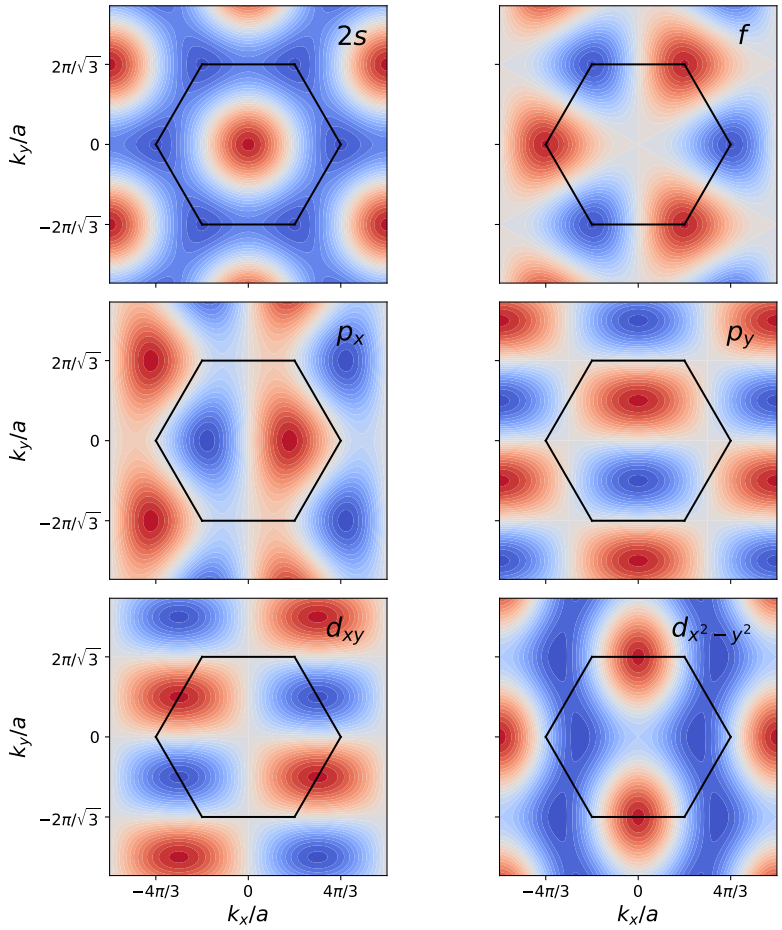

Figure 2.2: Plot of the seven first basis functions without considering normalisation.

Chapter 3

Bilayer model

The bilayer discussed in this thesis will consist of two layers of monoatomic thickness; one of the layers just being a normal metal (NM) while the other layer consists of an electrically insulating ferromagnetic material with a non-collinear spin structure. Specifically we choose to look at a non-collinear magnetic material that has a spiral structure as its ground state, which we will refer to as a spiral phase ferromagnetic insulator (SPFMI). An illustration of the complete bilayer system is shown in Figure 3.1.

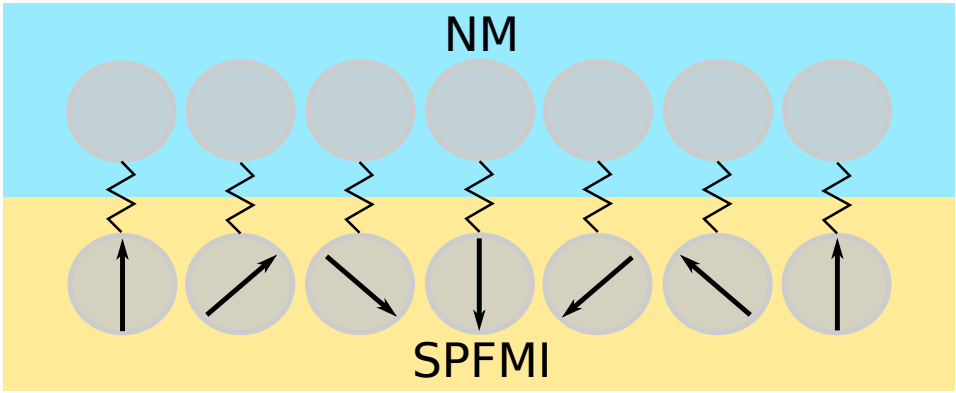

Figure 3.1: Schematic of the bilayer. Unlike previous studies the magnetic layer (SPFMI part) has a non-collinear spiral structure.

3.1 Tight binding normal metal

Seeing as the complete bilayer model will be complex enough as it is with the non-collinear spin structure in the magnet part of the system, we are motivated to keep the electronic part as simple as possible. Based on this we choose to let the material layer where the

electrons are conducted be a simple normal metal (NM) described by a tight binding model of electrons hopping between lattice sites on a triangular grid

$$\mathcal{H}_{\text{NM}} = -t \sum_{i,j,\sigma} c^\dagger_{i\sigma} c_{j\sigma} - \mu \sum_{i} c^\dagger_{i\sigma} c_{i\sigma}. \tag{3.1}$$

To find the electronic spectrum we must diagonalise this system, which is achieved by a basis of fermionic operators in k-space. We therefore introduce the Fourier transform of the operators and write the real space operators in terms of these

$$c_{i\sigma} = \frac{1}{\sqrt{N}} \sum_{\boldsymbol{k}} c_{\boldsymbol{k}\sigma} e^{-i\boldsymbol{k}\cdot\boldsymbol{r}_i}, \tag{3.2}$$

so that

$$\mathcal{H}_{\text{NM}} = \sum_{\boldsymbol{k},\sigma} (\epsilon_{\boldsymbol{k}} - \mu) c^\dagger_{\boldsymbol{k}\sigma} c_{\boldsymbol{k}\sigma}, \tag{3.3}$$

where the electron dispersion relation for a triangular grid is given by

$$\epsilon_{\boldsymbol{k}} = -2t \left(\cos\left(k_x a\right) + 2\cos\left(\frac{1}{2}k_x a\right) \cos\left(\frac{\sqrt{3}}{2}k_y a\right) \right). \tag{3.4}$$

In the long wavelength regime this can be approximated by a parabolic dispersion relation

$$\epsilon_{\boldsymbol{k}} \approx 3a^2 t(k_x^2 + k_y^2) - 6t \tag{3.5}$$

The density of states is given by

$$D(\epsilon) = \sum_{\boldsymbol{k}} \delta(\epsilon - \epsilon_{\boldsymbol{k}} + \mu) = -\frac{N}{\pi} \Im\big[G(\epsilon + i0^+)\big], \tag{3.6}$$

and we have introduced the electron Green's function

$$G(z) = \frac{1}{N} \sum_{\boldsymbol{k}} \frac{1}{z - \epsilon_{\boldsymbol{k}} + \mu}. \tag{3.7}$$

The density of k-states is

$$D(k) = \frac{\sqrt{3} N a^2 k}{2\pi}. \tag{3.8}$$

At the bottom of the electronic band structure where the dispersion is approximately parabolic the 2D density of states is constant, with the value

$$D(\epsilon) = \frac{\sqrt{3} N}{12\pi t}. \tag{3.9}$$

Calculating the DOS outside the low energy regime as given in Eq. (3.6) involves solving an elliptic integral of the first kind [30]. For a numerical treatment we calculate the DOS using the Python library `GfTool` [31]. The full electron spectrum and DOS is shown in Figure 3.2.

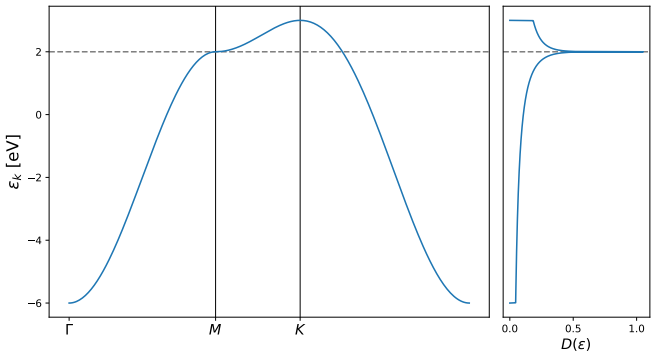

Figure 3.2: Spectrum and DOS per atom for a triangular tight binding model with $t = 1$ eV and $\mu = 0$. The gray stapled line indicates the Van Hove instability.

3.2 Spiral phase ferromagnetic insulator

The second part of the bilayer consists of a non-collinear ferromagnetic insulator, and we choose specifically to look at a spin structure that the author has studied in his project thesis [23]. This section is therefore mostly a reiteration of the main results found as a part of that work. We consider a magnetic ground state with a spin structure arising from a Dzyaloshinsky-Moriya interaction term in the FMI Hamiltonian, leading to a canting of the spins [11]. We specifically choose to look at a triangular lattice in two dimensions, and assume that there exists some feature so that the system breaks inversion symmetry without having to treat it as a bulk material. This is because the DMI vectors are determined by the crystal symmetry; the orientation decided by a set of rules found by Moriya [12]. In our case we require the DMI vectors $\boldsymbol{D}$ to lie in the lattice plane (which we choose to be the xy-plane) such that $D_z^{ij} = 0$ in all cases. For simplicity we consider only nearest neighbour interactions, and we will let all DMI vectors have the same magnitude regardless of their position on the lattice. We describe our canted ferromagnetic system with the following Hamiltonian

$$\mathcal{H} = -\sum_{\langle i,j \rangle} \left[J_x S_x^i S_x^j + J_y S_y^i S_y^j + J_z S_z^i S_z^j + \boldsymbol{D}^{ij} \cdot (\boldsymbol{S}^i \times \boldsymbol{S}^j) \right]. \tag{3.10}$$

We see from the cross product that the role of the DMI vectors $\boldsymbol{D}^{ij}$ is to twist the spins toward a perpendicular configuration. They constitute the anti-symmetric part of the exchange interaction [12], [32], [33], which becomes clear by writing the Hamiltonian in terms of a 3×3 exchange interaction matrix

$$\mathcal{H} = -\sum_{\langle i,j \rangle} (\boldsymbol{S}^i)^T \begin{bmatrix} J_x & D_z^{ij} & -D_y^{ij} \\ -D_z^{ij} & J_y & D_x^{ij} \\ D_y^{ij} & -D_x^{ij} & J_z \end{bmatrix} \boldsymbol{S}^j. \tag{3.11}$$

First of all, it now has an elegant and compact form which will simplify notation a lot when introducing HP-transformations for a non-collinear ground state. We see that the DMI contribution to the exchange interaction matrix is indeed the off-diagonal anti-symmetric part.

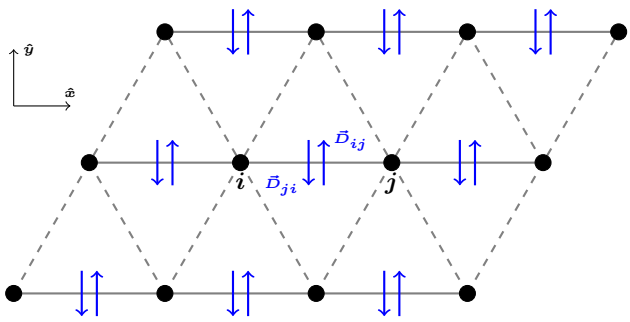

Figure 3.3: Triangular lattice with Dzyaloshinskii-Moriya interaction vectors (blue) in the lattice plane. Solid lines denote nearest neighbours with both exchange interactions Dzyaloshinskii-Moriya interactions, while dashed lines denote only exchange interactions.

In this case the symmetric part is just a diagonal matrix of what we here will refer to as the "exchange interaction" (which in general is anisotropic) with elements J_x, J_y and J_z. The non-collinear structure is a result of competition between the exchange interaction favouring parallel spins and the DMI favouring perpendicular spins. In a more general treatment one would include off-diagonal elements of the symmetric part of the exchange interaction matrix, which could be included for a system with completely general interactions [33]. One can achieve the more generalised version of the Hamiltonian in Eq. (3.11) by considering a general many-body problem for interacting electrons in a crystal with spin-orbit coupling to second order in the hopping parameter [34].

The task is now to express the Hamiltonian in terms of bosonic ladder-operators by applying the HP transformation, which would be easy if we were considering a simple collinear FMI since we then could use the same HP transformation everywhere. Our problem however involves non-collinear spins as a consequence of the DMI, and so the local spin coordinate axes will be rotated relative to each other according to the so-called generalised rotation model presented by Fishman and Haraldsen [35], [36]. It is therefore necessary to introduce a different HP transformation for each different rotation of the spins. The theory presented here is an adaptation of Fishman and Haraldsen's general rotation model to include DMI while ignoring interactions from external magnetic fields and easy axis anisotropy. The spin operators $\boldsymbol{S}$ must be rotated to each site's local spin coordinate system. We can achieve this by applying a rotation matrix to each spin operator:

$$\tilde{\boldsymbol{S}}^i = U^i \boldsymbol{S}^i. \tag{3.12}$$

Seeing as we only need two Euler angles θ_i, ψ_i to perform a rotation to any point on the Bloch sphere we let the rotation matrix be as follows

$$U^i = \begin{bmatrix} \cos\theta_i \cos\psi_i & \cos\theta_i \sin\psi_i & -\sin\theta_i \\ -\sin\psi_i & \cos\psi_i & 0 \\ \sin\theta_i \cos\psi_i & \sin\theta_i \sin\psi_i & \cos\theta_i \end{bmatrix}, \qquad (U^i)^{-1} = (U^i)^T. \tag{3.13}$$

Eq. (3.11) can now be rewritten in terms of the rotated spins

$$\mathcal{H} = -\sum_{\langle i,j \rangle} (\tilde{\boldsymbol{S}}^i)^T W^{ij} \tilde{\boldsymbol{S}}^j, \tag{3.14}$$

where

$$W^{ij} = \begin{bmatrix} W^{ij}_{xx} & W^{ij}_{xy} & W^{ij}_{xz} \\ W^{ij}_{yx} & W^{ij}_{yy} & W^{ij}_{yz} \\ W^{ij}_{zx} & W^{ij}_{zy} & W^{ij}_{zz} \end{bmatrix} = U^i \begin{bmatrix} J_x & D^{ij}_z & -D^{ij}_y \\ -D^{ij}_z & J_y & D^{ij}_x \\ D^{ij}_y & -D^{ij}_x & J_z \end{bmatrix} (U^j)^T. \tag{3.15}$$

The elements of the rotated interaction matrix W^{ij} are listed in appendix A.1 since they are somewhat lengthy expressions. We now make linearised HP transformations at each lattice site described in the local coordinates

$$\begin{aligned} \tilde{S}^i_z &= s - a^\dagger_i a_i \\ \tilde{S}^i_+ &\approx \sqrt{2s}\, a_i \\ \tilde{S}^i_- &\approx \sqrt{2s}\, a^\dagger_i. \end{aligned} \tag{3.16}$$

We can now swap out the spin operators in Eq. (3.14) with terms of boson ladder operators a, $a^\dagger$. The Hamiltonian then takes the form

$$\mathcal{H} = \mathcal{H}^{(0)} + \mathcal{H}^{(1)} + \mathcal{H}^{(2)}, \tag{3.17}$$

where $\mathcal{H}^{(0)}$, $\mathcal{H}^{(1)}$ and $\mathcal{H}^{(2)}$ are terms in zeroth, first and second order of the boson operators respectively. Since we are dealing with linear spin wave theory we neglect all terms of higher order (ie. we consider no boson-boson interactions).

Zeroth order Hamiltonian

The zeroth order terms describe the classical ground state of the system. We assume that the quantum mechanical ground state is given by magnetic fluctuations around the classical ground state, in a similar fashion to how one treats the collinear AFMI ground state as fluctuations around a Néel structure. Having replaced the spin operators with bosonic ladder operators we get the zeroth order Hamiltonian by grouping the constant terms together, yielding

$$\mathcal{H}^{(0)} = -s^2 \sum_{\langle i,j \rangle} W^{ij}_{zz}. \tag{3.18}$$

The task finding the classical ground state means finding the spin angles (θ_i, ψ_i) at each lattice site that minimise Eq. (3.18). Assuming we have N lattice sites this becomes a problem of finding the minimum of a $2N$-variable function. In this thesis we will consider DMI interactions only between two of the six nearest neighbours as shown in Figure 3.3, where the DMI interactions all lie on the same line. The result is that all spin rotations lie in the same plane so that our 2D system actually looks a lot like several connected "1D spin chains" of rotating spins [37], where the "connection" between different chains is just a normal exchange interaction. We mostly chose to work with this system because

it is simple; the "pseudo-1D" nature of the minimisation problem means we can find an analytic solution for the classical ground state with the added bonus that we can work with relatively few different spin orientations. It is one of the simplest non-collinear spin structures we can study, and the fact that we only get two-dimensional spin spirals will prove to simplify interactions with the NM massively.

Furthermore, to keep the system relatively simple we choose to look at isotropic exchange coupling so that $J_x = J_y = J_z$ which we will simply denote as J. The spin rotation must obviously be uniform with every spin rotated an angle $\Delta\theta$ from the adjacent spins along the direction of rotation. We must however account for the fact that our "spin chains" on the triangular lattice are connected, so that two adjacent chains may be rotated relative to each other to get a lower energy. We take this into account when writing the single site contribution to the classical energy:

$$\begin{aligned} E_i = &-2s^2 J\left[2\cos(\Delta\theta) + \cos(\alpha) + \cos(\beta) + \cos(\alpha - \Delta\theta) + \cos(\beta - \Delta\theta)\right] \\ &- 4s^2|\boldsymbol{D}|\sin(\Delta\theta), \end{aligned} \tag{3.19}$$

where the site i is located on a given "spin chain" and the angles α and β are the relative rotations of the two neighbouring chains. We minimise with respect to α, β and $\Delta\theta$ in order to find the ground state spin structure. Minimisation w.r.t α

$$\frac{\partial E_i}{\partial \alpha} = 2s^2 J[\sin(\alpha) + \sin(\alpha - \Delta\theta)] = 0, \tag{3.20}$$

yields $\alpha = \Delta\theta/2$, and likewise we can show that $\beta = \Delta\theta/2$. Thus we have shown that our 2D lattice of connected "spin chains" is actually just two alternating spin spirals with a relative rotation of $\Delta\theta/2$. Inserting what we have found into Eq. (3.19), we get

$$E_i = -4s^2 J\left[\cos(\Delta\theta) + 2\cos\left(\frac{1}{2}\Delta\theta\right)\right] - 4s^2|\boldsymbol{D}|\sin(\Delta\theta), \tag{3.21}$$

and subsequently minimising this w.r.t $\Delta\theta$ provides the following analytical relation between DMI and exchange interaction for any given spin rotation periodicity

$$\frac{|\boldsymbol{D}|}{J} = \frac{\sin(\Delta\theta) + \sin(\frac{1}{2}\Delta\theta)}{\cos(\Delta\theta)}. \tag{3.22}$$

Accordingly the smallest possible spiral period is 5 atoms for a non-zero exchange interaction. Having determined the angles (θ_i, ψ_i) of our magnetic structure and the relation $\frac{|\boldsymbol{D}|}{J}$ in order to generate this structure we can start analysing higher order parts of the Hamiltonian.

First order Hamiltonian

We now move on to look at all the terms that are linear in boson operators a_i, $a_i^\dagger$ from our HP transformations. Grouping them together we find the first order Hamiltonian

$$\mathcal{H}^{(1)} = -s\sqrt{\frac{s}{2}}\sum_{\langle i,j\rangle}\left[W_{xz}^{ij}(a_i + a_i^\dagger) + iW_{yz}^{ij}(a_i^\dagger - a_i) + W_{zx}^{ij}(a_j + a_j^\dagger) + iW_{zy}^{ij}(a_j^\dagger - a_j)\right] \tag{3.23}$$

Since the total Hamiltonian now is expressed as a function of boson operators $\mathcal{H} = \mathcal{H}(\{a_i, a_i^\dagger\})$ and the ground state is the minimum of this function, it follows that all operator terms of linear order must necessarily vanish. Since the ground state is a minimum then differentiation with respect to the operators $(a_i, a_i^\dagger)$ must give zero, and consequently we have $\mathcal{H}^{(1)} = 0$ at the ground state. We can show that this does indeed hold for our system by dividing Eq. (3.23) into a real and imaginary part (the elements of the rotated interaction matrix are purely real numbers). For the linear boson operator terms to vanish our system must therefore satisfy the following constraints at each site i:

$$\sum_{\langle j \rangle} (W_{zy}^{ij} + W_{yz}^{ji}) = 0, \tag{3.24}$$

$$\sum_{\langle j \rangle} (W_{xz}^{ij} + W_{zx}^{ji}) = 0. \tag{3.25}$$

Here $\langle j \rangle$ is the set of nearest neighbours to site i. One can show that these constraints are equivalent to finding the extrema of equation (3.18), which means that finding the correct angles $\{\theta_i, \psi_i\}$ for the classical ground state automatically ensures the linear operator terms vanish.

Second order Hamiltonian

Finally we consider the terms of second order in bosonic operators.

$$\mathcal{H}^{(2)} = s \sum_{\langle i,j \rangle} \left[G_1^{ij\,*} a_i a_j^\dagger + G_1^{ij} a_i^\dagger a_j + G_2^{ij} a_i a_j + G_2^{ij\,*} a_i^\dagger a_j^\dagger + W_{zz}^{ij} (a_i^\dagger a_i + a_j^\dagger a_j) \right] \tag{3.26}$$

This is the spin wave Hamiltonian and describes fluctuations of the localised spins. While the zeroth order Hamiltonian was only important for determining the magnetic ground state and the first order Hamiltonian vanished, the second order Hamiltonian is the part of the magnetic layer Hamiltonian that we need when describing the magnons and their interactions with electrons in the NM layer. The operator $a_i^\dagger a_i$ gives a count of how many fluctuations there are at site i, while $a_i^\dagger a_j$ moves a spin fluctuation from i to site j. To make the notation more tidy we have introduced the coefficients

$$G_1^{ij} \equiv -\frac{1}{2}[W_{xx}^{ij} + W_{yy}^{ij} - i(W_{yx}^{ij} - W_{xy}^{ij})], \tag{3.27}$$

$$G_2^{ij} \equiv -\frac{1}{2}[W_{xx}^{ij} - W_{yy}^{ij} - i(W_{yx}^{ij} - W_{xy}^{ij})]. \tag{3.28}$$

In general, having such site dependent coefficients complicates diagonalisation of the spin wave Hamiltonian significantly. In our case the periodicity of the ground state spin structure allows us to divide the lattice into a certain amount of sub-lattices where each sub-lattice contains equally oriented spins. We can then characterise a lattice site i instead by what sub-lattice r it belongs to and its position i' on that sub-lattice. The nearest neighbours j of this site in general live on different sub-lattices t, each with position j' on their

given sub-lattice. We therefore rewrite the sum over i and j as a sum over two sub-lattices r and t and the sites i' and j' in each of these sub-lattices

$$\begin{aligned}\mathcal{H}^{(2)} = s\sum_{\langle r,t\rangle}\sum_{\langle i',j'\rangle}\Big[&G_1^{i'j'rt\,*}a_{i',r}a^\dagger_{j',t} + G_1^{i'j'rt}a^\dagger_{i',r}a_{j',t}\\ &+ G_2^{i'j'rt}a_{i',r}a_{j',t} + G_2^{i'j'rt\,*}a^\dagger_{i',r}a^\dagger_{j',t} + W_{zz}^{i'j'rt}(a^\dagger_{i',r}a_{i',r} + a^\dagger_{j',t}a_{j',t})\Big].\end{aligned} \tag{3.29}$$

Eq. (3.29) is written in a very general way, but we will see that it simplifies a lot since the spin angles hidden in the coefficients only depend on the sub-lattice. We introduce the Fourier transformed boson operators on each sub-lattice $a_{\boldsymbol{q},r}$, $a^\dagger_{\boldsymbol{q},r}$ describing collective excitations with a wavevector $\boldsymbol{q}$

$$a_{i',r} = \frac{1}{\sqrt{N_r}}\sum_{\boldsymbol{q}} a_{\boldsymbol{q},r}e^{-i\boldsymbol{q}\cdot\boldsymbol{r}_{i'}}, \tag{3.30}$$

$$a^\dagger_{i',r} = \frac{1}{\sqrt{N_r}}\sum_{\boldsymbol{q}} a^\dagger_{\boldsymbol{q},r}e^{i\boldsymbol{q}\cdot\boldsymbol{r}_{i'}}, \tag{3.31}$$

where N_r is the number of sites on sub-lattice r. In our case all the sub-lattices contain the same amount of sites. Writing Eq. (3.29) in terms of these collective bosons rather than single site operators finally gives us

$$\begin{aligned}\mathcal{H}^{(2)} = s\sum_{\boldsymbol{q}}\sum_{\langle r,t\rangle}\Big[&\Gamma_1^{rt\,*}(\boldsymbol{q})\,a_{\boldsymbol{q},r}a^\dagger_{\boldsymbol{q},t} + \Gamma_1^{rt}(\boldsymbol{q})\,a^\dagger_{\boldsymbol{q},r}a_{\boldsymbol{q},t}\\ &+ \Gamma_2^{rs}(\boldsymbol{q})\,a_{-\boldsymbol{q},r}a_{\boldsymbol{q},t} + \Gamma_2^{rt\,*}(\boldsymbol{q})\,a^\dagger_{-\boldsymbol{q},r}a^\dagger_{\boldsymbol{q},t} + 2\zeta^{rt}\,a^\dagger_{\boldsymbol{q},r}a_{\boldsymbol{q},r}\Big].\end{aligned} \tag{3.32}$$

Note that we have defined new q-space coefficients

$$\Gamma_1^{rt}(\boldsymbol{q}) \equiv \sum_{j'} G_1^{rt}(\boldsymbol{d}_{rtj'})\,e^{-i\boldsymbol{q}\cdot\boldsymbol{d}_{rtj'}} \tag{3.33}$$

$$\Gamma_2^{rt}(\boldsymbol{q}) \equiv \sum_{j'} G_2^{rt}(\boldsymbol{d}_{rtj'})\,e^{-i\boldsymbol{q}\cdot\boldsymbol{d}_{rtj'}} \tag{3.34}$$

$$\zeta^{rs} \equiv \sum_{j'} W_{zz}^{rs}(\boldsymbol{d}_{rsj'}). \tag{3.35}$$

where $\{\boldsymbol{d}_{rtj'}\}$ is the set of vectors from a site on sub-lattice r to its nearest neighbours on sub-lattice t. Here the coefficients $G_1^{i'j'rt}$ and $G_2^{i'j'rt}$ have simplified since we look at a system where DMI is independent of lattice site the coefficients. They are written as as functions of $\boldsymbol{d}_{rtj'}$, reflecting the fact that the DMI vectors only depend on the orientation of the nearest neighbour vectors $\boldsymbol{d}_{rtj'}$. It now remains to diagonalise $\mathcal{H}^{(2)}$. There is some resemblance of this Hamiltonian to a Bogoliubov Hamiltonian, and it turns out that we can write it in the form of Eq. (2.20) by performing a few simple steps. We just swap $\boldsymbol{q}$ with $-\boldsymbol{q}$ for some of the indices and perform some commutations, giving us

$$\begin{aligned}\mathcal{H}^{(2)} = \sum_{\boldsymbol{q}}\sum_{\langle r,t\rangle}\Big[&\eta_{rt}(\boldsymbol{q})\,a^\dagger_{\boldsymbol{q},r}a_{\boldsymbol{q},t} + \nu_{rt}(\boldsymbol{q})\,a_{-\boldsymbol{q},r}a_{\boldsymbol{q},t}\\ &+ \nu^*_{rt}(-\boldsymbol{q})\,a^\dagger_{\boldsymbol{q},r}a^\dagger_{-\boldsymbol{q},t} + \eta^*_{rt}(-\boldsymbol{q})\,a_{-\boldsymbol{q},r}a^\dagger_{-\boldsymbol{q},t}\Big].\end{aligned} \tag{3.36}$$

Constant terms have been ignored seeing as they only shift the ground state energy by some amount. We write the expression $\mathcal{H}^{(2)} = \sum_{\boldsymbol{q}} \mathcal{H}^{(2)}_{\boldsymbol{q}}$ in the matrix form we used in Section 2.3

$$\mathcal{H}^{(2)}_{\boldsymbol{q}} = \boldsymbol{\alpha}^\dagger M \boldsymbol{\alpha} = \begin{bmatrix} \boldsymbol{a}^\dagger_{\boldsymbol{q}} & \boldsymbol{a}_{-\boldsymbol{q}} \end{bmatrix} \begin{bmatrix} \eta(\boldsymbol{q}) & \nu^*(-\boldsymbol{q}) \\ \nu(\boldsymbol{q}) & \eta^*(-\boldsymbol{q}) \end{bmatrix} \begin{bmatrix} \boldsymbol{a}_{\boldsymbol{q}} \\ \boldsymbol{a}^\dagger_{-\boldsymbol{q}} \end{bmatrix}, \tag{3.37}$$

where M is a block matrix constructed from four matrices $\eta(\boldsymbol{q})$, $\eta^*(-\boldsymbol{q})$, $\nu(\boldsymbol{q})$ and $\nu^*(-\boldsymbol{q})$; it is the grand-dynamical matrix from Eq. (2.23). The matrix blocks contain the elements

$$\eta_{rt}(\boldsymbol{q}) = s\,\Gamma^{rt}_1(\boldsymbol{q}) + s\sum_t \zeta^{rt}\delta_{r,t}, \tag{3.38}$$

$$\nu_{rs}(\boldsymbol{q}) = s\,\Gamma^{rt}_2(\boldsymbol{q}). \tag{3.39}$$

Using the diagonalisation scheme presented in Section 2.3 we can now find the Bogoliubov transformation T that diagonalises the Hamiltonian into a basis of long-lived magnons.

$$\mathcal{H}^{(2)}_{\boldsymbol{q}} = \boldsymbol{\mathcal{A}}^\dagger D \boldsymbol{\mathcal{A}}, \qquad \boldsymbol{\mathcal{A}} = T\boldsymbol{\alpha} \tag{3.40}$$

The spin wave Hamiltonian can thus be written

$$\mathcal{H}^{(2)} = \sum_{\boldsymbol{q}} \sum_{r=1}^{m} \left[\omega_r(\boldsymbol{q}) A^\dagger_{\boldsymbol{q},r} A_{\boldsymbol{q},r} + \omega_{r+m}(\boldsymbol{q}) A_{-\boldsymbol{q},r} A^\dagger_{-\boldsymbol{q},r} \right], \tag{3.41}$$

where m denotes how many sub-lattices our system is partitioned into, while $\omega_{r+m}(\boldsymbol{q})$ are spectrum bands for magnons with wavevector $-\boldsymbol{q}$. These are just equal to the positive momenta bands $\omega_r(\boldsymbol{q}) = \omega_{r+m}(-\boldsymbol{q})$, so that

$$\mathcal{H}^{(2)} = 2\sum_{\boldsymbol{q}} \sum_{r=1}^{m} \omega_r(\boldsymbol{q}) \left(A^\dagger_{\boldsymbol{q},r} A_{\boldsymbol{q},r} + \frac{1}{2} \right). \tag{3.42}$$

Our magnon spectrum therefore consists of m different bands, each representing a certain mixing of collective excitations on the m sub-lattices. Our system is however deceptively large, as the smallest possible spin spiral periodicity was 5 atoms but with two alternating "spin chains" it means we have at least $m = 10$ sub-lattices. Since we diagonalise a $2m \times 2m$ system a numerical treatment seems inevitable. We define the inverse transformation matrix to be

$$T^{-1} = \begin{bmatrix} U_{\boldsymbol{q}} & V_{-\boldsymbol{q}} \\ V^*_{\boldsymbol{q}} & U^*_{-\boldsymbol{q}} \end{bmatrix}, \tag{3.43}$$

the choice of notation motivated by the "textbook" u-v notation often used for simple cases of $m = 1$ Bogoliubov transformations. The decision of working with the inverse transformation T^{-1} rather than the transformation T itself is a deliberate choice, since T^{-1} is the matrix that is calculated in Colpa's diagonalisation scheme. Furthermore, since we are interested in replacing the specific sub-lattice excitations with the diagonalised operators using $\boldsymbol{\alpha} = T^{-1}\boldsymbol{\mathcal{A}}$ it becomes natural to only work with T^{-1}. The inverse transformation is written as the following linear combination

$$a_{\boldsymbol{q}r} = \sum_{i=1}^{m} \left(u_{\boldsymbol{q}ri} A_{\boldsymbol{q}i} + v_{\boldsymbol{q}ri} A^\dagger_{-\boldsymbol{q}i} \right), \tag{3.44}$$

$$a^{\dagger}_{-\boldsymbol{q}r} = \sum_{i=1}^{m} \left(v^{*}_{-\boldsymbol{q}ri} A_{\boldsymbol{q}i} + u^{*}_{-\boldsymbol{q}ri} A^{\dagger}_{-\boldsymbol{q}i} \right). \tag{3.45}$$

Indeed for $m = 1$ we find that the expressions do give the familiar u-v notation [15]. After calculating the different bands $\omega_r(\boldsymbol{q})$ numerically for certain wave vectors $\boldsymbol{q}$ along some high-symmetry directions we plot the resulting spectrum (shown in Figure 3.4) in the case of a spiral phase with a 6-atom period and $J = 10$ meV. There are therefore 12 different sub-lattices resulting in 12 different magnon bands. A few features of this spectrum should be highlighted; the particular choice of DMI vector placement in the model results in the 1st BZ for the magnons being rectangular rather than triangular (similar to the situation of [38]). Also the spectrum has a mass-gap for the excitation of magnons, and some of the bands become seemingly degenerate on the border of the magnon 1st BZ between the Y and S point.

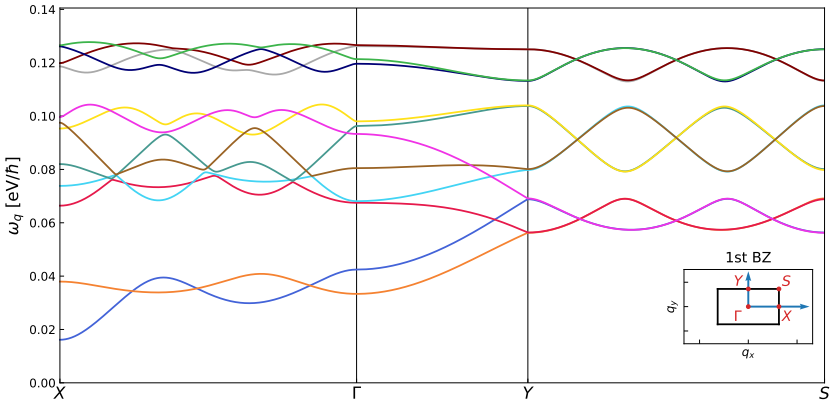

Figure 3.4: Magnon spectrum along a few high symmetry directions for a SPFMI of uniform rotation with a spin period of 6 atoms and isotropic exchange.

3.3 Exchange coupling in the bilayer interface

Let us remind ourselves what the idea of studying superconductivity in the interface of SPFMI / NM bilayer was; rather than a traditional phonon-mediated phenomenon the superconductivity should instead be mediated by magnons in the SPFMI. There must be some mechanism that allows for interactions between the localised electrons in the SPFMI layer and the free electrons in the NM layer in order to get this magnon mediated effect, and a natural idea is to extend the concept of exchange interactions from the magnetic layer by accounting for exchange interactions between the two layers [6]–[10]. Since we defined both the SPFMI and NM on triangular grid we have a one-to-one connection between sites in the two different layers. The exchange interaction between localised spins $\boldsymbol{S}_i$ in the

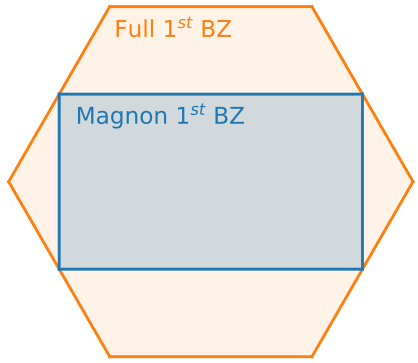

Figure 3.5: Comparison of the full 1st Brillouin Zone and the magnon 1st Brillouin Zone.

SPFMI and free electrons on the corresponding site in the NM is written

$$\mathcal{H}_{e-m} = -2\sum_i \bar{J}_i c_i^\dagger \boldsymbol{\tau} c_i \cdot \boldsymbol{S}_i. \tag{3.46}$$

For specific calculations in later sections we will consider the case where the exchange coupling $\bar{J}_i$ between materials is equal at every lattice site, a so-called fully compensated coupling. In general different sites could have different interaction strengths, making the coupling uncompensated to a certain extent. Having now defined all the necessary parts of our SPFMI / NM bilayer model we must choose the size of the different parameters. The parameters listed in Table 3.1 will be used for the rest of the thesis. As mentioned earlier it is important to note that the magnon 1st BZ is not the same as the full 1st BZ (see Figure 3.5), with sums over $\boldsymbol{q}$ and $\boldsymbol{k}$ understood to go over the former and latter BZ respectively.

Parameter	Size
t	1 eV
J	10 meV
$\bar{J}$	10 meV
s	1

Table 3.1: Chosen values for certain parameters which are used throughout the thesis.

Chapter 4

Magnon mediated electron-electron interaction

4.1 Electron-magnon coupling

We now take a closer look at the part of the Hamiltonian that couples the two materials.

$$\mathcal{H}_{e-m} = -2\sum_i \bar{J}_i c_i^\dagger \boldsymbol{\tau} c_i \cdot \boldsymbol{S}_i \tag{4.1}$$

Here we have introduced a notation with the spinors $c_i^\dagger = (c_{i\uparrow}^\dagger, c_{i\downarrow}^\dagger)$. Since the SPFMI part has a non-collinear magnetic structure we rewrite $\boldsymbol{S}_i$ as a rotation of a spin aligned along the z-axis in spin space. Like in the derivation of the magnon dispersion this is done in order to facilitate the introduction of spin fluctuation creation and destruction operators using the HP transformation, with the same rotation matrix (3.13).

$$\mathcal{H}_{e-m}^{(\Omega)} = -2\sum_{i\in\Omega} \bar{J}_\Omega c_i^\dagger \boldsymbol{\tau} c_i \cdot \left(U(\theta_\Omega, \psi_\Omega)^T \tilde{\boldsymbol{S}}_i\right) \tag{4.2}$$

Substituting the spin operators with bosonic creation/destruction operators and performing the dot product yields a somewhat lengthy expression

$$\begin{aligned}
\mathcal{H}_{e-m}^{(\Omega)} = &-2\sqrt{\frac{s}{2}}\bar{J}_\Omega \cos(\psi_\Omega) \sum_{i\in\Omega,\sigma} \left(a_{i,\Omega}(\cos(\theta_\Omega) - \sigma) c_{i\sigma}^\dagger c_{i,-\sigma} + \text{h.c}\right) \\
&+ 2\sqrt{\frac{s}{2}}\bar{J}_\Omega \sin(\theta_\Omega) \sum_{i\in\Omega,\sigma} \left(\sigma a_{i,\Omega} c_{i\sigma}^\dagger c_{i\sigma} + \text{h.c}\right) \\
&- 2\bar{J}_\Omega \cos(\theta_\Omega) \sum_{i\in\Omega,\sigma} \sigma(s - a_{i,\Omega}^\dagger a_{i,\Omega}) c_{i\sigma}^\dagger c_{i\sigma} \\
&- 2\bar{J}_\Omega \sin(\theta_\Omega)\cos(\psi_\Omega) \sum_{i\in\Omega,\sigma} (s - a_{i,\Omega}^\dagger a_{i,\Omega}) c_{i\sigma}^\dagger c_{i,-\sigma}.
\end{aligned} \tag{4.3}$$

The terms including two boson operators will henceforth be ignored. Since the separate Hamiltonians of both the FMI and NM are diagonalised in k-space it is reasonable to also analyse the bilayer system in k-space. Furthermore, since constraints on momenta are a central part of BCS theory, which will be the focus of the next chapter, it is natural to consider an analysis in k-space. Thus a Fourier transform of the interaction term is necessary, where the three-operator terms can then be rewritten using

$$\sum_{i\in\Omega} a_{\Omega,i} c^\dagger_{i\sigma} c_{i\sigma'} = \frac{\sqrt{N_\Omega}}{N} \sum_{\boldsymbol{k},\boldsymbol{q}} a_{\Omega,\boldsymbol{q}} c^\dagger_{\boldsymbol{k}+\boldsymbol{q},\sigma} c_{\boldsymbol{k},\sigma'}. \tag{4.4}$$

We have neglected umklapp processes since this is outside the scope of this thesis. Thus one obtains

$$\begin{aligned}\mathcal{H}^{(\Omega)}_{e-m} = &-2\sqrt{\frac{sN_\Omega}{2N^2}}\bar{J}_\Omega \cos(\psi_\Omega) \sum_{\boldsymbol{k},\boldsymbol{q},\sigma} \left(a_{\boldsymbol{q},\Omega}(\cos(\theta_\Omega) - \sigma) c^\dagger_{\boldsymbol{k}+\boldsymbol{q},\sigma} c_{\boldsymbol{k},-\sigma} + \text{h.c} \right) \\ &+ 2\sqrt{\frac{sN_\Omega}{2N^2}}\bar{J}_\Omega \sin(\theta_\Omega) \sum_{\boldsymbol{k},\boldsymbol{q},\sigma} \left(\sigma a_{\boldsymbol{q},\Omega} c^\dagger_{\boldsymbol{k}+\boldsymbol{q},\sigma} c_{\boldsymbol{k},\sigma} + \text{h.c} \right) \\ &- \frac{2\bar{J}_\Omega s N_\Omega}{N} \left(\cos(\theta_\Omega) \sum_{\boldsymbol{k},\sigma} \sigma c^\dagger_{\boldsymbol{k},\sigma} c_{\boldsymbol{k},\sigma} + \sin(\theta_\Omega)\cos(\psi_\Omega) \sum_{\boldsymbol{k},\sigma} c^\dagger_{\boldsymbol{k},\sigma} c_{\boldsymbol{k},-\sigma} \right).\end{aligned} \tag{4.5}$$

Note that $\sigma \in \{-1, 1\}$ labeling "spin up" and "spin down". A closer look at this expression is in order. In general there are terms coupling magnons both to electron spin flip processes and electron scattering without spin flip. Note that when we use the term "scattering without spin flip" it is in the context of a global spin space z-axis. A magnon must always have spin 1 as discussed in Section 2.1 and so there must be a spin flip along some axis of quantisation, however it does not have to be along the global z-axis. There are also some purely fermionic terms that correspond to a change in electronic properties of the NM. This includes the possibility of lifting the energy band degeneracy in the NM and changing the NM electron eigenstates. These terms may therefore be moved to the NM part of the Hamiltonian so that

$$\begin{aligned}\mathcal{H}_{\text{NM}} = &\sum_{\boldsymbol{k},\sigma} \left(\epsilon_{\boldsymbol{k}} + \mu - \frac{2s\sigma}{N} \sum_\Omega \bar{J}_\Omega N_\Omega \cos(\theta_\Omega) \right) c^\dagger_{\boldsymbol{k},\sigma} c_{\boldsymbol{k},\sigma} \\ &- \frac{2s}{N} \sum_{\boldsymbol{k},\sigma} \sum_\Omega \bar{J}_\Omega N_\Omega \sin(\theta_\Omega)\cos(\psi_\Omega) c^\dagger_{\boldsymbol{k},\sigma} c_{\boldsymbol{k},-\sigma}.\end{aligned} \tag{4.6}$$

One notices that the new terms in $\mathcal{H}_{\text{NM}}$ are non-zero if the net magnetisation is non-zero. In that case the fermionic operators must be re-diagonalised if the magnetisation is not aligned along the z-axis in spin space. However, the FMI structure we consider is a spiral with zero net magnetisation, and so it is readily seen that the new contributions to $\mathcal{H}_{\text{NM}}$ vanish. Thus there is no need for a re-diagonalisation of the creation/destruction operators

either. The electron-magnon interaction containing only coupling terms now reads

$$\mathcal{H}_{e-m}^{(\Omega)} = \sum_{\boldsymbol{k},\boldsymbol{q},\sigma} \left(g_1^{\Omega\sigma} a_{\boldsymbol{q},\Omega} c^\dagger_{\boldsymbol{k}+\boldsymbol{q},\sigma} c_{\boldsymbol{k},-\sigma} + g_2^{\Omega\sigma} a_{\boldsymbol{q},\Omega} c^\dagger_{\boldsymbol{k}+\boldsymbol{q},\sigma} c_{\boldsymbol{k},\sigma} + \text{h.c} \right), \tag{4.7}$$

where the magnon-electron coupling strengths for scattering with and without spin-flip are defined respectively as

$$g_1^{\Omega\sigma} = -2\sqrt{\frac{sN_\Omega}{2N^2}}\,\bar{J}_\Omega \cos(\psi_\Omega)(\cos(\theta_\Omega) - \sigma) \tag{4.8}$$

and

$$g_2^{\Omega\sigma} = 2\sqrt{\frac{sN_\Omega}{2N^2}}\,\bar{J}_\Omega \sigma \sin(\theta_\Omega). \tag{4.9}$$

So far the interactions are written in terms of magnetic excitations contained to each sublattice. These must be rewritten as combinations of the long-lived magnons in the FMI. We remind ourselves of the Bogoliubov transformation used to diagonalise the FMI Hamiltonian

$$a_{\boldsymbol{q}\Omega} = \sum_{\Gamma=1}^{m} \left(u_{\boldsymbol{q}\Omega\Gamma} A_{\boldsymbol{q}\Gamma} + v_{\boldsymbol{q}\Omega\Gamma} A^\dagger_{-\boldsymbol{q}\Gamma} \right), \tag{4.10}$$

$$a^\dagger_{-\boldsymbol{q}\Omega} = \sum_{\Gamma=1}^{m} \left(v^*_{-\boldsymbol{q}\Omega\Gamma} A_{\boldsymbol{q}\Gamma} + u^*_{-\boldsymbol{q}\Omega\Gamma} A^\dagger_{-\boldsymbol{q}\Gamma} \right). \tag{4.11}$$

It proves useful to also write this in matrix form:

$$\begin{bmatrix} \boldsymbol{a}_{\boldsymbol{q}} \\ \boldsymbol{a}^\dagger_{-\boldsymbol{q}} \end{bmatrix} = \underbrace{\begin{bmatrix} U_{\boldsymbol{q}} & V_{\boldsymbol{q}} \\ V^*_{-\boldsymbol{q}} & U^*_{-\boldsymbol{q}} \end{bmatrix}}_{T_{\boldsymbol{q}}^{-1}} \begin{bmatrix} \boldsymbol{A}_{\boldsymbol{q}} \\ \boldsymbol{A}^\dagger_{-\boldsymbol{q}} \end{bmatrix}. \tag{4.12}$$

The interaction term is therefore written

$$\mathcal{H}_{e-m}^{(\Omega)} = \sum_{\substack{\boldsymbol{k},\boldsymbol{q},\Gamma \\ \alpha,\alpha'}} \left(g_\Omega^{\alpha\alpha'} \left(u_{\boldsymbol{q}\Omega\Gamma} A_{\boldsymbol{q}\Gamma} + v_{\boldsymbol{q}\Omega\Gamma} A^\dagger_{-\boldsymbol{q}\Gamma} \right) c^\dagger_{\boldsymbol{k}+\boldsymbol{q},\alpha} c_{\boldsymbol{k},\alpha'} + \text{h.c} \right), \tag{4.13}$$

where we have made the notation more compact by introducing

$$g_\Omega^{\alpha\alpha'} = \begin{cases} g_1^{\Omega\alpha}, & \alpha = -\alpha' \\ g_2^{\Omega\alpha}, & \alpha = \alpha' \end{cases}. \tag{4.14}$$

Armed with an electron-magnon coupling written in terms of the diagonalised fermion operators and diagonalised boson operators we proceed with a derivation of the effective interaction.

4.2 Effective interaction

There are a few ways of deriving an effective interaction from the electron-magnon coupling in Eq. (4.7). Greens function treatments in either S-matrix perturbation theory or functional integral formalism are two possibilities [39]. These methods give some nice physical insight, but are somewhat cumbersome. Instead we take some inspiration from studies of magnetic impurities and use the Schrieffer-Wolff transformation that we discussed in Section 2.2, as this gives a somewhat simpler mathematical treatment and has been used in many previous studies of superconductivity at the interface of other bilayers or trilayers [6]–[9]. We write the total Hamiltonian as

$$\mathcal{H} = \mathcal{H}_0 + \eta\mathcal{H}_1, \tag{4.15}$$

where we have defined the interaction term as a perturbation to an uncoupled system

$$\mathcal{H}_0 = \mathcal{H}_{\text{NM}} + \mathcal{H}_{\text{FMI}}, \qquad \eta\mathcal{H}_1 = \mathcal{H}_{e-m}. \tag{4.16}$$

The task is first to find a suitable transformation that should have a similar form as Eq. (4.7). We make the following ansatz:

$$\eta\mathcal{S}^{(\Omega)} = \sum_{\substack{\boldsymbol{k},\boldsymbol{q},\Gamma \\ \alpha,\alpha'}} \left(g_{\Omega}^{\alpha\alpha'} \left(\mathcal{X}_{\boldsymbol{kq}\Gamma}^{\alpha\alpha'} u_{\boldsymbol{q}\Omega\Gamma} A_{\boldsymbol{q}\Gamma} + \mathcal{Y}_{\boldsymbol{kq}\Gamma}^{\alpha\alpha'} v_{\boldsymbol{q}\Omega\Gamma} A_{-\boldsymbol{q}\Gamma}^{\dagger} \right) c_{\boldsymbol{k}+\boldsymbol{q},\alpha}^{\dagger} c_{\boldsymbol{k},\alpha'} - \text{h.c} \right). \tag{4.17}$$

In order to find the coefficients $\mathcal{X}_{\boldsymbol{kq}\Gamma}^{\alpha\alpha'}$ and $\mathcal{Y}_{\boldsymbol{kq}\Gamma}^{\alpha\alpha'}$ we make use of a clever trick by introducing states $|n\rangle$ and $|m\rangle$ describing a single electron having some momentum and spin in the presence or absence of a Γ-mode magnon [40]. Thus we can use it to pick out individual terms of $\mathcal{H}_1$ in order to find the coefficient of the corresponding term in $\eta\mathcal{S}^{(\Omega)}$, using the following relation

$$\langle n| \eta\mathcal{H}_1 |m\rangle = \langle n| \left(\mathcal{H}_0\eta S - \eta S\mathcal{H}_0\right) |m\rangle . \tag{4.18}$$

The coefficients are found to be

$$\mathcal{X}_{\boldsymbol{kq}\Gamma}^{\alpha\alpha'} = \frac{1}{E_{\boldsymbol{k}+\boldsymbol{q},\alpha} - E_{\boldsymbol{k},\alpha'} - \omega_{\Gamma,\boldsymbol{q}}}, \qquad \mathcal{Y}_{\boldsymbol{kq}\Gamma}^{\alpha\alpha'} = \frac{1}{E_{\boldsymbol{k}+\boldsymbol{q},\alpha} - E_{\boldsymbol{k},\alpha'} + \omega_{\Gamma,\boldsymbol{q}}}. \tag{4.19}$$

Note that these are indeed the magnon propagators one would find in a Green's function treatment [18]. We repeat what the effective Hamiltonian looks like in the Schrieffer-Wolff transformation:

$$\mathcal{H}_{\text{Eff}} = \mathcal{H}_0 - \frac{1}{2} \sum_{\Omega,\Omega'} \left[\eta\mathcal{H}_1^{(\Omega)}, \eta\mathcal{S}^{(\Omega')} \right]. \tag{4.20}$$

We are specifically interested in the electron pair interaction term, which now reads

$$\mathcal{H}_{\text{Pair}} = -\frac{1}{2} \sum_{\Omega\Omega'\Gamma} \sum_{\boldsymbol{kk'q}} \sum_{\substack{\alpha\alpha' \\ \beta\beta'}} \sum_{j=1}^{8} \mathcal{H}_{\text{Pair}}^{(j)}. \tag{4.21}$$

In order to keep a somewhat readable notation we here have introduced $\mathcal{H}^{(j)}_{\text{Pair}}$ to denote the different operator structure terms

$$\mathcal{H}^{(1)}_{\text{Pair}} = \frac{g^{\alpha\alpha'}_{\Omega} g^{\beta\beta'}_{\Omega'} u_{\boldsymbol{q}\Omega\Gamma} v_{-\boldsymbol{q}\Omega'\Gamma}}{E_{\boldsymbol{k'}-\boldsymbol{q},\beta} - E_{\boldsymbol{k'},\beta'} + \omega_{\Gamma,\boldsymbol{q}}} \times c^{\dagger}_{\boldsymbol{k}+\boldsymbol{q},\alpha} c_{\boldsymbol{k},\alpha'} c^{\dagger}_{\boldsymbol{k'}-\boldsymbol{q},\beta} c_{\boldsymbol{k'},\beta'}, \tag{4.22}$$

$$\mathcal{H}^{(2)}_{\text{Pair}} = \frac{-g^{\alpha\alpha'}_{\Omega} g^{\beta\beta'}_{\Omega'} v_{\boldsymbol{q}\Omega\Gamma} u_{-\boldsymbol{q}\Omega'\Gamma}}{E_{\boldsymbol{k'}-\boldsymbol{q},\beta} - E_{\boldsymbol{k'},\beta'} - \omega_{\Gamma,\boldsymbol{q}}} \times c^{\dagger}_{\boldsymbol{k}+\boldsymbol{q},\alpha} c_{\boldsymbol{k},\alpha'} c^{\dagger}_{\boldsymbol{k'}-\boldsymbol{q},\beta} c_{\boldsymbol{k'},\beta'}, \tag{4.23}$$

$$\mathcal{H}^{(3)}_{\text{Pair}} = \frac{g^{\alpha\alpha'}_{\Omega} g^{\beta\beta'}_{\Omega'} u^{*}_{\boldsymbol{q}\Omega\Gamma} v^{*}_{-\boldsymbol{q}\Omega'\Gamma}}{E_{\boldsymbol{k'}-\boldsymbol{q},\beta} - E_{\boldsymbol{k'},\beta'} + \omega_{\Gamma,\boldsymbol{q}}} \times c^{\dagger}_{\boldsymbol{k},\alpha'} c_{\boldsymbol{k}+\boldsymbol{q},\alpha} c^{\dagger}_{\boldsymbol{k'},\beta'} c_{\boldsymbol{k'}-\boldsymbol{q},\beta}, \tag{4.24}$$

$$\mathcal{H}^{(4)}_{\text{Pair}} = \frac{-g^{\alpha\alpha'}_{\Omega} g^{\beta\beta'}_{\Omega'} v^{*}_{\boldsymbol{q}\Omega\Gamma} u^{*}_{-\boldsymbol{q}\Omega'\Gamma}}{E_{\boldsymbol{k'}-\boldsymbol{q},\beta} - E_{\boldsymbol{k'},\beta'} - \omega_{\Gamma,\boldsymbol{q}}} \times c^{\dagger}_{\boldsymbol{k},\alpha'} c_{\boldsymbol{k}+\boldsymbol{q},\alpha} c^{\dagger}_{\boldsymbol{k'},\beta'} c_{\boldsymbol{k'}-\boldsymbol{q},\beta}, \tag{4.25}$$

$$\mathcal{H}^{(5)}_{\text{Pair}} = \frac{-g^{\alpha\alpha'}_{\Omega} g^{\beta\beta'}_{\Omega'} u_{\boldsymbol{q}\Omega\Gamma} u^{*}_{\boldsymbol{q}\Omega'\Gamma}}{E_{\boldsymbol{k'}+\boldsymbol{q},\beta} - E_{\boldsymbol{k'},\beta'} - \omega_{\Gamma,\boldsymbol{q}}} \times c^{\dagger}_{\boldsymbol{k}+\boldsymbol{q},\alpha} c_{\boldsymbol{k},\alpha'} c^{\dagger}_{\boldsymbol{k'},\beta'} c_{\boldsymbol{k'}+\boldsymbol{q},\beta}, \tag{4.26}$$

$$\mathcal{H}^{(6)}_{\text{Pair}} = \frac{g^{\alpha\alpha'}_{\Omega} g^{\beta\beta'}_{\Omega'} v_{\boldsymbol{q}\Omega\Gamma} v^{*}_{\boldsymbol{q}\Omega'\Gamma}}{E_{\boldsymbol{k'}+\boldsymbol{q},\beta} - E_{\boldsymbol{k'},\beta'} + \omega_{\Gamma,\boldsymbol{q}}} \times c^{\dagger}_{\boldsymbol{k}+\boldsymbol{q},\alpha} c_{\boldsymbol{k},\alpha'} c^{\dagger}_{\boldsymbol{k'},\beta'} c_{\boldsymbol{k'}+\boldsymbol{q},\beta}, \tag{4.27}$$

$$\mathcal{H}^{(7)}_{\text{Pair}} = \frac{-g^{\alpha\alpha'}_{\Omega} g^{\beta\beta'}_{\Omega'} u^{*}_{\boldsymbol{q}\Omega\Gamma} u_{\boldsymbol{q}\Omega'\Gamma}}{E_{\boldsymbol{k'}+\boldsymbol{q},\beta} - E_{\boldsymbol{k'},\beta'} - \omega_{\Gamma,\boldsymbol{q}}} \times c^{\dagger}_{\boldsymbol{k},\alpha'} c_{\boldsymbol{k}+\boldsymbol{q},\alpha} c^{\dagger}_{\boldsymbol{k'}+\boldsymbol{q},\beta} c_{\boldsymbol{k'},\beta'}, \tag{4.28}$$

$$\mathcal{H}^{(8)}_{\text{Pair}} = \frac{g^{\alpha\alpha'}_{\Omega} g^{\beta\beta'}_{\Omega'} v^{*}_{\boldsymbol{q}\Omega\Gamma} v_{\boldsymbol{q}\Omega'\Gamma}}{E_{\boldsymbol{k'}+\boldsymbol{q},\beta} - E_{\boldsymbol{k'},\beta'} + \omega_{\Gamma,\boldsymbol{q}}} \times c^{\dagger}_{\boldsymbol{k},\alpha'} c_{\boldsymbol{k}+\boldsymbol{q},\alpha} c^{\dagger}_{\boldsymbol{k'}+\boldsymbol{q},\beta} c_{\boldsymbol{k'},\beta'}. \tag{4.29}$$

To simplify notation we will relabel these terms so that they all have the same fermion operator structure as Eqs. (4.22) and (4.23). For Eqs. (4.24) and (4.25) this means relabeling momenta $\boldsymbol{k} \to \boldsymbol{k} - \boldsymbol{q}$, $\boldsymbol{k'} \to \boldsymbol{k'} + \boldsymbol{q}$ and spins $\alpha \leftrightarrow \beta'$, $\beta \leftrightarrow \alpha'$, followed by swapping $\boldsymbol{k} \leftrightarrow \boldsymbol{k'}$ and anti-commuting the operators so that

$$\mathcal{H}^{(3)}_{\text{Pair}} \to \frac{g^{\beta'\beta}_{\Omega} g^{\alpha'\alpha}_{\Omega'} u^{*}_{\boldsymbol{q}\Omega\Gamma} v^{*}_{-\boldsymbol{q}\Omega'\Gamma}}{E_{\boldsymbol{k},\alpha'} - E_{\boldsymbol{k}+\boldsymbol{q},\alpha} + \omega_{\Gamma,\boldsymbol{q}}} \times c^{\dagger}_{\boldsymbol{k}+\boldsymbol{q},\alpha} c_{\boldsymbol{k},\alpha'} c^{\dagger}_{\boldsymbol{k'}-\boldsymbol{q},\beta} c_{\boldsymbol{k'},\beta'}, \tag{4.30}$$

$$\mathcal{H}^{(4)}_{\text{Pair}} \to \frac{-g^{\beta'\beta}_{\Omega} g^{\alpha'\alpha}_{\Omega'} v^{*}_{\boldsymbol{q}\Omega\Gamma} u^{*}_{-\boldsymbol{q}\Omega'\Gamma}}{E_{\boldsymbol{k},\alpha'} - E_{\boldsymbol{k}+\boldsymbol{q},\alpha} - \omega_{\Gamma,\boldsymbol{q}}} \times c^{\dagger}_{\boldsymbol{k}+\boldsymbol{q},\alpha} c_{\boldsymbol{k},\alpha'} c^{\dagger}_{\boldsymbol{k'}-\boldsymbol{q},\beta} c_{\boldsymbol{k'},\beta'}. \tag{4.31}$$

For Eqs. (4.26) and (4.27) we only need to relabel $\boldsymbol{k'} \to \boldsymbol{k'} - \boldsymbol{q}$ and $\beta \leftrightarrow \beta'$ to get

$$\mathcal{H}^{(5)}_{\text{Pair}} \to \frac{-g^{\alpha\alpha'}_{\Omega} g^{\beta'\beta}_{\Omega'} u_{\boldsymbol{q}\Omega\Gamma} u^{*}_{\boldsymbol{q}\Omega'\Gamma}}{E_{\boldsymbol{k'},\beta'} - E_{\boldsymbol{k'}-\boldsymbol{q},\beta} - \omega_{\Gamma,\boldsymbol{q}}} \times c^{\dagger}_{\boldsymbol{k}+\boldsymbol{q},\alpha} c_{\boldsymbol{k},\alpha'} c^{\dagger}_{\boldsymbol{k'}-\boldsymbol{q},\beta} c_{\boldsymbol{k'},\beta'}, \tag{4.32}$$

$$\mathcal{H}^{(6)}_{\text{Pair}} \to \frac{g^{\alpha\alpha'}_{\Omega} g^{\beta'\beta}_{\Omega'} v_{\boldsymbol{q}\Omega\Gamma} v^{*}_{\boldsymbol{q}\Omega'\Gamma}}{E_{\boldsymbol{k'},\beta'} - E_{\boldsymbol{k'}-\boldsymbol{q},\beta} + \omega_{\Gamma,\boldsymbol{q}}} \times c^{\dagger}_{\boldsymbol{k}+\boldsymbol{q},\alpha} c_{\boldsymbol{k},\alpha'} c^{\dagger}_{\boldsymbol{k'}-\boldsymbol{q},\beta} c_{\boldsymbol{k'},\beta'}. \tag{4.33}$$

For Eqs. (4.28) and (4.29) we must relabel $\boldsymbol{k} \to \boldsymbol{k} - \boldsymbol{q}$ and spins $\alpha \leftrightarrow \beta$, $\alpha' \leftrightarrow \beta'$, and subsequently perform the swaps $\beta \leftrightarrow \beta'$ and $\boldsymbol{k} \leftrightarrow \boldsymbol{k'}$. Again we anti-commute the

operators to get

$$\mathcal{H}^{(7)}_{\text{Pair}} \to \frac{-g^{\beta'\beta}_{\Omega} g^{\alpha\alpha'}_{\Omega'} u^{*}_{\boldsymbol{q}\Omega\Gamma} u_{\boldsymbol{q}\Omega'\Gamma}}{E_{\boldsymbol{k}+\boldsymbol{q},\alpha} - E_{\boldsymbol{k},\alpha'} - \omega_{\Gamma,\boldsymbol{q}}} \times c^{\dagger}_{\boldsymbol{k}+\boldsymbol{q},\alpha} c_{\boldsymbol{k},\alpha'} c^{\dagger}_{\boldsymbol{k'}-\boldsymbol{q},\beta} c_{\boldsymbol{k'},\beta'}, \tag{4.34}$$

$$\mathcal{H}^{(8)}_{\text{Pair}} \to \frac{g^{\beta'\beta}_{\Omega} g^{\alpha\alpha'}_{\Omega'} v^{*}_{\boldsymbol{q}\Omega\Gamma} v_{\boldsymbol{q}\Omega'\Gamma}}{E_{\boldsymbol{k}+\boldsymbol{q},\alpha} - E_{\boldsymbol{k},\alpha'} + \omega_{\Gamma,\boldsymbol{q}}} \times c^{\dagger}_{\boldsymbol{k}+\boldsymbol{q},\alpha} c_{\boldsymbol{k},\alpha'} c^{\dagger}_{\boldsymbol{k'}-\boldsymbol{q},\beta} c_{\boldsymbol{k'},\beta'}. \tag{4.35}$$

We can then rewrite

$$\begin{aligned}\mathcal{H}_{\text{Pair}} = \frac{1}{2} \sum_{\substack{\boldsymbol{k}\boldsymbol{k'}\boldsymbol{q} \\ \Gamma}} \sum_{\substack{\alpha\alpha' \\ \beta\beta'}} \Bigg[&\left(\frac{A_1(\boldsymbol{q},\Gamma,\alpha,\alpha',\beta,\beta')}{E_{\boldsymbol{k}+\boldsymbol{q},\alpha} - E_{\boldsymbol{k},\alpha'} - \omega_{\Gamma,\boldsymbol{q}}} - \frac{A_2(\boldsymbol{q},\Gamma,\alpha,\alpha',\beta,\beta')}{E_{\boldsymbol{k}+\boldsymbol{q},\alpha} - E_{\boldsymbol{k},\alpha'} + \omega_{\Gamma,\boldsymbol{q}}} \right) \\ &+ \left(\frac{B_1(\boldsymbol{q},\Gamma,\alpha,\alpha',\beta,\beta')}{E_{\boldsymbol{k'},\beta'} - E_{\boldsymbol{k'}-\boldsymbol{q},\beta} - \omega_{\Gamma,\boldsymbol{q}}} - \frac{B_2(\boldsymbol{q},\Gamma,\alpha,\alpha',\beta,\beta')}{E_{\boldsymbol{k'},\beta'} - E_{\boldsymbol{k'}-\boldsymbol{q},\beta} + \omega_{\Gamma,\boldsymbol{q}}} \right) \Bigg] \\ &\times c^{\dagger}_{\boldsymbol{k}+\boldsymbol{q},\alpha} c_{\boldsymbol{k},\alpha'} c^{\dagger}_{\boldsymbol{k'}-\boldsymbol{q},\beta} c_{\boldsymbol{k'},\beta'}.\end{aligned} \tag{4.36}$$

with

$$A_1(\boldsymbol{q},\Gamma,\alpha,\alpha',\beta,\beta') = \sum_{\Omega\Omega'} \left(g^{\beta'\beta}_{\Omega} g^{\alpha\alpha'}_{\Omega'} u^{*}_{\boldsymbol{q}\Omega\Gamma} u_{\boldsymbol{q}\Omega'\Gamma} + g^{\beta'\beta}_{\Omega} g^{\alpha'\alpha}_{\Omega'} u^{*}_{\boldsymbol{q}\Omega\Gamma} v^{*}_{-\boldsymbol{q}\Omega'\Gamma} \right), \tag{4.37}$$

$$A_2(\boldsymbol{q},\Gamma,\alpha,\alpha',\beta,\beta') = \sum_{\Omega\Omega'} \left(g^{\beta'\beta}_{\Omega} g^{\alpha\alpha'}_{\Omega'} v^{*}_{\boldsymbol{q}\Omega\Gamma} v_{\boldsymbol{q}\Omega'\Gamma} + g^{\beta'\beta}_{\Omega} g^{\alpha'\alpha}_{\Omega'} v^{*}_{\boldsymbol{q}\Omega\Gamma} u^{*}_{-\boldsymbol{q}\Omega'\Gamma} \right), \tag{4.38}$$

$$B_1(\boldsymbol{q},\Gamma,\alpha,\alpha',\beta,\beta') = \sum_{\Omega\Omega'} \left(g^{\alpha\alpha'}_{\Omega} g^{\beta'\beta}_{\Omega'} u_{\boldsymbol{q}\Omega\Gamma} u^{*}_{\boldsymbol{q}\Omega'\Gamma} + g^{\alpha\alpha'}_{\Omega} g^{\beta\beta'}_{\Omega'} u_{\boldsymbol{q}\Omega\Gamma} v_{-\boldsymbol{q}\Omega'\Gamma} \right), \tag{4.39}$$

$$B_2(\boldsymbol{q},\Gamma,\alpha,\alpha',\beta,\beta') = \sum_{\Omega\Omega'} \left(g^{\alpha\alpha'}_{\Omega} g^{\beta'\beta}_{\Omega'} v_{\boldsymbol{q}\Omega\Gamma} v^{*}_{\boldsymbol{q}\Omega'\Gamma} + g^{\alpha\alpha'}_{\Omega} g^{\beta\beta'}_{\Omega'} v_{\boldsymbol{q}\Omega\Gamma} u_{-\boldsymbol{q}\Omega'\Gamma} \right). \tag{4.40}$$

The entire prefactor in front of the fermion operators can be interpreted as a scattering matrix element $V^{\alpha\alpha'\beta\beta'}_{\boldsymbol{k}\boldsymbol{k'}\boldsymbol{q}}$ so that

$$\mathcal{H}_{\text{Pair}} = \sum_{\boldsymbol{k}\boldsymbol{k'}\boldsymbol{q}} \sum_{\substack{\alpha\alpha' \\ \beta\beta'}} V^{\alpha\alpha'\beta\beta'}_{\boldsymbol{k}\boldsymbol{k'}\boldsymbol{q}} c^{\dagger}_{\boldsymbol{k}+\boldsymbol{q},\alpha} c_{\boldsymbol{k},\alpha'} c^{\dagger}_{\boldsymbol{k'}-\boldsymbol{q},\beta} c_{\boldsymbol{k'},\beta'} \tag{4.41}$$

At this point it is prudent to take a closer look at the squeezing parameters that appear in the coefficients (4.37– 4.40), seeing as these will in general be complex numbers once we venture beyond the simplest examples of collinear FMIs and AFMIs. We know that the inverse Bogoliubov transformation $T^{-1}_{\boldsymbol{q}}$ with squeezing parameters as elements is not unique, as its columns are made up of eigenvectors that can each be multiplied by any phase $e^{i\theta}$. We must therefore be very careful to check that no such arbitrary chosen phases manifest themselves in our electron pair potential, seeing as we perform a numerical calculation of $T^{-1}_{\boldsymbol{q}}$ at each point $\boldsymbol{q}$ in the 1$^{\text{st}}$ BZ. Assume the Γ-th eigenvector $\boldsymbol{w}_{\Gamma}(\boldsymbol{q})$ (ie. the Γ-th column of $T^{-1}_{\boldsymbol{q}}$) is multiplied with the phase $e^{i\theta_{\Gamma}(\boldsymbol{q})}$. It is easy to see that the first term in each of Eqs. (4.37– 4.40) is the product of an element in $\boldsymbol{w}_{\Gamma}(\boldsymbol{q})$ and the complex conjugate of another element in the same eigenvector such that an arbitrary chosen phase

factor will cancel out. Indeed the same applies for the second term of each coefficient, however now it can be a bit harder to see. Taking a look at (4.12) we for instance see that $u_{\boldsymbol{q}\Omega\Gamma}$ and $v^*_{-\boldsymbol{q}\Omega'\Gamma}$ are elements of the same eigenvector $\boldsymbol{w}_\Gamma(\boldsymbol{q})$. Thus any arbitrary applied phase also cancels for the second term in (4.39), and likewise one can show that the same holds for the other three coefficients.

4.2.1 BCS pairing

We will focus on the BCS pairing mechanism, where one only considers opposite momenta scattering processes $\boldsymbol{k'} = -\boldsymbol{k}$. Inserting this relation into (4.36) we can get rid of the redundant momentum variable by relabeling $\boldsymbol{k} + \boldsymbol{q} \to \boldsymbol{k}$ and $\boldsymbol{k} \to \boldsymbol{k'}$. We then have

$$\mathcal{H}_{\text{BCS}} = \sum_{\boldsymbol{k}\boldsymbol{k'}} \sum_{\substack{\alpha\alpha' \\ \beta\beta'}} V^{\alpha\beta\beta'\alpha'}_{\boldsymbol{k}\boldsymbol{k'}} c^\dagger_{\boldsymbol{k},\alpha} c^\dagger_{-\boldsymbol{k},\beta} c_{-\boldsymbol{k'},\beta'} c_{\boldsymbol{k'},\alpha'}, \tag{4.42}$$

with

$$\begin{aligned} V^{\alpha\beta\beta'\alpha'}_{\boldsymbol{k}\boldsymbol{k'}} = \frac{1}{2} \sum_\Gamma \Bigg[&\left(\frac{A_1(\boldsymbol{k}-\boldsymbol{k'},\Gamma,\alpha,\alpha',\beta,\beta')}{E_{\boldsymbol{k},\alpha} - E_{\boldsymbol{k'},\alpha'} - \omega_{\Gamma,\boldsymbol{k}-\boldsymbol{k'}}} - \frac{A_2(\boldsymbol{k}-\boldsymbol{k'},\Gamma,\alpha,\alpha',\beta,\beta')}{E_{\boldsymbol{k},\alpha} - E_{\boldsymbol{k'},\alpha'} + \omega_{\Gamma,\boldsymbol{k}-\boldsymbol{k'}}} \right) \\ &+ \left(\frac{B_1(\boldsymbol{k}-\boldsymbol{k'},\Gamma,\alpha,\alpha',\beta,\beta')}{E_{-\boldsymbol{k'},\beta'} - E_{-\boldsymbol{k},\beta} - \omega_{\Gamma,\boldsymbol{k}-\boldsymbol{k'}}} - \frac{B_2(\boldsymbol{k}-\boldsymbol{k'},\Gamma,\alpha,\alpha',\beta,\beta')}{E_{-\boldsymbol{k'},\beta'} - E_{-\boldsymbol{k},\beta} + \omega_{\Gamma,\boldsymbol{k}-\boldsymbol{k'}}} \right) \Bigg]. \end{aligned} \tag{4.43}$$

We note that in our case we have an electron dispersion relation that is even in $\boldsymbol{k}$ so that $E_{\boldsymbol{k},\alpha} = E_{-\boldsymbol{k},\alpha}$, and since the net magnetisation of the FMI spin structure is zero the dispersion relation $E_{\boldsymbol{k},\alpha} = E_{\boldsymbol{k}}$ is also independent of spin. Thus the pair scattering matrix simplifies further into

$$\begin{aligned} V^{\alpha\beta\beta'\alpha'}_{\boldsymbol{k}\boldsymbol{k'}} = \frac{1}{2} \sum_\Gamma \Bigg(&\frac{A_1(\boldsymbol{k}-\boldsymbol{k'},\Gamma,\alpha,\alpha',\beta,\beta') + B_2(\boldsymbol{k}-\boldsymbol{k'},\Gamma,\alpha,\alpha',\beta,\beta')}{E_{\boldsymbol{k}} - E_{\boldsymbol{k'}} - \omega_{\Gamma,\boldsymbol{k}-\boldsymbol{k'}}} \\ &- \frac{A_2(\boldsymbol{k}-\boldsymbol{k'},\Gamma,\alpha,\alpha',\beta,\beta') + B_1(\boldsymbol{k}-\boldsymbol{k'},\Gamma,\alpha,\alpha',\beta,\beta')}{E_{\boldsymbol{k}} - E_{\boldsymbol{k'}} + \omega_{\Gamma,\boldsymbol{k}-\boldsymbol{k'}}} \Bigg), \end{aligned} \tag{4.44}$$

which in turn can be written in a similar form to the canonical BCS potential multiplied by the factor $A(\boldsymbol{k}-\boldsymbol{k'},\Gamma,\alpha,\alpha',\beta,\beta')$, and with the inclusion of an additional term.

$$\begin{aligned} V^{\alpha\beta\beta'\alpha'}_{\boldsymbol{k}\boldsymbol{k'}} = \frac{1}{2} \sum_\Gamma \Bigg(&\frac{\omega_{\Gamma,\boldsymbol{k}-\boldsymbol{k'}}}{(E_{\boldsymbol{k}} - E_{\boldsymbol{k'}})^2 - \omega^2_{\Gamma,\boldsymbol{k}-\boldsymbol{k'}}} A(\boldsymbol{k}-\boldsymbol{k'},\Gamma,\alpha,\alpha',\beta,\beta') \\ &+ \frac{E_{\boldsymbol{k}} - E_{\boldsymbol{k'}}}{(E_{\boldsymbol{k}} - E_{\boldsymbol{k'}})^2 - \omega^2_{\Gamma,\boldsymbol{k}-\boldsymbol{k'}}} B(\boldsymbol{k}-\boldsymbol{k'},\Gamma,\alpha,\alpha',\beta,\beta') \Bigg). \end{aligned} \tag{4.45}$$

Here we have defined the coefficients

$$\begin{aligned} A(\boldsymbol{k}-\boldsymbol{k'},\Gamma,\alpha,\alpha',\beta,\beta') = &A_1(\boldsymbol{k}-\boldsymbol{k'},\Gamma,\alpha,\alpha',\beta,\beta') + B_2(\boldsymbol{k}-\boldsymbol{k'},\Gamma,\alpha,\alpha',\beta,\beta') \\ &+ A_2(\boldsymbol{k}-\boldsymbol{k'},\Gamma,\alpha,\alpha',\beta,\beta') + B_1(\boldsymbol{k}-\boldsymbol{k'},\Gamma,\alpha,\alpha',\beta,\beta'). \end{aligned} \tag{4.46}$$

$$B(\boldsymbol{k}-\boldsymbol{k'},\Gamma,\alpha,\alpha',\beta,\beta') = A_1(\boldsymbol{k}-\boldsymbol{k'},\Gamma,\alpha,\alpha',\beta,\beta') + B_2(\boldsymbol{k}-\boldsymbol{k'},\Gamma,\alpha,\alpha',\beta,\beta') - A_2(\boldsymbol{k}-\boldsymbol{k'},\Gamma,\alpha,\alpha',\beta,\beta') - B_1(\boldsymbol{k}-\boldsymbol{k'},\Gamma,\alpha,\alpha',\beta,\beta'). \tag{4.47}$$

We have until now not made any assumptions about the arrangement of spin indices in the pair scattering matrix. From a physical point of view we must however have a conservation of spin, which rules out any scattering matrix elements with an odd number of "spin up" and "spin down" indices. Therefore the pair scattering matrix can only be non-zero if either all indices are the same, or if half of the indices are "spin up" and the other half are "spin down". We separate the Hamiltonian into a part contributing to unpolarised ($S_z = 0$) and polarised ($S_z = \pm 1$) Cooper pairs respectively

$$\mathcal{H}_{\text{BCS}}^{\text{unpol}} = \sum_{\boldsymbol{k}\boldsymbol{k'}} \tilde{V}_{\boldsymbol{k}\boldsymbol{k'}} c^\dagger_{\boldsymbol{k},\downarrow} c^\dagger_{-\boldsymbol{k},\uparrow} c_{-\boldsymbol{k'},\uparrow} c_{\boldsymbol{k'},\downarrow}, \tag{4.48}$$

$$\begin{aligned}\mathcal{H}_{\text{BCS}}^{\text{pol}} = \sum_{\boldsymbol{k}\boldsymbol{k'}} \Big(& V^{\uparrow\uparrow\uparrow\uparrow}_{\boldsymbol{k}\boldsymbol{k'}} c^\dagger_{\boldsymbol{k},\uparrow} c^\dagger_{-\boldsymbol{k},\uparrow} c_{-\boldsymbol{k'},\uparrow} c_{\boldsymbol{k'},\uparrow} + V^{\downarrow\downarrow\downarrow\downarrow}_{\boldsymbol{k}\boldsymbol{k'}} c^\dagger_{\boldsymbol{k},\downarrow} c^\dagger_{-\boldsymbol{k},\downarrow} c_{-\boldsymbol{k'},\downarrow} c_{\boldsymbol{k'},\downarrow} \\ & + V^{\uparrow\uparrow\downarrow\downarrow}_{\boldsymbol{k}\boldsymbol{k'}} c^\dagger_{\boldsymbol{k},\uparrow} c^\dagger_{-\boldsymbol{k},\uparrow} c_{-\boldsymbol{k'},\downarrow} c_{\boldsymbol{k'},\downarrow} + V^{\downarrow\downarrow\uparrow\uparrow}_{\boldsymbol{k}\boldsymbol{k'}} c^\dagger_{\boldsymbol{k},\downarrow} c^\dagger_{-\boldsymbol{k},\downarrow} c_{-\boldsymbol{k'},\uparrow} c_{\boldsymbol{k'},\uparrow} \Big).\end{aligned} \tag{4.49}$$

Note that we have used the fermionic anti-commutation property in order to gather the different unpolarised Cooper pair terms into a single term of the same operator structure as the conventional phonon-mediated BCS theory, where

$$\tilde{V}_{\boldsymbol{k}\boldsymbol{k'}} = V^{\downarrow\uparrow\uparrow\downarrow}_{\boldsymbol{k},\boldsymbol{k'}} + V^{\uparrow\downarrow\downarrow\uparrow}_{-\boldsymbol{k},-\boldsymbol{k'}} - V^{\uparrow\downarrow\uparrow\downarrow}_{-\boldsymbol{k},\boldsymbol{k'}} - V^{\downarrow\uparrow\downarrow\uparrow}_{\boldsymbol{k},-\boldsymbol{k'}}. \tag{4.50}$$

Now is a good time to take a step back and reflect on what has been found, for unlike many of the previous studies of magnon mediated superconductivity in bilayers or trilayers with collinear FMIs and AFMIs, we now have terms in our Hamiltonian that could give rise to the polarised spin triplet states $|\uparrow\uparrow\rangle$ and $|\downarrow\downarrow\rangle$. It is reasonable to assume that this is a feature of the non-collinear spin structure that we study here, explained by the fact that the electron-electron interaction is mediated by a nearest neighbour exchange between two lattice sites of different magnetisation in the SPFMI layer. Non-collinear spin structures have already been suggested to enable spin polarised Cooper pairs in other types of superconducting systems [4]. One could picture the electron-electron scattering as two Stern-Gerlach like measurements, where the act of an electron spin flip is akin to a "measurement" of the spin direction. If the incoming electrons scatter at sites with magnetisation directions of (θ_1, ψ_1) and (θ_2, ψ_2), then the resulting spin states after the scattering will be measured to be

$$|\varphi_1\rangle = \cos(\theta_1/2)\,|\downarrow\rangle + e^{i\psi_1}\sin(\theta_1/2)\,|\uparrow\rangle\,, \tag{4.51}$$

$$|\varphi_2\rangle = \cos(\theta_2/2)\,|\downarrow\rangle + e^{i\psi_2}\sin(\theta_2/2)\,|\uparrow\rangle\,. \tag{4.52}$$

Thus there is a possibility for mixing states with different combinations of $|\uparrow\downarrow\rangle$, $|\uparrow\uparrow\rangle$ and $|\downarrow\downarrow\rangle$, and so one could indeed get polarised triplet states. This is a result of scattering on the SPFMI spin structure essentially rotating the spins.

4.3 Collinear AFMI potential

As a way to check the result derived in the previous section we consider the simple example of a collinear AFMI on a square lattice, which is described by a bipartite lattice with Néel ordering. The motivation behind looking at such a system is that the magnonic properties have well known analytical solutions. We label the two sub-lattices $\Omega \in \{A, B\}$ and choose the z-axis as the axis of quantisation. There are equally many sites in the two sub-lattices such that we may write $N_A = N_B = N/2$. The sub-lattice angles are then given by $(\theta_A, \psi_A) = (0, 0)$ and $(\theta_B, \psi_B) = (\pi, \pi)$, with the result that all terms with the factor $\sin(\theta_\Omega)$ are zero. Thus from Eqs. (4.8) and (4.9) we immediately see that

$$g_1^{A\downarrow} = -2\sqrt{\frac{s}{N}}\bar{J}_A, \qquad g_1^{B\uparrow} = -2\sqrt{\frac{s}{N}}\bar{J}_B, \qquad g_1^{A\uparrow} = g_1^{B\downarrow} = 0, \tag{4.53}$$

and

$$g_2^{A\downarrow} = g_2^{A\uparrow} = g_2^{B\downarrow} = g_2^{B\uparrow} = 0. \tag{4.54}$$

As a result of Eqn. (4.54) all terms where $\alpha = \alpha'$ and/or $\beta = \beta'$ vanish:

$$V_{\boldsymbol{k}\boldsymbol{k}'}^{\uparrow\uparrow\uparrow\uparrow} = V_{\boldsymbol{k}\boldsymbol{k}'}^{\downarrow\downarrow\downarrow\downarrow} = V_{\boldsymbol{k}\boldsymbol{k}'}^{\downarrow\uparrow\uparrow\downarrow} = V_{\boldsymbol{k}\boldsymbol{k}'}^{\uparrow\downarrow\downarrow\uparrow} = 0. \tag{4.55}$$

Having ruled out half of the terms we must look at the factors (4.46) and (4.47) for the other terms. We note that the magnon dispersion relations for the collinear AFMI are degenerate ($\omega_A = \omega_B$) and isotropic ($\omega_{\boldsymbol{q}} = \omega_{-\boldsymbol{q}}$). The inverse Bogoliubov transformation for the AFMI is

$$a_{\boldsymbol{q}} = u_{\boldsymbol{q}} A_{\boldsymbol{q}} + v_{\boldsymbol{q}} B_{-\boldsymbol{q}}^\dagger, \qquad b_{\boldsymbol{q}} = u_{\boldsymbol{q}} B_{\boldsymbol{q}} + v_{\boldsymbol{q}} A_{-\boldsymbol{q}}^\dagger. \tag{4.56}$$

Here the squeezing parameters $u_{\boldsymbol{q}}$ and $v_{\boldsymbol{q}}$ are real numbers that are even in $\boldsymbol{q}$. In matrix form with the more generalised boson operator basis, the inverse Bogoliuabov transformation reads

$$T_{\boldsymbol{q}}^{-1} = \begin{bmatrix} u_{\boldsymbol{q}} & 0 & 0 & v_{\boldsymbol{q}} \\ 0 & u_{\boldsymbol{q}} & v_{\boldsymbol{q}} & 0 \\ 0 & v_{\boldsymbol{q}} & u_{\boldsymbol{q}} & 0 \\ v_{\boldsymbol{q}} & 0 & 0 & u_{\boldsymbol{q}} \end{bmatrix}. \tag{4.57}$$

As a result the only non-zero enhancement factors in the pair scattering matrix are

$$A_1(\boldsymbol{q}, B, \uparrow, \downarrow, \downarrow, \uparrow) = B_1(\boldsymbol{q}, B, \uparrow, \downarrow, \downarrow, \uparrow) = g_1^{B\uparrow} g_1^{B\uparrow} u_{\boldsymbol{q}}^2 + g_1^{B\uparrow} g_1^{A\downarrow} u_{\boldsymbol{q}} v_{\boldsymbol{q}}, \tag{4.58}$$

$$A_2(\boldsymbol{q}, A, \uparrow, \downarrow, \downarrow, \uparrow) = B_2(\boldsymbol{q}, A, \uparrow, \downarrow, \downarrow, \uparrow) = g_1^{B\uparrow} g_1^{B\uparrow} v_{\boldsymbol{q}}^2 + g_1^{B\uparrow} g_1^{A\downarrow} v_{\boldsymbol{q}} u_{\boldsymbol{q}}, \tag{4.59}$$

$$A_1(\boldsymbol{q}, A, \downarrow, \uparrow, \uparrow, \downarrow) = B_1(\boldsymbol{q}, A, \downarrow, \uparrow, \uparrow, \downarrow) = g_1^{A\downarrow} g_1^{A\downarrow} u_{\boldsymbol{q}}^2 + g_1^{A\downarrow} g_1^{B\uparrow} u_{\boldsymbol{q}} v_{\boldsymbol{q}}, \tag{4.60}$$

$$A_2(\boldsymbol{q}, B, \downarrow, \uparrow, \uparrow, \downarrow) = B_2(\boldsymbol{q}, B, \downarrow, \uparrow, \uparrow, \downarrow) = g_1^{A\downarrow} g_1^{A\downarrow} v_{\boldsymbol{q}}^2 + g_1^{A\downarrow} g_1^{B\uparrow} v_{\boldsymbol{q}} u_{\boldsymbol{q}}. \tag{4.61}$$

The fact that the magnon dispersion relations are degenerate means that the two non-zero pair scattering matrix elements can be written

$$V_{\boldsymbol{k}\boldsymbol{k}'}^{\uparrow\downarrow\uparrow\downarrow} = \frac{1}{2} \frac{\omega_{\boldsymbol{k}-\boldsymbol{k}'}}{(E_{\boldsymbol{k}} - E_{\boldsymbol{k}'})^2 - \omega_{\boldsymbol{k}-\boldsymbol{k}'}^2} \sum_\Gamma A(\boldsymbol{k} - \boldsymbol{k}', \Gamma, \uparrow, \downarrow, \downarrow, \uparrow), \tag{4.62}$$

$$V^{\downarrow\uparrow\downarrow\uparrow}_{\boldsymbol{k}\boldsymbol{k}'} = \frac{1}{2}\frac{\omega_{\boldsymbol{k}-\boldsymbol{k}'}}{(E_{\boldsymbol{k}}-E_{\boldsymbol{k}'})^2-\omega^2_{\boldsymbol{k}-\boldsymbol{k}'}}\sum_{\Gamma} A(\boldsymbol{k}-\boldsymbol{k}',\Gamma,\downarrow,\uparrow,\uparrow,\downarrow). \tag{4.63}$$

We define $\bar{J}_B = \bar{J}$ and $\bar{J}_A = C\bar{J}$ where the parameter C determines the relative difference of coupling strength to the NM for the two different sub-lattices. The pair scattering part of the AFMI BCS Hamiltonian is

$$\mathcal{H}^{\text{AFMI}}_{\text{BCS}} = \sum_{\boldsymbol{k}\boldsymbol{k}'} \tilde{V}_{\boldsymbol{k}\boldsymbol{k}'} c^{\dagger}_{\boldsymbol{k},\downarrow} c^{\dagger}_{-\boldsymbol{k},\uparrow} c_{-\boldsymbol{k}',\uparrow} c_{\boldsymbol{k}',\downarrow}, \tag{4.64}$$

where

$$\tilde{V}_{\boldsymbol{k}\boldsymbol{k}'} = -\left(V^{\uparrow\downarrow\uparrow\downarrow}_{-\boldsymbol{k},\boldsymbol{k}'} + V^{\downarrow\uparrow\downarrow\uparrow}_{\boldsymbol{k},-\boldsymbol{k}'}\right) = -\frac{2s\bar{J}^2}{N}\frac{\omega_{\boldsymbol{k}+\boldsymbol{k}'}}{(E_{\boldsymbol{k}}-E_{\boldsymbol{k}'})^2-\omega^2_{\boldsymbol{k}+\boldsymbol{k}'}}\tilde{A}(\boldsymbol{k}-\boldsymbol{k}',C), \tag{4.65}$$

and

$$\begin{aligned}\tilde{A}(\boldsymbol{k}-\boldsymbol{k}',C) &= \sum_{\Gamma}\left(A(\boldsymbol{k}-\boldsymbol{k}',\Gamma,\uparrow,\downarrow,\downarrow,\uparrow)+A(\boldsymbol{k}-\boldsymbol{k}',\Gamma,\downarrow,\uparrow,\uparrow,\downarrow)\right)\\ &= 2(1+C^2)(u^2_{\boldsymbol{q}}+v^2_{\boldsymbol{q}})+8Cu_{\boldsymbol{q}}v_{\boldsymbol{q}}.\end{aligned} \tag{4.66}$$

This result is in exact agreement with the findings of [8] for the BCS potential of an AFMI / NM bilayer.

4.4 Investigating the pair potential: Numerical analysis

We now find ourselves at an impasse for analytical calculations regarding the pair potential, seeing as it contains magnon variables that must be treated numerically as discussed previously. Thus in order to calculate any results for the system we must again turn to numerical methods. We are for instance interested in knowing what the pair scattering potential actually looks like and how its enhancement factor compares to the FMI and AFMI bilayers. To get an idea of what the BCS potential may look like in the case of a SPFMI / NM bilayer we choose a spiral period of 6 and a certain incoming wavevector $\boldsymbol{k}$ on the Fermi surface (for a sufficiently low filling so that the Fermi surface is approximately a circle of radius $k_F = a^{-1}$). We then calculate the potential around the Fermi surface and additionally for a few different high-symmetry directions. The results are displayed in Figures 4.1 and 4.2.

We observe that for an unpolarised interaction $\tilde{V}_{\boldsymbol{k}\boldsymbol{k}'}$ is repulsive on the Fermi surface. It is important to note that a positive valued (repulsive) $\tilde{V}_{\boldsymbol{k}\boldsymbol{k}'}$ does not necessarily rule out superconductivity. Even if all the scattering matrix elements are positive, as long as it has an odd part in $\boldsymbol{k}$ we can have superconductivity from triplet Cooper pairs. However one would in this case expect singlet Cooper pair superconductivity to be suppressed. Along the high-symmetry cuts of the BZ we see that there is only a thin strip surrounding the Fermi surface that actually contributes non-zero values to the pair scattering matrix. The width of this strip is determined by the highest frequency in the magnon band structure; each mode gives rise to a singularity in the potential where the energy and momentum difference of the incoming and outgoing electron matches the corresponding magnon energy

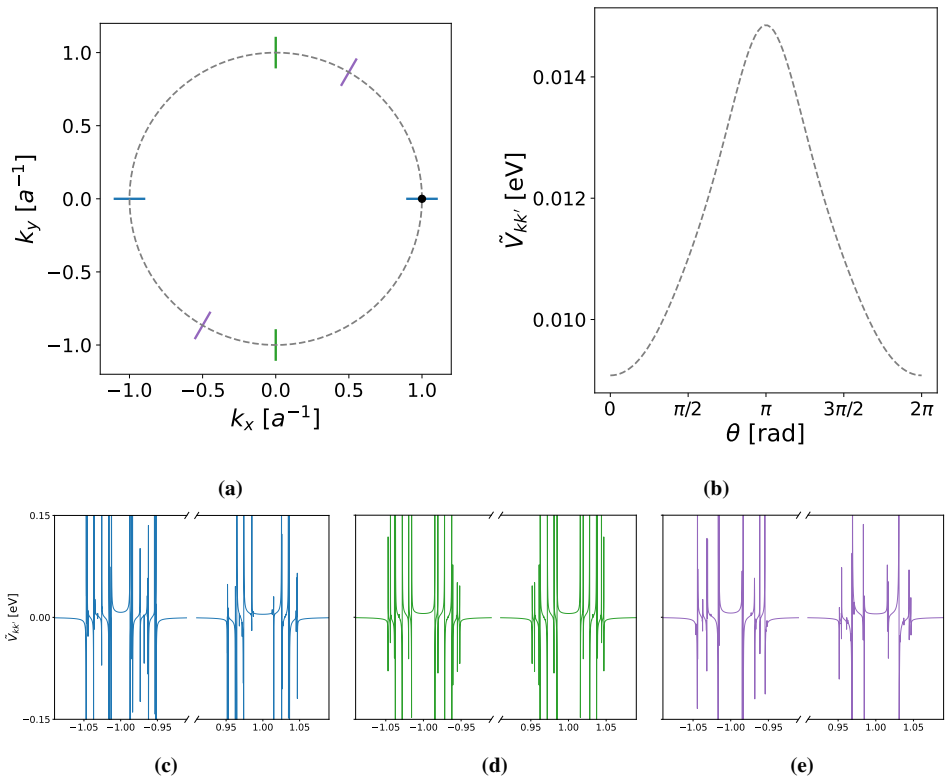

Figure 4.1: Illustrations of the pair scattering potential for an electron with incoming wavevector $\boldsymbol{k} = [1, 0]$. Figure a) shows the incoming wavevector (black dot) and the four different cuts where the pair potential is analysed (figures b-e)). Figure b) shows $\tilde{V}_{\boldsymbol{k}\boldsymbol{k}'}$ for outgoing wavevectors $\boldsymbol{k}'$ on the Fermi surface (a circle with $k_F = a^{-1}$). Figures c-e) show $\tilde{V}_{\boldsymbol{k}\boldsymbol{k}'}$ for outgoing wavevectors $\boldsymbol{k}'$ in three different high-symmetry directions.

and momentum. Since we have quite a lot of magnon modes the potential becomes quite messy around the Fermi surface, however since our magnon spectrum in this case has a small mass gap there is a thin interval surrounding the Fermi surface where there will be no singularities, defined in this case by the smallest energy in the magnon spectrum.

Next we take a look at the BCS potential enhancement factors that we defined in Eqs. (4.46) and (4.47). Since these coefficients are dependent on the magnon mode we must also take the magnon dispersion part of the BCS potential into account, which for the collinear FMI and AFMI cases is unnecessary as the magnon bands in both those cases are degenerate. For a comparison of the different systems we therefore find the enhancement factors multiplied by the magnon dispersion since the electron-magnon energy difference in the denominator of Eq. (4.45) should be regarded to have the same form for all modes close to the allowed energies (given by the propagator singularities). We plot these BCS potential enhancement factors along some high-symmetry directions to get an idea of their magnitude in the NM / SPFMI bilayer, in addition to see what modes contribute at different

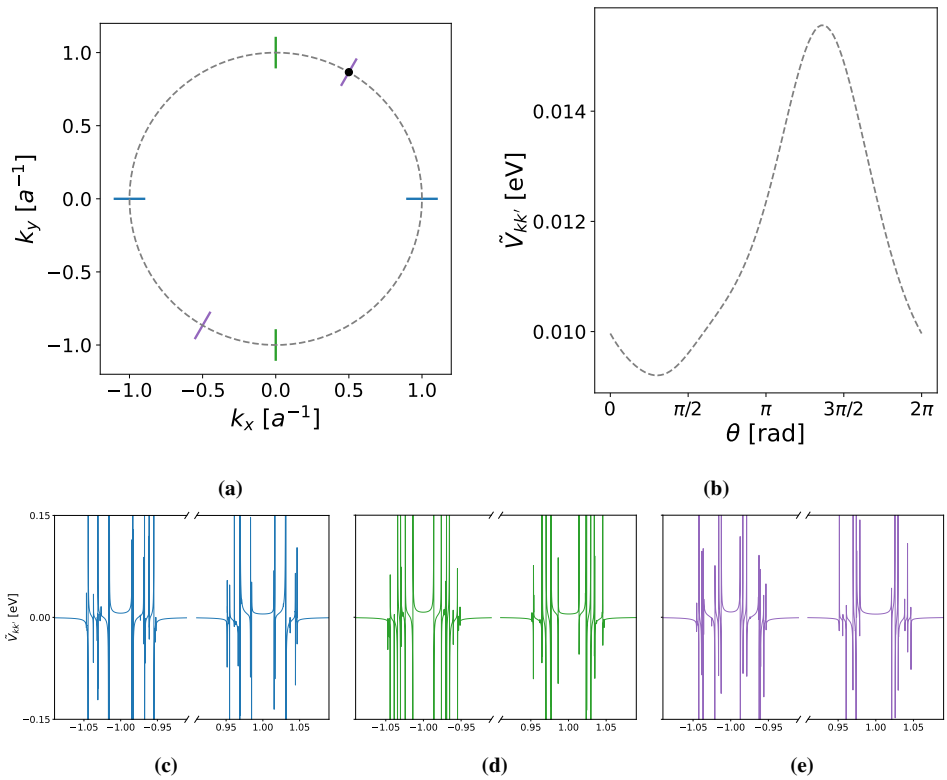

Figure 4.2: Illustrations of the pair scattering potential for an electron with incoming wavevector $\boldsymbol{k} = [1/2, \sqrt{3}/2]$. Figure a) shows the incoming wavevector (black dot) and the four different cuts where the pair potential is analysed (figures b-e)). Figure b) shows $\tilde{V}_{\boldsymbol{kk'}}$ for outgoing wavevectors $\boldsymbol{k'}$ on the Fermi surface (a circle with $k_F = a^{-1}$). Figures c-e) show $\tilde{V}_{\boldsymbol{kk'}}$ for outgoing wavevectors $\boldsymbol{k'}$ in three different high-symmetry directions.

magnon momenta. It turns out that the contributions from the factors (4.47) vanish, and so we are left with a potential that indeed does have the canonical BCS form, at least for the magnetic spiral structures considered in this thesis. As for the factors (4.46), values for different magnon momenta are shown in Figures 4.3, 4.4, 4.5 and 4.6. It is interesting to note how the sum of all the different mode contributions seems to be a very well-behaved function of the magnon momentum, even as many different modes appear and disappear when the momentum varies. The type of switching between modes could be related to a crossing of the two different mode bands, and these transitions have a surprising likeness to q-dependent phonon factors in a Master's thesis by Lockert (see Figure 6.4 in [41]). Another interesting observation is the fact that only one mode seems to contribute along the path between the points Γ and Y in the case of scattering without spin flip. Note that even though some modes seem to have discontinuous contributions this is not the case, as one will see by just "zooming" close enough in. The contributions do however appear to not be smooth at the Y-point.

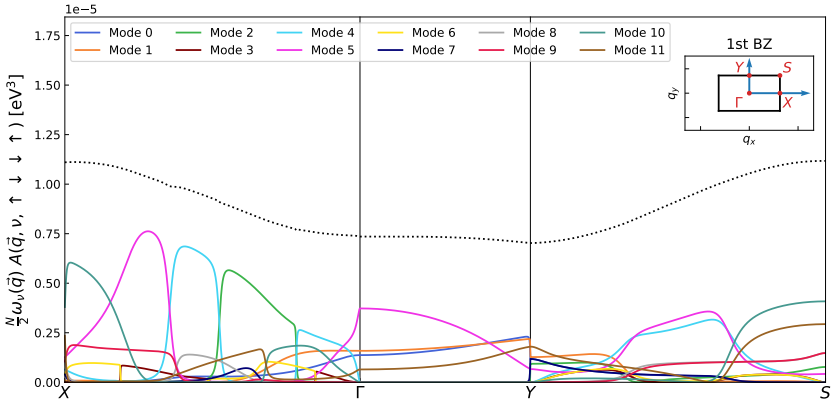

Figure 4.3: BCS potential enhancement factor along some high-symmetry directions of a spin flip scattering process for two incoming/outgoing opposite spin electrons for the different magnon modes. Here the SPFMI has a spin periodicity of 6 atoms. The sum of all mode contributions is indicated by the black dotted line.

We know already that a bilayer with a collinear AFMI will give the optimal enhancement, since the squeezing coefficients in this special case diverge in the magnonic long wavelength limit. We do not see any sort of divergences in our case. Comparing to the collinear FMI enhancement [6] for similar exchange parameters (see Table 3.1)

$$\frac{48J\bar{J}^2s^2}{N}\left(1-\frac{1}{6}\sum_{\boldsymbol{d}}e^{i\boldsymbol{q}\cdot\boldsymbol{d}}\right)\leq\frac{4.8\cdot10^{-5}}{N}\mathrm{eV}^3, \tag{4.67}$$

we get a somewhat larger upper limit to the enhancement in the case of the FMI as opposed to our bilayer with a SPFMI. Of course without a large gap in the FMI spectrum there will be areas with much smaller enhancement at long magnon wavelengths, while the SPFMI enhancement remains on the same order of magnitude across the magnon BZ. In any case it seems like the squeezing parameters from our chosen non-collinear spin structure do not help to enhance the superconductivity, possibly making it slightly worse.

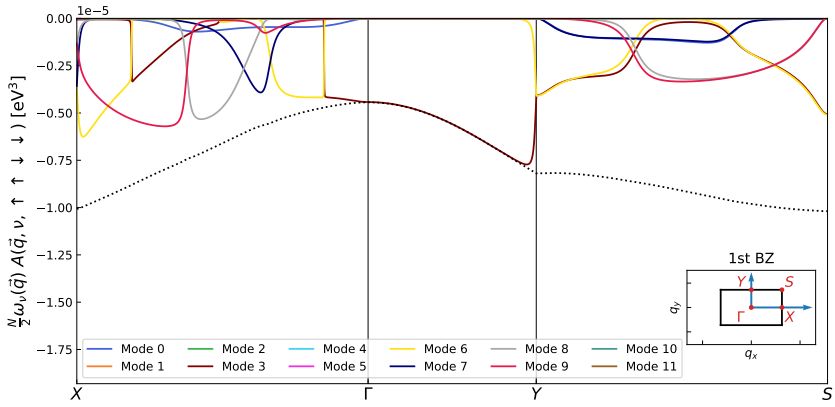

Figure 4.4: BCS potential enhancement factor along some high-symmetry directions of a scattering process without spin flip for two incoming/outgoing opposite spin electrons for the different magnon modes. Here the SPFMI has a spin periodicity of 6 atoms. The sum of all mode contributions is indicated by the black dotted line.

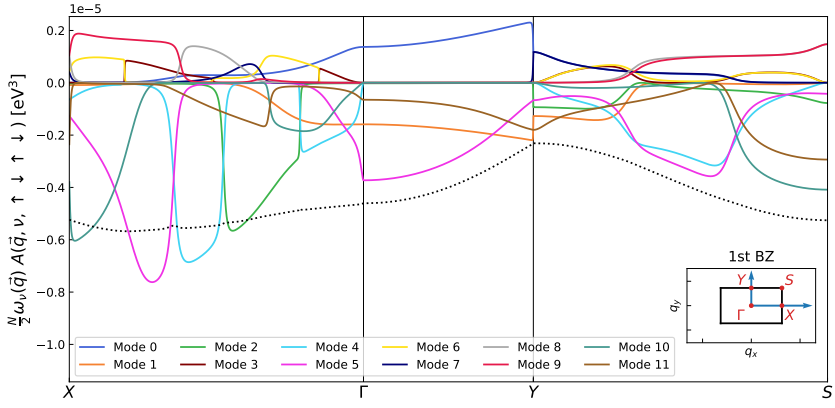

Figure 4.5: BCS potential enhancement factor along some high-symmetry directions of a spin flip scattering process for two incoming/outgoing equal spin electrons for the different magnon modes. Here the SPFMI has a spin periodicity of 6 atoms. The sum of all mode contributions is indicated by the black dotted line.

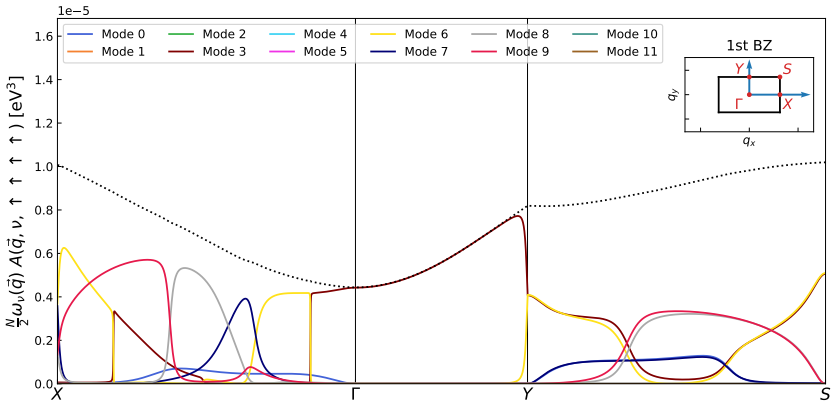

Figure 4.6: BCS potential enhancement factor along some high-symmetry directions of a scattering process without spin flip for two incoming/outgoing equal spin electrons for the different magnon modes. Here the SPFMI has a spin periodicity of 6 atoms. The sum of all mode contributions is indicated by the black dotted line.

Chapter 5

Superconductivity

5.1 Generalised BCS theory

The starting point of the BCS theory is a Hamiltonian consisting of a single particle occupation energy and a two-particle scattering term

$$\mathcal{H} = \sum_{\boldsymbol{k},\sigma} \epsilon_{\boldsymbol{k}} c^\dagger_{\boldsymbol{k}\sigma} c_{\boldsymbol{k}\sigma} + \frac{1}{2} \sum_{\boldsymbol{k},\boldsymbol{k'}} \sum_{\sigma_1,\sigma_2,\sigma_3,\sigma_4} \tilde{V}^{\sigma_1\sigma_2\sigma_3\sigma_4}_{\boldsymbol{k}\boldsymbol{k'}} c^\dagger_{\boldsymbol{k}\sigma_1} c^\dagger_{-\boldsymbol{k}\sigma_2} c_{-\boldsymbol{k'}\sigma_3} c_{\boldsymbol{k'}\sigma_4}. \tag{5.1}$$

The system must be diagonalised to find the electron excitation spectrum, and in order to deal with the four-operator terms we make use of a mean field approximation. Defining the Cooper pair mean field as the ensemble average

$$b_{\boldsymbol{k}\sigma\sigma'} = \langle c_{-\boldsymbol{k}\sigma} c_{\boldsymbol{k}\sigma'} \rangle, \tag{5.2}$$

with a fluctuation

$$\delta b_{\boldsymbol{k}\sigma\sigma'} = c_{-\boldsymbol{k}\sigma} c_{\boldsymbol{k}\sigma'} - \langle c_{-\boldsymbol{k}\sigma} c_{\boldsymbol{k}\sigma'} \rangle, \tag{5.3}$$

we write the four-operator term as

$$\mathcal{H}_{\text{Pair}} = \frac{1}{2} \sum_{\boldsymbol{k},\boldsymbol{k'}} \sum_{\substack{\sigma_1,\sigma_2 \\ \sigma_3,\sigma_4}} \tilde{V}^{\sigma_1\sigma_2\sigma_3\sigma_4}_{\boldsymbol{k}\boldsymbol{k'}} (b^\dagger_{\boldsymbol{k}\sigma_2\sigma_1} + \delta b^\dagger_{\boldsymbol{k}\sigma_2\sigma_1})(b_{\boldsymbol{k'}\sigma_3\sigma_4} + \delta b_{\boldsymbol{k'}\sigma_3\sigma_4}). \tag{5.4}$$

Making the approximation that

$$\delta b^\dagger_{\boldsymbol{k}\sigma_2\sigma_1} \delta b_{\boldsymbol{k}\sigma_3\sigma_4} \approx 0, \tag{5.5}$$

we find that the BCS Hamiltonian can be written in terms of only two-operator interactions [15]

$$\begin{aligned} \mathcal{H} = &\sum_{\boldsymbol{k},\sigma} \epsilon_{\boldsymbol{k}} c^\dagger_{\boldsymbol{k}\sigma} c_{\boldsymbol{k}\sigma} - \frac{1}{2} \sum_{\boldsymbol{k}} \sum_{\sigma_1,\sigma_2} \left(\Delta_{\boldsymbol{k}\sigma_1\sigma_2} c^\dagger_{\boldsymbol{k}\sigma_1} c^\dagger_{-\boldsymbol{k}\sigma_2} + \Delta^\dagger_{\boldsymbol{k}\sigma_1\sigma_2} c_{-\boldsymbol{k}\sigma_1} c_{\boldsymbol{k}\sigma_2} \right) \\ &+ \frac{1}{2} \sum_{\boldsymbol{k}} \sum_{\sigma_1,\sigma_2} \Delta_{\boldsymbol{k}\sigma_1\sigma_2} b^\dagger_{\boldsymbol{k}\sigma_2\sigma_1}, \end{aligned} \tag{5.6}$$

where we have introduced the following quantities

$$\Delta_{\boldsymbol{k}\sigma_1\sigma_2} = -\sum_{\boldsymbol{k'}\sigma_3\sigma_4} \tilde{V}^{\sigma_1\sigma_2\sigma_3\sigma_4}_{\boldsymbol{k}\boldsymbol{k'}} b_{\boldsymbol{k'}\sigma_3\sigma_4}, \tag{5.7}$$

$$\Delta^{\dagger}_{\boldsymbol{k}\sigma_1\sigma_2} = -\sum_{\boldsymbol{k'}\sigma_3\sigma_4} \tilde{V}^{\sigma_3\sigma_4\sigma_1\sigma_2}_{\boldsymbol{k}\boldsymbol{k'}} b^{\dagger}_{\boldsymbol{k'}\sigma_3\sigma_4}. \tag{5.8}$$

These are the superconducting order parameters; more well known as the gap functions since they describe the onset of a gap in the dispersion relation of a superconducting phase. They can be written as elements of a 2×2 matrix

$$\hat{\Delta}(\boldsymbol{k}) = \begin{bmatrix} \Delta_{\boldsymbol{k}\uparrow\uparrow} & \Delta_{\boldsymbol{k}\uparrow\downarrow} \\ \Delta_{\boldsymbol{k}\downarrow\uparrow} & \Delta_{\boldsymbol{k}\downarrow\downarrow} \end{bmatrix}. \tag{5.9}$$

The fact that these are order parameters is evident from Eqn. (5.6). In the case where $\langle c_{-\boldsymbol{k}\sigma} c_{\boldsymbol{k}\sigma'} \rangle = 0$ there are on average no Cooper pairs and Eqn. (5.6) is already diagonalised in the NM phase. However for $\langle c_{-\boldsymbol{k}\sigma} c_{\boldsymbol{k}\sigma'} \rangle \neq 0$ the system is no longer diagonalised in the old electron operator basis, meaning that a transition from the NM phase to a new phase must have occurred. The new phase is ordered in the sense that electrons pair up in bound k-space states called Cooper pairs. The phase transition occurs at some critical temperature T_c for which the lack of thermal fluctuations allows the electrons to condensate into Cooper pairs that are energetically favourable. In order to determine this critical temperature it is necessary to diagonalise the system (for example by the means of a Bogoliubov transformation) and then minimise the free energy with respect to the order parameter. This yields a self-consistent equation

$$\Delta_{\boldsymbol{k}\sigma_1\sigma_2} = -\sum_{\boldsymbol{k'}\sigma_3\sigma_4} \tilde{V}^{\sigma_1\sigma_2\sigma_3\sigma_4}_{\boldsymbol{k}\boldsymbol{k'}} \Delta_{\boldsymbol{k}\sigma_4\sigma_3} \chi_{\boldsymbol{k}}(T), \tag{5.10}$$

with

$$\chi_{\boldsymbol{k}}(T) = \frac{1}{2E_{\boldsymbol{k}}} \tanh\left(\frac{E_{\boldsymbol{k}}}{2k_B T}\right), \qquad E_{\boldsymbol{k}} = \sqrt{\epsilon^2_{\boldsymbol{k}} + \frac{1}{2}\mathrm{Tr}\hat{\Delta}(\boldsymbol{k})\hat{\Delta}^{\dagger}(\boldsymbol{k})}, \tag{5.11}$$

in the case of a unitary order parameter matrix $\hat{\Delta}(\boldsymbol{k})$ [42].

5.1.1 Spin symmetry of the Cooper Pair scattering matrix

Taking a look at the scattering potential operator in the BCS Hamiltonian (5.1)

$$\mathcal{V} = \frac{1}{2}\sum_{\boldsymbol{k},\boldsymbol{k'}} \sum_{\sigma_1,\sigma_2,\sigma_3,\sigma_4} \tilde{V}^{\sigma_1\sigma_2\sigma_3\sigma_4}_{\boldsymbol{k}\boldsymbol{k'}} c^{\dagger}_{\boldsymbol{k}\sigma_1} c^{\dagger}_{-\boldsymbol{k}\sigma_2} c_{-\boldsymbol{k'}\sigma_3} c_{\boldsymbol{k'}\sigma_4}, \tag{5.12}$$

we see that the pair scattering matrix elements are given by [42]

$$\tilde{V}^{\sigma_1\sigma_2\sigma_3\sigma_4}_{\boldsymbol{k}\boldsymbol{k'}} = \langle \boldsymbol{k}, \sigma_1; -\boldsymbol{k}, \sigma_2 | \, 2\mathcal{V} \, | -\boldsymbol{k'}, \sigma_3; \boldsymbol{k'}, \sigma_4 \rangle \, . \tag{5.13}$$

Anti-commutation of the fermionic operators therefore requires that the scattering matrix must have the following structure

$$\tilde{V}^{\sigma_1\sigma_2\sigma_3\sigma_4}_{\boldsymbol{k},\boldsymbol{k'}} = -\tilde{V}^{\sigma_2\sigma_1\sigma_3\sigma_4}_{-\boldsymbol{k},\boldsymbol{k'}} = -\tilde{V}^{\sigma_1\sigma_2\sigma_4\sigma_3}_{\boldsymbol{k},-\boldsymbol{k'}} = \tilde{V}^{\sigma_2\sigma_1\sigma_4\sigma_3}_{-\boldsymbol{k},-\boldsymbol{k'}}. \tag{5.14}$$

The first obvious result of this is that all the spin polarised scattering matrix elements must be odd in $\boldsymbol{k}$

$$\begin{aligned} \tilde{V}^{\uparrow\uparrow\uparrow\uparrow}_{\boldsymbol{k},\boldsymbol{k'}} &= -\tilde{V}^{\uparrow\uparrow\uparrow\uparrow}_{-\boldsymbol{k},\boldsymbol{k'}} \qquad \tilde{V}^{\downarrow\downarrow\downarrow\downarrow}_{\boldsymbol{k},\boldsymbol{k'}} = -\tilde{V}^{\downarrow\downarrow\downarrow\downarrow}_{-\boldsymbol{k},\boldsymbol{k'}} \\ \tilde{V}^{\uparrow\uparrow\downarrow\downarrow}_{\boldsymbol{k},\boldsymbol{k'}} &= -\tilde{V}^{\uparrow\uparrow\downarrow\downarrow}_{-\boldsymbol{k},\boldsymbol{k'}} \qquad \tilde{V}^{\downarrow\downarrow\uparrow\uparrow}_{\boldsymbol{k},\boldsymbol{k'}} = -\tilde{V}^{\downarrow\downarrow\uparrow\uparrow}_{-\boldsymbol{k},\boldsymbol{k'}}. \end{aligned} \tag{5.15}$$

Again we can gather all the unpolarised spin terms together in the form of Eqn. (4.48) with

$$\tilde{V}_{\boldsymbol{k}\boldsymbol{k'}} = \frac{1}{2}\left(\tilde{V}^{\downarrow\uparrow\uparrow\downarrow}_{\boldsymbol{k},\boldsymbol{k'}} + \tilde{V}^{\uparrow\downarrow\downarrow\uparrow}_{-\boldsymbol{k},-\boldsymbol{k'}} - \tilde{V}^{\uparrow\downarrow\uparrow\downarrow}_{-\boldsymbol{k},\boldsymbol{k'}} - \tilde{V}^{\downarrow\uparrow\downarrow\uparrow}_{\boldsymbol{k},-\boldsymbol{k'}}\right), \tag{5.16}$$

where we have written $\tilde{V}_{\boldsymbol{k}\boldsymbol{k'}}$ in terms of scattering matrix elements that obey (5.14). This is the same quantity we defined in (4.50), however we note that in the previous case it was written as a sum of matrix elements that had not been balanced in order to satisfy (5.14). We will later find it useful to define this potential in terms of the even and odd parts in $\boldsymbol{k}$

$$\tilde{V}^{E(\boldsymbol{k})}_{\boldsymbol{k}\boldsymbol{k'}} = \frac{1}{2}\left(\tilde{V}_{\boldsymbol{k}\boldsymbol{k'}} + \tilde{V}_{-\boldsymbol{k}\boldsymbol{k'}}\right), \tag{5.17}$$

$$\tilde{V}^{O(\boldsymbol{k})}_{\boldsymbol{k}\boldsymbol{k'}} = \frac{1}{2}\left(\tilde{V}_{\boldsymbol{k}\boldsymbol{k'}} - \tilde{V}_{-\boldsymbol{k}\boldsymbol{k'}}\right). \tag{5.18}$$

Using the fact that $\tilde{V}^{\downarrow\uparrow\uparrow\downarrow}_{\boldsymbol{k}\boldsymbol{k'}} = \tilde{V}^{\uparrow\downarrow\downarrow\uparrow}_{\boldsymbol{k},\boldsymbol{k'}}$ together with Eqns. (5.14) and (5.16) we can now write

$$\tilde{V}^{E(\boldsymbol{k})}_{\boldsymbol{k}\boldsymbol{k'}} = \tilde{V}^{\downarrow\uparrow\uparrow\downarrow}_{\boldsymbol{k}\boldsymbol{k'}} + \tilde{V}^{\downarrow\uparrow\uparrow\downarrow}_{-\boldsymbol{k}\boldsymbol{k'}} = \tilde{V}^{\uparrow\downarrow\downarrow\uparrow}_{\boldsymbol{k},\boldsymbol{k'}} + \tilde{V}^{\uparrow\downarrow\downarrow\uparrow}_{-\boldsymbol{k},\boldsymbol{k'}}, \tag{5.19}$$

$$\tilde{V}^{O(\boldsymbol{k})}_{\boldsymbol{k}\boldsymbol{k'}} = \tilde{V}^{\downarrow\uparrow\uparrow\downarrow}_{\boldsymbol{k}\boldsymbol{k'}} - \tilde{V}^{\downarrow\uparrow\uparrow\downarrow}_{-\boldsymbol{k}\boldsymbol{k'}} = \tilde{V}^{\uparrow\downarrow\downarrow\uparrow}_{\boldsymbol{k},\boldsymbol{k'}} - \tilde{V}^{\uparrow\downarrow\downarrow\uparrow}_{-\boldsymbol{k},\boldsymbol{k'}}. \tag{5.20}$$

These relations will prove useful when discussing the superconducting order parameter.

5.1.2 The superconducting order parameter

The superconducting order parameter can in general take quite a complicated form, as we have seen that the inclusion of triplet Cooper pairs makes it necessary to consider an order parameter described by a matrix rather than just a scalar. The triplet pairings can furthermore give a non-unitary order parameter matrix which complicates the diagonalisation of the BCS Hamiltonian considerably. As can be seen from Eqn. (5.10) the gap function matrix elements are described by four pairwise coupled equations. It turns out that we can decouple the two unpolarised gap matrix elements by introducing order parameters that are odd and even in spin labeling

$$\Delta^{O(s)}_{\boldsymbol{k},\uparrow\downarrow} \equiv \Delta_{\boldsymbol{k},\uparrow\downarrow} - \Delta_{\boldsymbol{k},\downarrow\uparrow}, \tag{5.21}$$

$$\Delta^{E(s)}_{\boldsymbol{k},\uparrow\downarrow} \equiv \Delta_{\boldsymbol{k},\uparrow\downarrow} + \Delta_{\boldsymbol{k},\downarrow\uparrow}. \tag{5.22}$$

Inserting the two unpolarised gap functions into these relations and using the relations (5.19) and (5.20) it is quite easily shown (see Appendix C.1) that

$$\Delta^{O(s)}_{\boldsymbol{k},\uparrow\downarrow} = -\sum_{\boldsymbol{k'}} \tilde{V}^{E(\boldsymbol{k})}_{\boldsymbol{k}\boldsymbol{k'}}\, \Delta^{O(s)}_{\boldsymbol{k'},\uparrow\downarrow}\, \chi_{\boldsymbol{k'}}, \tag{5.23}$$

$$\Delta^{E(s)}_{\boldsymbol{k},\uparrow\downarrow} = -\sum_{\boldsymbol{k'}} \tilde{V}^{O(\boldsymbol{k})}_{\boldsymbol{k}\boldsymbol{k'}}\, \Delta^{E(s)}_{\boldsymbol{k'},\uparrow\downarrow}\, \chi_{\boldsymbol{k'}}. \tag{5.24}$$

In the case of the polarised gaps we already know that only triplet pairing is involved, and that we are restricted to odd potentials in $\boldsymbol{k}$. We therefore do not decouple these two matrix elements, but rather write them as a single matrix equation

$$\begin{pmatrix} \Delta_{\boldsymbol{k},\uparrow\uparrow} \\ \Delta_{\boldsymbol{k},\downarrow\downarrow} \end{pmatrix} = -\sum_{\boldsymbol{k'}} \begin{pmatrix} \tilde{V}^{\uparrow\uparrow\uparrow\uparrow}_{\boldsymbol{k}\boldsymbol{k'}} & \tilde{V}^{\uparrow\uparrow\downarrow\downarrow}_{\boldsymbol{k}\boldsymbol{k'}} \\ \tilde{V}^{\downarrow\downarrow\uparrow\uparrow}_{\boldsymbol{k}\boldsymbol{k'}} & \tilde{V}^{\downarrow\downarrow\downarrow\downarrow}_{\boldsymbol{k}\boldsymbol{k'}} \end{pmatrix} \begin{pmatrix} \Delta_{\boldsymbol{k'},\uparrow\uparrow} \\ \Delta_{\boldsymbol{k'},\downarrow\downarrow} \end{pmatrix} \chi_{\boldsymbol{k'}}. \tag{5.25}$$

In the case where $\tilde{V}^{\uparrow\uparrow\uparrow\uparrow}_{\boldsymbol{k}\boldsymbol{k'}} = \tilde{V}^{\downarrow\downarrow\downarrow\downarrow}_{\boldsymbol{k}\boldsymbol{k'}}$ and $\tilde{V}^{\uparrow\uparrow\downarrow\downarrow}_{\boldsymbol{k}\boldsymbol{k'}} = \tilde{V}^{\downarrow\downarrow\uparrow\uparrow}_{\boldsymbol{k}\boldsymbol{k'}}$ this simplifies to a scalar equation

$$\Delta^{(p)}_{\boldsymbol{k}} = -\sum_{\boldsymbol{k'}} \tilde{V}^{(p)}_{\boldsymbol{k}\boldsymbol{k'}} \Delta^{(p)}_{\boldsymbol{k'}}\, \chi_{\boldsymbol{k'}}, \tag{5.26}$$

where we denote $\Delta^{(p)}_{\boldsymbol{k}} = \Delta_{\boldsymbol{k},\uparrow\uparrow} = \Delta_{\boldsymbol{k},\downarrow\downarrow}$ and $\tilde{V}^{(p)}_{\boldsymbol{k}\boldsymbol{k'}} = \tilde{V}^{\uparrow\uparrow\uparrow\uparrow}_{\boldsymbol{k}\boldsymbol{k'}} + \tilde{V}^{\uparrow\uparrow\downarrow\downarrow}_{\boldsymbol{k}\boldsymbol{k'}}$.

5.1.3 Momentum symmetry channels for the pair potential

In order to get an idea of the symmetry of the superconducting state it is natural to explore the k-space symmetry of the pair potential given the relation between the two quantities described by the gap function. We can already make a few observations based on the results from Section 4.4, where it was found that the unpolarised part of the pair potential is purely positive for scattering events restricted to the Fermi surface. This would suggest that there should not be any s-wave superconductivity. Thus we must investigate other symmetry channels in our search for superconductivity which are described by the lattice harmonics presented in Section 2.4. The potential in this case originates from a system of triangular lattices, and so it is reasonable to assume that the shape of the potential reflects this lattice symmetry and therefore can be expanded in terms of the triangular lattice harmonics as follows

$$V_{\boldsymbol{k}\boldsymbol{k'}} = \sum_{\alpha} \Gamma_\alpha B_\alpha(\boldsymbol{k}) B_\alpha(\boldsymbol{k'}), \tag{5.27}$$

with the different lattice harmonics labeled here by α [43]. As of yet we have not made any assumptions whether the potential $V_{\boldsymbol{k}\boldsymbol{k'}}$ describes a spin singlet or triplet state, and in the latter case if it is spin polarised or not. We will however define $V_{\boldsymbol{k}\boldsymbol{k'}}$ to be independent of the lattice size (for example $V_{\boldsymbol{k}\boldsymbol{k'}} = N\tilde{V}_{\boldsymbol{k}\boldsymbol{k'}}$ in the case of an unpolarised Cooper pair). Multiplying both sides by basis functions $B_\beta(\boldsymbol{k})$ and $B_\beta(\boldsymbol{k'})$ before taking a double integral over the 1$^{\text{st}}$ BZ gives an expression for the symmetry coefficient

$$\Gamma_\beta = \int_{\text{BZ}} d\boldsymbol{k} d\boldsymbol{k'}\, V_{\boldsymbol{k}\boldsymbol{k'}} B_\beta(\boldsymbol{k}) B_\beta(\boldsymbol{k'}), \tag{5.28}$$

where we have utilised the orthonormality of the basis functions. Similarly, the superconducting gap can be expanded in terms of the lattice harmonics

$$\Delta_{\boldsymbol{k}} = \sum_{\alpha} \Delta_{\alpha} B_{\alpha}(\boldsymbol{k}), \tag{5.29}$$

where Δ_{α} is a coefficient determining the contribution of the symmetry α to the superconducting gap. Inserting the symmetry expanded expressions of the potential and superconducting gap into the gap function we find

$$\sum_{\alpha} \Delta_{\alpha} B_{\alpha}(\boldsymbol{k}) = -\sum_{\boldsymbol{k'}} \sum_{\alpha} \Gamma_{\alpha} B_{\alpha}(\boldsymbol{k}) B_{\alpha}(\boldsymbol{k'}) \sum_{\beta} \Delta_{\beta} B_{\beta}(\boldsymbol{k'}) \chi_{\boldsymbol{k'}}. \tag{5.30}$$

Again we make use of the orthonormality by multiplying with a basis function on both sides and taking the integral over the 1st BZ

$$\sum_{\alpha} \Delta_{\alpha} \underbrace{\int d\boldsymbol{k}\, B_{\alpha}(\boldsymbol{k}) B_{\zeta}(\boldsymbol{k})}_{=\delta_{\alpha\zeta}} = -\sum_{\boldsymbol{k'}} \sum_{\alpha,\beta} \underbrace{\int d\boldsymbol{k}\, B_{\alpha}(\boldsymbol{k}) B_{\zeta}(\boldsymbol{k})}_{=\delta_{\alpha\zeta}} \Gamma_{\alpha} B_{\alpha}(\boldsymbol{k'}) \Delta_{\beta} B_{\beta}(\boldsymbol{k'}) \chi_{\boldsymbol{k'}}. \tag{5.31}$$

Thus we end up with the following expression for the gap coefficients

$$\Delta_{\zeta} = \sum_{\beta} \left(-\sum_{\boldsymbol{k'}} \Gamma_{\zeta} B_{\zeta}(\boldsymbol{k'}) B_{\beta}(\boldsymbol{k'}) \chi_{\boldsymbol{k'}} \right) \Delta_{\beta} = \sum_{\beta} M_{\zeta\beta} \Delta_{\beta}. \tag{5.32}$$

Note that each gap coefficient can in general have contributions from several symmetries, however even (odd) symmetries cannot contribute to odd (even) coefficients since $\chi_{\boldsymbol{k'}}$ is isotropic and therefore even in $\boldsymbol{k}$ such that the sum vanishes in the case where only one of α and β is odd. We could therefore choose to decouple Eq. (5.32) into two separate equations; where one contains the even coefficients while the other contains the odd coefficients.

5.2 Analysis on the Fermi Surface

It is now time to calculate some results from the expressions derived previously in this chapter, and again this requires a numerical treatment. We note however that the size of the problem is much larger than a lot of our previous simulations as a result of there being two momentum labels in the BCS potentials. For example, calculating a result for Eq. (5.28) requires a double integral over the entire 1st BZ, which is a sizable computational task if one wishes to have a good resolution of points in k-space. Looking back at the results from Section 4.4 there is a lot of variation in the potential close to the Fermi surface since there are so many magnon modes. Thus one expects that a very good sampling resolution is needed around the Fermi surface for a complete analysis of the pair potential symmetry and superconducting gap, and we should indeed be wary of any result where the k-space might be insufficient. Rather than looking at the entire BZ we follow the example of [8] and restrict ourselves to scattering events where $\boldsymbol{k}$ and $\boldsymbol{k'}$ both lie on the

Fermi surface, with the intention of getting some idea what the actual results may look like. It should therefore be made clear that the results of this section serve only as rough approximations, however in this case we are able to bypass the k-space resolution problem. For very low temperatures we can argue that this approximation is valid when discussing the superconducting gap since the function $\chi_{\boldsymbol{k}}$ is dominated by momenta situated on the Fermi surface.

5.2.1 The pairing symmetry coefficient

We start off with a calculation of Eq. (5.28), which now is modified to be a double sum over the Fermi surface

$$\Gamma_\alpha(\epsilon_F) = \int_{\text{FS}} d\boldsymbol{k} d\boldsymbol{k'}\, V_{\boldsymbol{k}\boldsymbol{k'}} B_\alpha(\boldsymbol{k}) B_\alpha(\boldsymbol{k'}). \tag{5.33}$$

Notice that Γ_α is now a function of the Fermi energy; in other words how large the filling factor is. In the case of a spin singlet we use the even part of the unpolarised pair scattering matrix so that

$$\Gamma_\alpha(\epsilon_F) \approx \left\langle \left\langle N\tilde{V}^{E(\boldsymbol{k})}_{\boldsymbol{k},\boldsymbol{k'}} B_\alpha(\boldsymbol{k}) B_\alpha(\boldsymbol{k'}) \right\rangle \right\rangle_{\text{FS},\boldsymbol{k},\boldsymbol{k'}}, \qquad \alpha \in \{s, 2s, d_{xy}, d_{x^2-y^2}\}. \tag{5.34}$$

Since we are dealing with a finite number of points in k-space the integral is rewritten as a double average over the Fermi surface which we denote by $\langle\langle \ldots \rangle\rangle_{\text{FS},\boldsymbol{k},\boldsymbol{k'}}$ (defining the Fermi surface average over N_{samp} sampled points as $\langle x_{\boldsymbol{k},\boldsymbol{k'}} \rangle_{\text{FS},\boldsymbol{k},\boldsymbol{k'}} = \sum_{\text{FS}} x_{\boldsymbol{k},\boldsymbol{k'}} / N_{\text{samp}}$, with $\boldsymbol{k}, \boldsymbol{k'} \in$ FS). The coefficients Γ_α for some different spin singlet symmetries have been plotted in Figure 5.1 for different Fermi energies. We restrict ourselves to values up to $\epsilon_F = 0.5$ eV where the Fermi surface does not deviate too much from a circle since we have neglected any umklapp processes. Note that for the spin singlet symmetries the coefficients are always positive. From Eq. (5.32) and the shape of the triangular lattice harmonics we see that a positive Γ_α is typically linked to suppression of superconductivity in the symmetry channel α, since most of the lattice harmonics will be approximately orthogonal on the Fermi surface (at least as long the Fermi surface is nearly circular). An exception is coupling between the s and $2s$ symmetries since these will not be close to orthogonal on the Fermi surface, so that the sign of Γ_α will not tell the entire story. However from Section 4.4 we found that the unpolarised pair scattering matrix was positive everywhere on the Fermi surface, and so we would still expect singlet pairing to not play an important role in any emergent superconducting state.

Similarly in the case of the unpolarised triplet we take the double average over the Fermi surface, this time with the odd part of the potential

$$\Gamma_\alpha(\epsilon_F) \approx \left\langle \left\langle N\tilde{V}^{O(\boldsymbol{k})}_{\boldsymbol{k},\boldsymbol{k'}} B_\alpha(\boldsymbol{k}) B_\alpha(\boldsymbol{k'}) \right\rangle \right\rangle_{\text{FS},\boldsymbol{k},\boldsymbol{k'}}, \qquad \alpha \in \{p_x, p_y, f\}. \tag{5.35}$$

The polarised triplet symmetry coefficients can be found by swapping $\tilde{V}^{O(\boldsymbol{k})}_{\boldsymbol{k},\boldsymbol{k'}}$ in Eq. (5.35) with a scattering matrix element for the polarised terms. In the case of spin triplet pairing all the symmetry channels are nearly orthogonal on the Fermi surface so that the matrix in Eq. (5.32) is dominated by the diagonal terms. If we follow the example of [43] by

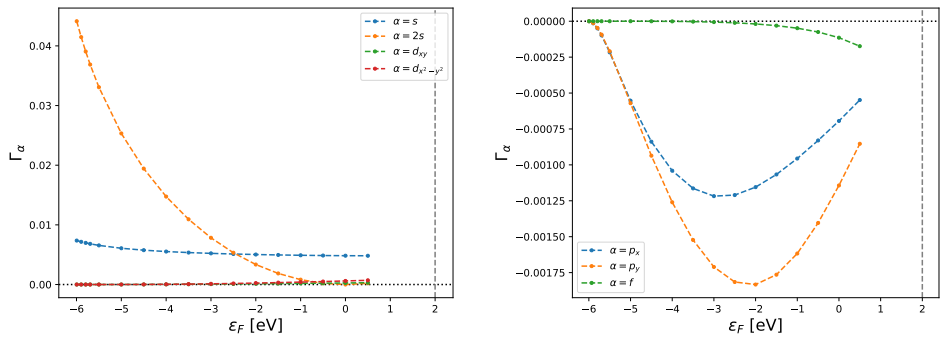

(a) **(b)**

Figure 5.1: Symmetry coefficient for unpolarised spin scattering, with singlet pairing in a) and triplet pairing in b).

approximating Eq. (5.32) as decoupled equations then there is a direct link between the sign of Γ_α and existence of a superconducting gap for the symmetry channel α. Looking at Figure 5.1 we see that there is a possibility for p-wave superconductivity, mainly in the p_y channel in the case for unpolarised triplet pairing. At large Fermi energies there also seems to be a small contribution to the f-wave channel. For the polarised triplet pairing the results displayed in Figure 5.2 indicate that only the p_x channel would contribute. Note however that it is an order of magnitude smaller than the unpolarised coefficient.

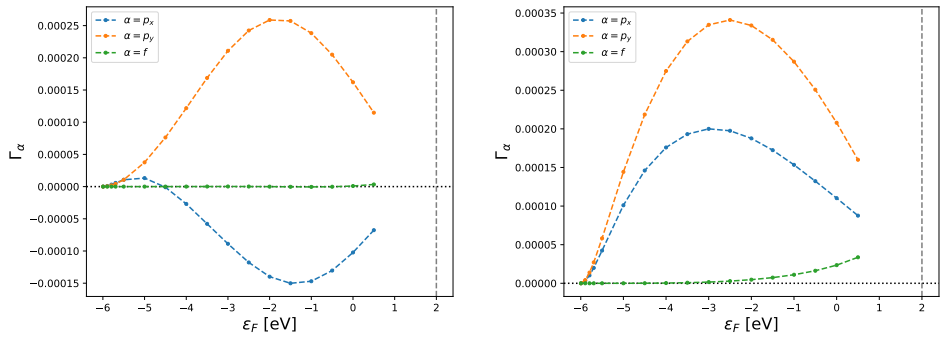

(a) **(b)**

Figure 5.2: Symmetry coefficient for two polarised spin scattering matrix elements. Figure a) shows the symmetry coefficient for $\tilde{V}^{\uparrow\uparrow\uparrow\uparrow}_{\boldsymbol{k},\boldsymbol{k}'}$, b) shows the symmetry coefficient for $\tilde{V}^{\uparrow\uparrow\downarrow\downarrow}_{\boldsymbol{k},\boldsymbol{k}'}$.

5.2.2 The linearised gap equation

In general it is not a simple case of just solving the self consistent gap in Eqs. (5.23) and (5.24), since these are large systems of nonlinear equations that may have many non-trivial

solutions. However, if we allow the temperature approach T_c from below the gap vanishes. Treating $\Delta_{\boldsymbol{k}}$ as an eigenvector, the norm approaches zero at the critical temperature, although $\Delta_{\boldsymbol{k}}$ still has some structure. This motivates removing the gap dependence of $\chi_{\boldsymbol{k'}}$ so that the gap structure is determined by the linear equation

$$\Delta_{\boldsymbol{k}} = -\sum_{\boldsymbol{k'}} V_{\boldsymbol{k}\boldsymbol{k'}}\, \Delta_{\boldsymbol{k'}}\, \frac{1}{2|\epsilon_{\boldsymbol{k'}}|} \tanh\left(\frac{|\epsilon_{\boldsymbol{k'}}|}{2k_B T_c}\right). \tag{5.36}$$

Here we let the sum go over a thin strip in k-space with energies between $\epsilon_F - \omega_c$ and $\epsilon_F + \omega_c$, where ω_c is a cutoff energy. Here we choose ω_c to be the maximum energy in the magnon spectrum. We now make an approximation in the spirit of the Bardeen, Schrieffer and Cooper's original treatment of conventional superconductors [3]; we assume that the potential does not vary in the radial direction on the strip, but is defined only by its value on the Fermi surface. In a sense we have made the "textbook" constant potential approximation in the radial direction, while keeping the full potential structure tangentially along the Fermi surface. Parameterising the momentum in terms of polar coordinates we write the potential as $V_{\boldsymbol{k}\boldsymbol{k'}} = V(k, \varphi, k', \varphi')$. We rewrite the sum as an integral in polar coordinates and make a change of integration variable from momentum to energy by using the relation $D(\epsilon)\, d\epsilon = D(k)\, dk$

$$\Delta(\varphi) = -\frac{N}{A_{\mathrm{BZ}}} \int_0^{2\pi} d\varphi'\, V(\varphi, \varphi')\Delta(\varphi') \int_{-\omega_c}^{\omega_c} d\epsilon\, \frac{k' D(\epsilon)}{D(k')} \frac{1}{2|\epsilon|} \tanh\left(\frac{|\epsilon|}{2k_B T_c}\right). \tag{5.37}$$

Inserting the expression for k-space DOS on a triangular lattice and making the approximation that $D(\epsilon)$ equals the Fermi surface density of states D_0 in the relevant energy range, we arrive at the expression

$$\Delta(\varphi) = -D_0 \left\langle V(\varphi, \varphi')\Delta(\varphi')\right\rangle_{\mathrm{FS},\varphi'} \int_{-\omega_c}^{\omega_c} d\epsilon\, \frac{1}{2|\epsilon|} \tanh\left(\frac{|\epsilon|}{2k_B T_c}\right), \tag{5.38}$$

where we have written the angular part of the integral into an average over angles on the Fermi surface

$$\left\langle V(\varphi, \varphi')\Delta(\varphi')\right\rangle_{\mathrm{FS},\varphi'} = \frac{1}{N_{\mathrm{samp}}} \sum_{\varphi'} V(\varphi, \varphi')\Delta(\varphi'). \tag{5.39}$$

Here N_{samp} is the number of points sampled on the Fermi surface. We now introduce the coupling constant λ, which we define as follows [8]

$$\frac{1}{\lambda} = \int_{-\omega_c}^{\omega_c} d\epsilon\, \frac{1}{2|\epsilon|} \tanh\left(\frac{|\epsilon|}{2k_B T_c}\right) \approx \ln\left(\frac{1.14\omega_c}{k_B T_c}\right). \tag{5.40}$$

Thus the linearised gap function is an eigenvalue equation of the form

$$\lambda\Delta(\varphi) = D_0 \left\langle V(\varphi, \varphi')\Delta(\varphi')\right\rangle_{\mathrm{FS},\varphi'}, \tag{5.41}$$

which can be formulated in terms of a matrix equation where the chosen angles φ, φ' correspond to indices of the vector/matrix elements.

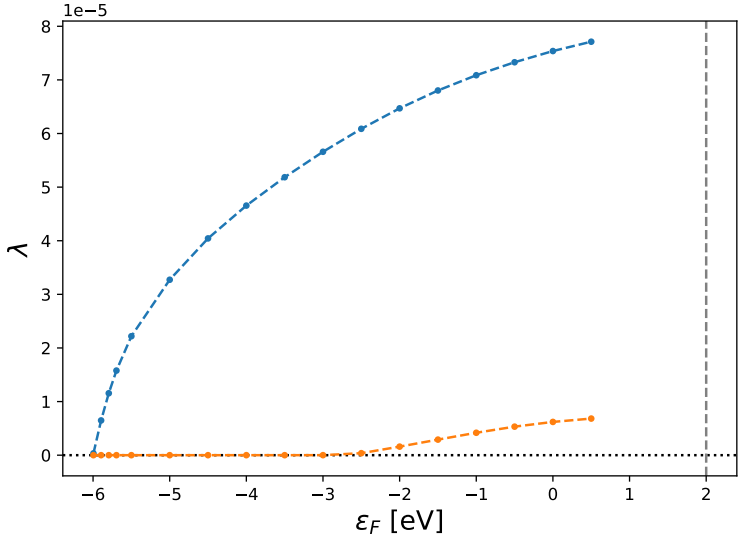

Figure 5.3: Coupling coefficient for scattering on the Fermi surface as a function of Fermi energy in the case of both unpolarised (blue) and polarised (yellow) spin triplet Cooper pairs. The gray stapled line indicates the Van Hove instability.

In order to get an idea of how the coupling constant λ varies with filling factor we solve the linearised gap eigenvalue problem for different Fermi energies, and the results are shown in Figure 5.3. Again we have chosen to look at the example where the SPFMI spin period is 6 atoms. Since the even part of the pair scattering matrix is always positive all eigenvalues should be negative for superconducting states that are even in momentum, so we ignore spin singlet pairing and focus only on spin triplets. For both unpolarised and polarised triplets the coupling increases with increasing Fermi energy, and we note that for low filling there seems to be a phase transition at $\epsilon_F \approx -2.5$ eV where the polarised triplet coupling becomes zero and consequently stops contributing to the superconductivity. While a positive valued λ tells us that we have a superconducting state, to determine what type of symmetry it has we must look at the structure of the eigenvector $\Delta_{\boldsymbol{k}}$. We plot the eigenvector structure for the unpolarised triplet in Figure 5.4, and note that it has a p_y-wave symmetry at high filling, as predicted from our results in Figure 5.1b. At low filling it turns out to have a p_x-wave symmetry.

It is also interesting to see how the coupling coefficient varies for different spin spiral periodicities in the SPFMI layer. Recalling that the smallest possible period of our system is 5 atoms we compute the coupling for a few larger periods in addition to 5, plotting the results for both unpolarised and polarised spin triplet pairs in Figure 5.5 at $\epsilon_F = -1$ eV. While the polarised triplet coupling quickly vanishes for increasing periodicities; again indicating some phase transition; the unpolarised triplet pairing seems to increase linearly at larger periods. Such a linear trend can obviously not continue indefinitely, at some point the spin period becomes so large that the magnetic system approaches something

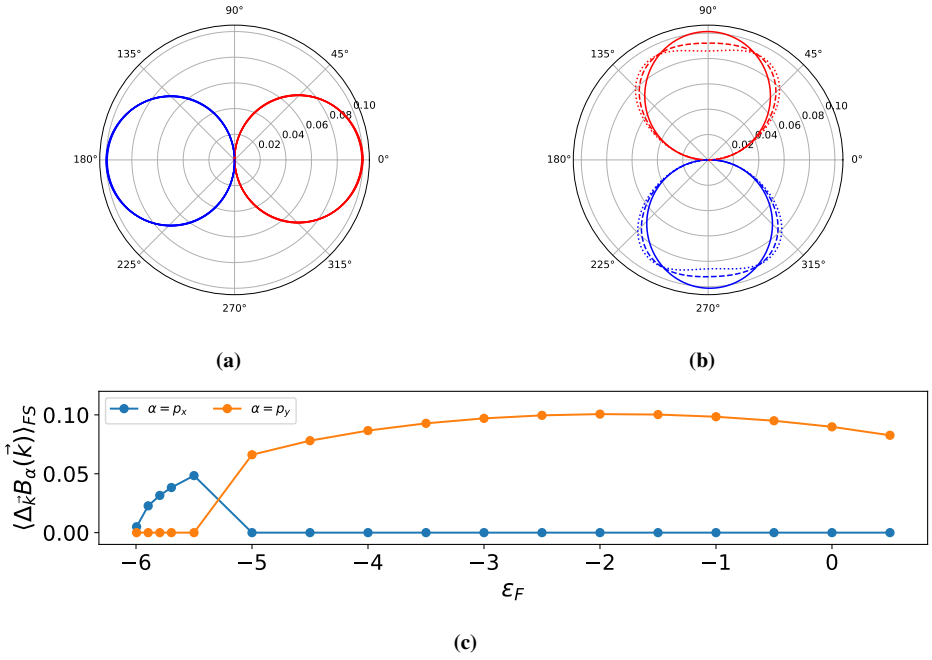

Figure 5.4: Gap structure on the Fermi surface for an unpolarised triplet state at the critical temperature. The normalised magnitude of $\Delta_{\boldsymbol{k}}$ is plotted in a) and b), with the colour indicating the sign difference (red/blue). Figure a) shows the p_x-wave structure at low filling ($\epsilon_F \leq -5.5$ eV), while b) shows a p_y-wave structure at high filling (solid line: $\epsilon_F = -5$ eV, dashed line: $\epsilon_F = 0$ eV, dotted line: $\epsilon_F = 0.5$ eV). Figure c) shows the gap projection onto both p-wave symmetry channels on the Fermi surface.

that looks like a collinear FMI. There is a point where the spin period is large enough that the assumption of a net-zero magnetisation not contributing to the NM spectrum becomes questionable. In any case, we see that the coupling coefficients for our system are very small and the resulting critical temperatures for these simulations would basically be zero given T_c's exponential dependence on λ. However, this extreme sensitivity to the coupling constant consequently makes critical temperature calculations very unreliable, and so for a qualitative understanding it is better to just analyse the variation of λ. The reason we get very small coupling constants in our approximation on the Fermi surface could be the fact that the magnon spectrum mass gap eliminates any divergences of the potential on the Fermi surface, unlike the FMI and AFMI examples of [6], [8] where there is no such magnon mass gap. In the case of a fully uncompensated collinear AFMI, the magnon squeezing parameters additionally provide the potential with an enormous enhancement factor for low-energy magnons.

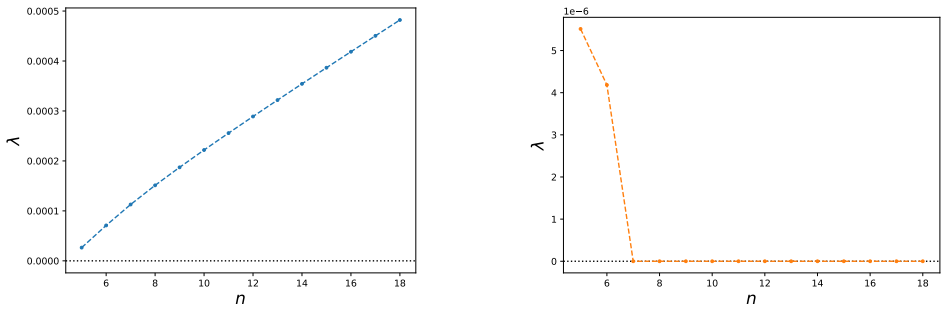

(a) **(b)**

Figure 5.5: Coupling coefficient for scattering on the Fermi surface at $\epsilon_F \approx -1$ eV as a function of the spin period in the SPFMI. Figures a) and b) show the cases of unpolarised and polarised spin triplet Cooper pairs respectively.

5.2.3 Remarks on a full BZ analysis of the superconducting gap

It is important to state that our results for the superconducting gap should be regarded as qualitative; a consequence of the rather severe approximation of ignoring the singularities in the BCS potential. A more correct treatment of the superconducting gap would be to follow the example of Thingstad et al. [44] by computing the gap function as an eigenvalue problem over the entire 1$^{\text{st}}$ BZ with additional sampled points closely around the Fermi surface where the BCS potential has a nontrivial structure. The continuum limit gap function which is described by an integral can be calculated numerically for such a non-uniform grid of k-points by approximating the integral as a weighted sum; with the weights given by a Delaunay triangulation. While such a treatment worked well for Thingstad et al. since they could invoke symmetry in order to analyse only a twelfth of the BZ in addition to considering no more than 4 bosonic modes, our problem becomes significantly more complicated. We made no assumptions of the symmetry of the superconducting state, as it is one of the things we would like to determine, and so we must analyse the entire BZ. Also, we have more than 10 magnon modes making the structure of the BCS potential very complicated in addition to it being significantly weaker than the phonon-mediated interaction studied in [44]. In order to faithfully capture the details of the potential we would therefore need a very good resolution of k-points close to the Fermi surface. It is also essential that one has sufficient resolution to resolve the shape of $\chi_{\boldsymbol{k}'}$ at T_c [45]. Although an attempt was made by using approximately 4000 points on the BZ (most of them on an annulus around the Fermi surface) it seems like a significantly better resolution is required.

5.3 The Eliashberg electron-boson spectral function

An alternative method of describing superconductivity is through Eliashberg theory, where one of the central quantities is the electron-boson spectral function $\alpha^2F(\omega)$ (sometimes just called the Eliashberg function). The electron-boson spectral function is defined as a

double average of the electron-boson coupling matrix over the Fermi surface [46]–[49], often written as

$$\alpha^2 F(\omega) = \frac{1}{D_0} \sum_{\boldsymbol{k},\boldsymbol{k'},\nu} \left| g^{\nu}_{\boldsymbol{k},\boldsymbol{k'}} \right|^2 \delta(\epsilon_{\boldsymbol{k}}) \delta(\epsilon_{\boldsymbol{k'}}) \delta(\omega - \omega_{\boldsymbol{k}-\boldsymbol{k'},\nu}). \tag{5.42}$$

Here D_0 is the density of states at the Fermi surface. We find the electron-boson coupling matrix $g^{\nu}_{\boldsymbol{k},\boldsymbol{k'}}$ from the electron-boson interaction in the Hamiltonian, which in general takes the form

$$\mathcal{H}_{e-b} = \sum_{\boldsymbol{k},\boldsymbol{q},\nu} \sum_{\sigma,\sigma'} \left(g^{\nu}_{\boldsymbol{k},\boldsymbol{q},\sigma,\sigma'} \varphi_{\boldsymbol{q},\nu} c^{\dagger}_{\boldsymbol{k}+\boldsymbol{q},\sigma} c_{\boldsymbol{k}^{\dagger},\sigma'} + \text{h.c} \right). \tag{5.43}$$

Whatever boson of mode ν and wavevector $\boldsymbol{q}$ chosen to mediate this interaction is created and annihilated by the operators $\varphi_{\boldsymbol{q},\nu}$ and $\varphi^{\dagger}_{\boldsymbol{q},\nu}$ respectively. As we have seen, the magnon modes of a non-collinear FMI can couple to several different electron spin structures. Typically phonon-mediated superconductivity is studied where there is only a single spin structure so that this is not a problem. We therefore generalise Eqn. (5.42) to include different spin structure coupling strengths

$$\alpha^2 F(\omega) = \frac{1}{D_0} \sum_{\boldsymbol{k},\boldsymbol{k'},\nu} \sum_{\alpha,\alpha'} \left| g^{\nu}_{\boldsymbol{k},\boldsymbol{k'},\alpha,\alpha'} \right|^2 \delta(\epsilon_{\boldsymbol{k},\alpha}) \delta(\epsilon_{\boldsymbol{k'},\alpha'}) \delta(\omega - \omega_{\boldsymbol{k}-\boldsymbol{k'},\nu}). \tag{5.44}$$

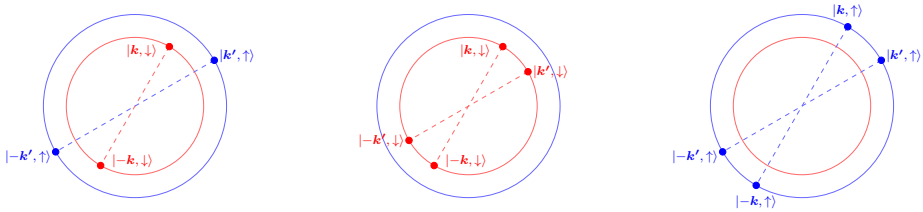

(a) **(b)** **(c)**

Figure 5.6: Schematic of the possible BCS scattering processes in the case of electron bands that are non-degenerate in spin quantum number.

With our choice of only opposite-momenta scattering processes there cannot be any contribution from unpolarised Cooper pairs if the single electron dispersion relation is non-degenerate for different spin (the possible scattering processes in this case are illustrated in Figure 5.6). In our case the electron dispersion is degenerate so that all pairings may contribute. We rewrite Eqn. (4.13) so that it resembles Eqn. (5.43)

$$\mathcal{H}^{(\rho)}_{e-m} = \sum_{\substack{\boldsymbol{k},\boldsymbol{q},\nu \\ \alpha,\alpha'}} \left[\left(g^{\alpha\alpha'}_{\rho} u_{\boldsymbol{q}\rho\nu} + g^{\alpha'\alpha}_{\rho} v^{*}_{-\boldsymbol{q}\rho\nu} \right) A_{\boldsymbol{q}\nu} c^{\dagger}_{\boldsymbol{k}+\boldsymbol{q},\alpha} c_{\boldsymbol{k},\alpha'} + \text{h.c} \right]. \tag{5.45}$$

Determining $g^{\nu}_{\boldsymbol{k},\boldsymbol{q},\sigma,\sigma'}$ in Eqn. (5.44) is now simply a matter of reading out the coefficient from Eqn. (5.45), which yields the following expression for the SPFMI / NM electron-magnon spectral function

$$\begin{aligned}\alpha^2F(\omega) = \frac{1}{D_0}\sum_{\boldsymbol{k},\boldsymbol{k'},\nu}\sum_{\alpha,\alpha'}\Bigg(\sum_{\rho,\rho'}\Big(g_{\rho}^{\alpha\alpha'}g_{\rho'}^{\alpha\alpha'}(u_{\boldsymbol{q}\rho\nu}u^*_{\boldsymbol{q}\rho'\nu}+v^*_{-\boldsymbol{q}\rho\nu}v_{-\boldsymbol{q}\rho'\nu}) \\ + g_{\rho}^{\alpha'\alpha}g_{\rho'}^{\alpha\alpha'}(v^*_{-\boldsymbol{q}\rho\nu}u^*_{\boldsymbol{q}\rho'\nu}+u_{\boldsymbol{q}\rho\nu}v_{-\boldsymbol{q}\rho'\nu})\Big)\Bigg)\times\delta(\epsilon_{\boldsymbol{k}})\delta(\epsilon_{\boldsymbol{k'}})\delta(\omega-\omega_{\boldsymbol{q},\nu}).\end{aligned} \tag{5.46}$$

For notation purposes we have kept the label $\boldsymbol{q} = \boldsymbol{k} - \boldsymbol{k'}$. There are some problems to address before a numerical calculation of this expression can be done. Even though the delta functions in single particle electron dispersion restricts the sum of $\boldsymbol{k}$'s to momenta on the Fermi surface one cannot hope to achieve a sufficient resolution so that a delta function in magnon dispersion gives correct results. Consequently we approximate $\delta(\omega-\omega_{\boldsymbol{k}-\boldsymbol{k'},\nu})$ by instead using a narrow rectangular function of unit area. We must also get rid of the system size dependence in order to perform an analysis in the continuum limit. Looking at the form of D_0 and $g_{\rho}^{\alpha\alpha'}$ we see that in total the sum has a factor of $1/N^2$, so we may rewrite the sum to an integral that is independent of N

$$\begin{aligned}\alpha^2F(\omega) = \frac{N^2}{D_0}\sum_{\alpha,\alpha',\nu}\int_{\mathrm{FS}}\frac{d\boldsymbol{k}d\boldsymbol{k'}}{A^2_{\mathrm{BZ}}}\Bigg(\sum_{\rho,\rho'}\Big(g_{\rho}^{\alpha\alpha'}g_{\rho'}^{\alpha\alpha'}(u_{\boldsymbol{q}\rho\nu}u^*_{\boldsymbol{q}\rho'\nu}+v^*_{-\boldsymbol{q}\rho\nu}v_{-\boldsymbol{q}\rho'\nu}) \\ + g_{\rho}^{\alpha'\alpha}g_{\rho'}^{\alpha\alpha'}(v^*_{-\boldsymbol{q}\rho\nu}u^*_{\boldsymbol{q}\rho'\nu}+u_{\boldsymbol{q}\rho\nu}v_{-\boldsymbol{q}\rho'\nu})\Big)\Bigg)\times\frac{1}{\Delta\omega}\mathrm{rect}\left(\frac{\omega-\omega_{\boldsymbol{q},\nu}}{\Delta\omega}\right).\end{aligned} \tag{5.47}$$

In a similar fashion to Eq. (5.38) we find here that the expression can be calculated as an average of sampled points over the Fermi surface. One of the important quantities we can calculate from the electron-boson spectral function is the Eliashberg electron-boson coupling constant

$$\lambda = 2\int_0^{\infty}\frac{d\omega}{\omega}\alpha^2F(\omega). \tag{5.48}$$

Figure 5.7 shows a numerical calculation of the Eliashberg electron-boson spectral function and coupling constant. Here we again get a quite small coupling strength, albeit a bit larger than that calculated from the gap function eigenvalue problem on the Fermi surface.

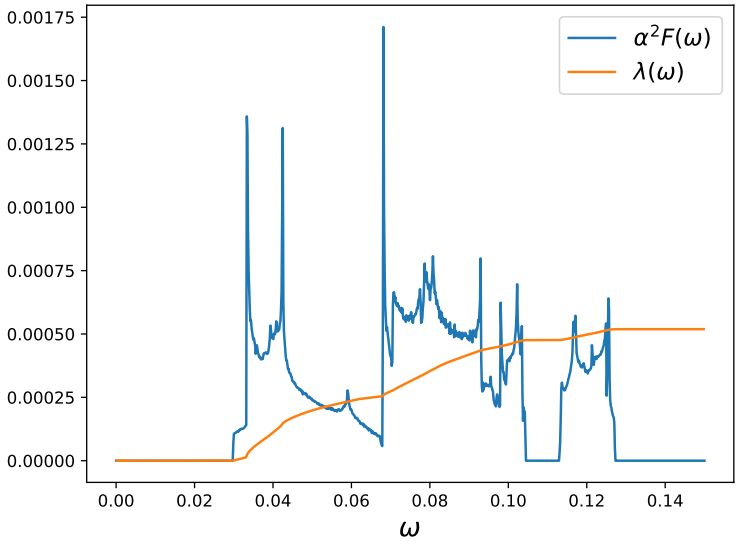

Figure 5.7: Eliashberg electron-boson spectral function and coupling constant for a SPFMI / NM bilayer with a spin period of 6 atoms at an approximately circular Fermi surface of radius $k_F = a^{-1}$.

Chapter 6

Conclusion and Outlook

We have utilised the general rotation model presented by Fishman [35] to develop a framework for working with magnon mediated superconductivity at the interface of a metal and a non-collinear in-plane magnetic structure of zero net magnetisation. Although the thesis limits itself to studying a 2D magnetic structure the same principles can easily be generalised to 3D skyrmion lattices, with the downside of yielding a theory of much uglier mathematical expressions. Furthermore we have tested that the framework in the specific case of a collinear antiferromagnetic insulator gives a description that agrees with previous studies [8]. The framework was also applied to a bilayer with a spiral spin structure on a triangular grid, for which both electronic and magnonic spectra were found and incorporated into an effective interaction describing the magnon mediated electron-electron coupling. This bilayer model was found to in theory allow for p-wave superconductivity with the addition of polarised $S_z = \pm 1$ Cooper pairs. However, the magnon mediated coupling for superconductivity in this specific system is estimated to be very weak even without considering Coulomb interactions, with the unpolarised triplet pairs dominating; although as a result of the complicated form of the pair potential the findings should be treated in a mostly qualitative manner. This was a necessary consequence of approximating the BCS potential to be constant in k-space magnitude, and while such approximations seem common in BCS theory there is the danger of losing too much information about the pair interaction. It would be desirable to perform a more complete calculation of the superconducting gap as done by Tingstad et al. [44], but with our significantly weaker and more complicated interaction a sufficient sampling of k-points was hard to achieve. An investigation of the Eliashberg electron-magnon spectral function provided further indications that the superconducting coupling constant will indeed be quite weak. We conclude that the spiral spin structure in a triangular lattice is not optimal for electron-magnon coupling, but the emergence of polarised triplet pairs is interesting. We attribute the creation of polarised triplet pairs to rotation of the spins as they scatter on the non-collinear spin structure.

Even if the specific non-collinear structure studied here with our given parameters may not give the best superconducting attributes this does not rule out other non-collinear struc-

tures being good superconducting mediators, and finding such a structure could be the focus of future investigations. One of the most interesting properties of the non-collinearity was the possible appearance of spin polarised Cooper pairs, which could be applied in spintronic logic devices, motivating the search for a bilayer with non-collinear structure where the polarised terms dominate. Another interesting avenue to explore would be a metal coupled to an insulating skyrmion crystal with topological magnonic states [50], or using a topological insulator instead of a metal, with the aim of finding a tunable ”topological superconductivity”. For an experimental study of such systems the metallic part should consist of a non-magnetic metal that does not become a superconductor at low temperatures, allowing us to be sure that any measured superconductivity is indeed mediated by magnons in the magnetic part. Some suggestions would be monoatomic layers of copper, silver or gold [13]. As for the non-collinear magnetic insulator part, a typical material seems to be Cu_2OSeO_3 [51], [52].

Bibliography

[1] H. K. Onnes *et al.*, *Through Measurement to Knowledge: the Selected Papers of Heike Kamerlingh Onnes 1853-1926*. 1991, [Online]. Available: http://link.springer.com/openurl?genre=book&isbn=978-94-010-7433-9.

[2] L. D. Landau and D. t. Haar, *Collected papers of L.D. Landau*. Oxford London Edinburgh: Pergamon Press, 1965.

[3] J. Bardeen *et al.*, "Theory of Superconductivity," *Physical Review*, vol. 108, no. 5, pp. 1175–1204, Dec. 1957, DOI: 10.1103/PhysRev.108.1175.

[4] J. Linder and J. W. A. Robinson, "Superconducting Spintronics," *Nature Physics*, vol. 11, no. 4, pp. 307–315, Apr. 2015, arXiv: 1510.00713, DOI: 10.1038/nphys3242.

[5] X. Gong *et al.*, "Time-reversal symmetry-breaking superconductivity in epitaxial bismuth/nickel bilayers," *Science Advances*, vol. 3, no. 3, e1602579, Mar. 2017, Publisher: American Association for the Advancement of Science, DOI: 10.1126/sciadv.1602579.

[6] N. Rohling *et al.*, "Superconductivity induced by interfacial coupling to magnons," *Physical Review B*, vol. 97, no. 11, p. 115 401, Mar. 2018, DOI: 10.1103/PhysRevB.97.115401.

[7] E. L. Fjærbu *et al.*, "Superconductivity at metal-antiferromagnetic insulator interfaces," *Physical Review B*, vol. 100, no. 12, p. 125 432, Sep. 2019, DOI: 10.1103/PhysRevB.100.125432.

[8] E. Erlandsen *et al.*, "Enhancement of superconductivity mediated by antiferromagnetic squeezed magnons," *Physical Review B*, vol. 100, no. 10, p. 100 503, Sep. 2019, DOI: 10.1103/PhysRevB.100.100503.

[9] E. Erlandsen *et al.*, "Magnon-mediated superconductivity on the surface of a topological insulator," *Physical Review B*, vol. 101, no. 9, p. 094 503, Mar. 2020, DOI: 10.1103/PhysRevB.101.094503.

[10] E. Erlandsen and A. Sudbø, "Schwinger boson study of superconductivity mediated by antiferromagnetic spin-fluctuations," *Physical Review B*, vol. 102, no. 21, p. 214 502, Dec. 2020, arXiv: 2009.07862, DOI: 10.1103/PhysRevB.102.214502.

[11] I. Dzyaloshinsky, "A thermodynamic theory of "weak" ferromagnetism of antiferromagnetics," *Journal of Physics and Chemistry of Solids*, vol. 4, no. 4, pp. 241–255, Jan. 1958, DOI: 10.1016/0022-3697(58)90076-3.

[12] T. Moriya, "Anisotropic Superexchange Interaction and Weak Ferromagnetism," *Physical Review*, vol. 120, no. 1, pp. 91–98, Oct. 1960, DOI: 10.1103/PhysRev.120.91.

[13] C. Kittel *et al.*, *Introduction to solid state physics*, 8th ed. Wiley, 2015.

[14] J. O. Andersen, *Introduction to statistical mechanics*, First edition. Trondheim, Norway: Akademika forlag, 2012.

[15] A. Sudbø, "Lecture notes in Quantum Theory of Solids," Unpublished, NTNU.

[16] T. Holstein and H. Primakoff, "Field Dependence of the Intrinsic Domain Magnetization of a Ferromagnet," *Physical Review*, vol. 58, no. 12, pp. 1098–1113, Dec. 1940, DOI: 10.1103/PhysRev.58.1098.

[17] S. V. Kusminskiy, *Quantum Magnetism, Spin Waves, and Light*. 2019, DOI: 10.1007/978-3-030-13345-0.

[18] J. R. Schrieffer and P. A. Wolff, "Relation between the Anderson and Kondo Hamiltonians," *Physical Review*, vol. 149, no. 2, pp. 491–492, Sep. 1966, Publisher: American Physical Society, DOI: 10.1103/PhysRev.149.491.

[19] C. Tsallis, "Diagonalization methods for the general bilinear Hamiltonian of an assembly of bosons," *Journal of Mathematical Physics*, vol. 19, no. 1, pp. 277–286, Jan. 1978, DOI: 10.1063/1.523549.

[20] J. H. P. Colpa, "Diagonalization of the quadratic boson hamiltonian," *Physica A: Statistical Mechanics and its Applications*, vol. 93, no. 3, pp. 327–353, Sep. 1978, DOI: 10.1016/0378-4371(78)90160-7.

[21] M.-w. Xiao, "Theory of transformation for the diagonalization of quadratic Hamiltonians," *arXiv:0908.0787 [math-ph]*, Aug. 2009, arXiv: 0908.0787, [Online]. Available: http://arxiv.org/abs/0908.0787.

[22] K. Mæland, "Excitation Spectrum of a Weakly Interacting Spin-Orbit Coupled Bose-Einstein Condensate," M.S. thesis, NTNU, Trondheim, Nov. 2020.

[23] J. Benestad, "Magnon-spectra in quantum magnets with non-collinear ground states," Unpublished, Trondheim, Dec. 2021.

[24] A. Akhmerov, *Connecting the dots*, [Online]. Available: quantumtinkerer.tudelft.nl/blog/connecting-the-dots/.

[25] C. W. Groth *et al.*, "Kwant: A software package for quantum transport," *New Journal of Physics*, vol. 16, no. 6, p. 063 065, Jun. 2014, Publisher: IOP Publishing, DOI: 10.1088/1367-2630/16/6/063065.

[26] H. W. Kuhn, "The Hungarian method for the assignment problem," *Naval Research Logistics Quarterly*, vol. 2, no. 1-2, pp. 83–97, 1955, DOI: https://doi.org/10.1002/nav.3800020109.

[27] E. Thingstad, "Triangular lattice basis functions," NTNU, Feb. 2021.

[28] E. Otnes, "Symmetrien til ordensparameteren i en høy T_c superleder," M.S. thesis, NTNU, Trondheim, Nov. 1996.

[29] F. Aryasetiawan, "Group Theory," Lund University, Jan. 2019, [Online]. Available: http://home.thep.lu.se/~malin/FYTN13/GroupTheoryFerdi19.pdf.

[30] E. Kogan and G. Gumbs, "Green's Functions and DOS for Some 2D Lattices," *SCIRP*, vol. 10, no. 1, pp. 1–12, Dec. 2020, Number: 1 Publisher: Scientific Research Publishing, DOI: 10.4236/graphene.2021.101001.

[31] A. Weh, *GfTool*, https://github.com/DerWeh/gftools/tree/0.11.0, May 2022.

[32] K. Yosida, "The Status of the Theories of Magnetic Anisotropy," *Journal of Applied Physics*, vol. 39, no. 2, pp. 511–518, Feb. 1968, DOI: 10.1063/1.2163506.

[33] T. Yildirim *et al.*, "Anisotropic spin Hamiltonians due to spin-orbit and Coulomb exchange interactions," *Physical Review B*, vol. 52, no. 14, pp. 10 239–10 267, Oct. 1995, DOI: 10.1103/PhysRevB.52.10239.

[34] Y. Sizyuk *et al.*, "Importance of anisotropic exchange interactions in honeycomb iridates: Minimal model for zigzag antiferromagnetic order in Na_2IrO_3," *Physical Review B*, vol. 90, no. 15, p. 155 126, Oct. 2014, DOI: 10.1103/PhysRevB.90.155126.

[35] R. S. Fishman, "Double exchange in a magnetically frustrated system," *Journal of Physics: Condensed Matter*, vol. 16, no. 30, pp. 5483–5501, Jul. 2004, Publisher: IOP Publishing, DOI: 10.1088/0953-8984/16/30/011.

[36] J. T. Haraldsen and R. S. Fishman, "Spin rotation technique for non-collinear magnetic systems: Application to the generalized Villain model," *Journal of Physics: Condensed Matter*, vol. 22, no. 50, p. 509 801, Dec. 2010, DOI: 10.1088/0953-8984/22/50/509801.

[37] A. Roldán-Molina *et al.*, "Quantum theory of spin waves in finite chiral spin chains," *Physical Review B*, vol. 89, no. 5, p. 054 403, Feb. 2014, DOI: 10.1103/PhysRevB.89.054403.

[38] A. Roldán-Molina *et al.*, "Quantum fluctuations stabilize skyrmion textures," *Physical Review B*, vol. 92, no. 24, p. 245 436, Dec. 2015, DOI: 10.1103/PhysRevB.92.245436.

[39] A. L. Fetter and J. D. Walecka, *Quantum theory of many-particle systems*. Mineola, N.Y: Dover Publications, 2003.

[40] C. Kittel and C. Y. Fong, *Quantum theory of solids*, 2nd rev. print. New York: Wiley, 1987.

[41] K. K. L. Lockert, "Phonon Coupled Luttinger Liquids in a Haldane Armchair Nanoribbon," M.S. thesis, NTNU, Trondheim, Jun. 2021.

[42] M. Sigrist and K. Ueda, "Phenomenological theory of unconventional superconductivity," *Reviews of Modern Physics*, vol. 63, no. 2, pp. 239–311, Apr. 1991, DOI: 10.1103/RevModPhys.63.239.

[43] N. H. Aase, "Slave-boson approach to the U=∞ Haldane-Hubbard model," M.S. thesis, NTNU, Trondheim, Jun. 2021.

[44] E. Thingstad *et al.*, "Phonon-mediated superconductivity in doped monolayer materials," *Physical Review B*, vol. 101, no. 21, p. 214 513, Jun. 2020, DOI: 10.1103/PhysRevB.101.214513.

[45] E. Thingstad, *Private communication*, 2022.

[46] P. B. Allen and B. Mitrović, "Theory of Superconducting Tc," in *Solid State Physics*, H. Ehrenreich *et al.*, Eds., vol. 37, Academic Press, Jan. 1983, pp. 1–92, DOI: 10.1016/S0081-1947(08)60665-7.

[47] G. Ummarino, "Eliashberg Theory," in *Emergent Phenomena in Correlated Matter Modeling and Simulation*, Forschungszentrum Jülich, 2013.

[48] M. V. Sadovskii, "Electron–Phonon Coupling in Eliashberg–McMillan Theory Beyond Adiabatic Approximation," *Journal of Experimental and Theoretical Physics*, vol. 128, no. 3, pp. 455–463, Mar. 2019, DOI: 10.1134/S1063776119020122.

[49] S. K. Bose and J. Kortus, "Electron-phonon coupling in metallic solids from density functional theory," in *Vibronic interactions and Electron-Phonon Interactions and Their Role in Modern Chemistry and Physics*, 2009.

[50] K. Mæland and A. Sudbø, "Quantum topological phase transitions in skyrmion crystals," May 2022, [Online]. Available: http://arxiv.org/abs/2205.12965.

[51] L. V. Abdurakhimov *et al.*, "Magnon-photon coupling in the noncollinear magnetic insulator Cu_2OSeO_3," *Physical Review B*, vol. 99, no. 14, p. 140 401, Apr. 2019, DOI: 10.1103/PhysRevB.99.140401.

[52] F. Qian *et al.*, "New magnetic phase of the chiral skyrmion material Cu_2OSeO_3," *Science Advances*, vol. 4, no. 9, Sep. 2018, Publisher: American Association for the Advancement of Science, DOI: 10.1126/sciadv.aat7323.

Appendix A

Non-collinear magnet

A.1 Elements of the rotated interaction matrix

The elements of W^{ij} are as follows:

$$\begin{aligned} W^{ij}_{xx} = &(J_x \cos\theta_i \cos\psi_i - D^{ij}_y \sin\theta_i - D^{ij}_z \cos\theta_i \sin\psi_i) \cos\theta_j \cos\psi_j \\ &+ (J_y \cos\theta_i \sin\psi_i + D^{ij}_x \sin\theta_i + D^{ij}_z \cos\theta_i \cos\psi_i) \cos\theta_j \sin\psi_j \\ &+ (J_z \sin\theta_i - D^{ij}_x \cos\theta_i \sin\psi_i + D^{ij}_y \cos\theta_i \cos\psi_i) \sin\theta_j, \end{aligned} \tag{A.1}$$

$$\begin{aligned} W^{ij}_{xy} = &(J_y \cos\theta_i \sin\psi_i + D^{ij}_x \sin\theta_i + D^{ij}_z \cos\theta_i \cos\psi_i) \cos\psi_j \\ &- (J_x \cos\theta_i \cos\psi_i - D^{ij}_y \sin\theta_i - D^{ij}_z \cos\theta_i \sin\psi_i) \sin\psi_j, \end{aligned} \tag{A.2}$$

$$\begin{aligned} W^{ij}_{xz} = &(J_x \cos\theta_i \cos\psi_i - D^{ij}_y \sin\theta_i - D^{ij}_z \cos\theta_i \sin\psi_i) \sin\theta_j \cos\psi_j \\ &+ (J_y \cos\theta_i \sin\psi_i + D^{ij}_x \sin\theta_i + D^{ij}_z \cos\theta_i \cos\psi_i) \sin\theta_j \sin\psi_j \\ &- (J \sin\theta_i - D^{ij}_x \cos\theta_i \sin\psi_i + D^{ij}_y \cos\theta_i \cos\psi_i) \cos\theta_j, \end{aligned} \tag{A.3}$$

$$\begin{aligned} W^{ij}_{yx} = &(J_y \cos\psi_i - D^{ij}_z \sin\psi_i) \cos\theta_j \sin\psi_j \\ &- (J_x \sin\psi_i + D^{ij}_z \cos\psi_i) \cos\theta_j \cos\psi_j \\ &- (D^{ij}_y \sin\psi_i + D^{ij}_x \cos\psi_i) \sin\theta_j, \end{aligned} \tag{A.4}$$

$$W^{ij}_{yy} = (J_x \sin\psi_i + D^{ij}_z \cos\psi_i) \sin\psi_j + (J_y \cos\psi_i - D^{ij}_z \sin\psi_i) \cos\psi_j, \tag{A.5}$$

$$\begin{aligned} W^{ij}_{yz} = &(J_y \cos\psi_i - D^{ij}_z \sin\psi_i) \sin\theta_j \sin\psi_j \\ &- (J_x \sin\psi_i + D^{ij}_z \cos\psi_i) \sin\theta_j \cos\psi_j \\ &+ (D^{ij}_x \cos\psi_i + D^{ij}_y \sin\psi_i) \cos\theta_j, \end{aligned} \tag{A.6}$$

$$
\begin{aligned}
W_{zx}^{ij} = {} & (J_x \sin\theta_i \cos\psi_i + D_y^{ij} \cos\theta_i - D_z^{ij} \sin\theta_i \sin\psi_i) \cos\theta_j \cos\psi_j \\
& + (J_y \sin\theta_i \sin\psi_i - D_x^{ij} \cos\theta_i + D_z^{ij} \sin\theta_i \cos\psi_i) \cos\theta_j \sin\psi_j \\
& - (J_z \cos\theta_i + D_x^{ij} \sin\theta_i \sin\psi_i - D_y^{ij} \sin\theta_i \cos\psi_i) \sin\theta_j ,
\end{aligned} \tag{A.7}
$$

$$
\begin{aligned}
W_{zy}^{ij} = {} & (J_y \sin\theta_i \sin\psi_i - D_x^{ij} \cos\theta_i + D_z^{ij} \sin\theta_i \cos\psi_i) \cos\psi_j \\
& - (J_x \sin\theta_i \cos\psi_i + D_y^{ij} \cos\theta_i - D_z^{ij} \sin\theta_i \sin\psi_i) \sin\psi_j ,
\end{aligned} \tag{A.8}
$$

$$
\begin{aligned}
W_{zz}^{ij} = {} & (J_x \sin\theta_i \cos\psi_i + D_y^{ij} \cos\theta_i - D_z^{ij} \sin\theta_i \sin\psi_i) \sin\theta_j \cos\psi_j \\
& + (J_y \sin\theta_i \sin\psi_i - D_x^{ij} \cos\theta_i + D_z^{ij} \sin\theta_i \cos\psi_i) \sin\theta_j \sin\psi_j \\
& + (J_z \cos\theta_i + D_x^{ij} \sin\theta_i \sin\psi_i - D_y^{ij} \sin\theta_i \cos\psi_i) \cos\theta_j .
\end{aligned} \tag{A.9}
$$

Appendix B

Effective interaction

B.1 Schrieffer-Wolff transformation

We identify the different parts of the interaction Hamiltonian

$$\begin{aligned}\eta\mathcal{H}_1^{(\Omega)} = \sum_{\substack{\boldsymbol{k},\boldsymbol{q},\Gamma\\ \alpha,\alpha'}} g_\Omega^{\alpha\alpha'}\Big(u_{\boldsymbol{q}\Omega\Gamma}\underbrace{A_{\boldsymbol{q}\Gamma}c^\dagger_{\boldsymbol{k}+\boldsymbol{q},\alpha}c_{\boldsymbol{k},\alpha'}}_{(1)} + v_{\boldsymbol{q}\Omega\Gamma}\underbrace{A^\dagger_{-\boldsymbol{q}\Gamma}c^\dagger_{\boldsymbol{k}+\boldsymbol{q},\alpha}c_{\boldsymbol{k},\alpha'}}_{(2)}\\ + u^*_{\boldsymbol{q}\Omega\Gamma}\underbrace{A^\dagger_{\boldsymbol{q}\Gamma}c^\dagger_{\boldsymbol{k},\alpha'}c_{\boldsymbol{k}+\boldsymbol{q},\alpha}}_{(3)} + v^*_{\boldsymbol{q}\Omega\Gamma}\underbrace{A_{-\boldsymbol{q}\Gamma}c^\dagger_{\boldsymbol{k},\alpha'}c_{\boldsymbol{k}+\boldsymbol{q},\alpha}}_{(4)}\Big),\end{aligned} \tag{B.1}$$

and write our ansatz for the corresponding generator of a canonical transformation that should give an effective Hamiltonian where the terms of linear order in boson operators:

$$\begin{aligned}\eta\mathcal{S}^{(\Omega)} = \sum_{\substack{\boldsymbol{k},\boldsymbol{q},\Gamma\\ \alpha,\alpha'}} g_\Omega^{\alpha\alpha'}\Big(\mathcal{X}^{(1)}u_{\boldsymbol{q}\Omega\Gamma}A_{\boldsymbol{q}\Gamma}c^\dagger_{\boldsymbol{k}+\boldsymbol{q},\alpha}c_{\boldsymbol{k},\alpha'} + \mathcal{X}^{(2)}v_{\boldsymbol{q}\Omega\Gamma}A^\dagger_{-\boldsymbol{q}\Gamma}c^\dagger_{\boldsymbol{k}+\boldsymbol{q},\alpha}c_{\boldsymbol{k},\alpha'}\\ + \mathcal{X}^{(3)}u^*_{\boldsymbol{q}\Omega\Gamma}A^\dagger_{\boldsymbol{q}\Gamma}c^\dagger_{\boldsymbol{k},\alpha'}c_{\boldsymbol{k}+\boldsymbol{q},\alpha} + \mathcal{X}^{(4)}v^*_{\boldsymbol{q}\Omega\Gamma}A_{-\boldsymbol{q}\Gamma}c^\dagger_{\boldsymbol{k},\alpha'}c_{\boldsymbol{k}+\boldsymbol{q},\alpha}\Big).\end{aligned} \tag{B.2}$$

The Hamiltonian describing isolated NM and SPFMI layers is

$$\mathcal{H}_0 = \sum_{\boldsymbol{k}\alpha} E_{\boldsymbol{k}\alpha}c^\dagger_{\boldsymbol{k},\alpha}c_{\boldsymbol{k},\alpha} + \sum_{\boldsymbol{q}}\omega_{\boldsymbol{q}\Gamma}a^\dagger_{\boldsymbol{q}\Gamma}a_{\boldsymbol{q}\Gamma} \tag{B.3}$$

The task is to determine the unknown coefficients in the generator, which we can find by using the fact that it has a similar form as the interaction Hamiltonian. This is done by projecting Eq. (2.18) onto certain states that count the number of fermions and bosons with quantum numbers matching the terms of the interaction Hamiltonian.

$$\langle n|\,\eta\mathcal{H}_1^{(\Omega)}\,|m\rangle = \langle n|\left(\mathcal{H}_0\eta S^{(\Omega)} - \eta S^{(\Omega)}\mathcal{H}_0\right)|m\rangle\,. \tag{B.4}$$

We now analyse term by term.

Term (1)

Let

$$\langle n| = \langle \boldsymbol{k}+\boldsymbol{q}, \alpha; 0| \,,$$

$$|m\rangle = |\boldsymbol{k}, \alpha'; \boldsymbol{q}, \Gamma\rangle \,.$$

Then

$$\langle n| \left(\mathcal{H}_0 \eta S^{(\Omega)} - \eta S^{(\Omega)} \mathcal{H}_0 \right) |m\rangle = \left(E_{\boldsymbol{k}+\boldsymbol{q},\alpha} - E_{\boldsymbol{k},\alpha'} - \omega_{\boldsymbol{q}\Gamma} \right) \langle n| \, \eta S^{(\Omega)} \, |m\rangle \,, \tag{B.5}$$

so that

$$\langle n| \, \eta S^{(\Omega)} \, |m\rangle = \mathcal{X}^{(1)} \, \langle n| \, \eta \mathcal{H}_1^{(\Omega)} \, |m\rangle = \frac{\langle n| \, \eta \mathcal{H}_1^{(\Omega)} \, |m\rangle}{E_{\boldsymbol{k}+\boldsymbol{q},\alpha} - E_{\boldsymbol{k},\alpha'} - \omega_{\boldsymbol{q}\Gamma}} \tag{B.6}$$

Term (2)

Let

$$\langle n| = \langle \boldsymbol{k}+\boldsymbol{q}, \alpha; -\boldsymbol{q}, \Gamma| \,,$$

$$|m\rangle = |\boldsymbol{k}, \alpha'; 0\rangle \,.$$

Then

$$\langle n| \left(\mathcal{H}_0 \eta S^{(\Omega)} - \eta S^{(\Omega)} \mathcal{H}_0 \right) |m\rangle = \left(E_{\boldsymbol{k}+\boldsymbol{q},\alpha} + \omega_{-\boldsymbol{q}\Gamma} - E_{\boldsymbol{k},\alpha'} \right) \langle n| \, \eta S^{(\Omega)} \, |m\rangle \,, \tag{B.7}$$

so that

$$\langle n| \, \eta S^{(\Omega)} \, |m\rangle = \mathcal{X}^{(2)} \, \langle n| \, \eta \mathcal{H}_1^{(\Omega)} \, |m\rangle = \frac{\langle n| \, \eta \mathcal{H}_1^{(\Omega)} \, |m\rangle}{E_{\boldsymbol{k}+\boldsymbol{q},\alpha} - E_{\boldsymbol{k},\alpha'} + \omega_{\boldsymbol{q}\Gamma}} \tag{B.8}$$

Term (3)

Let

$$\langle n| = \langle \boldsymbol{k}, \alpha'; \boldsymbol{q}, \Gamma| \,,$$

$$|m\rangle = |\boldsymbol{k}+\boldsymbol{q}, \alpha; 0\rangle \,.$$

Then

$$\langle n| \left(\mathcal{H}_0 \eta S^{(\Omega)} - \eta S^{(\Omega)} \mathcal{H}_0 \right) |m\rangle = \left(E_{\boldsymbol{k},\alpha'} + \omega_{\boldsymbol{q}\Gamma} - E_{\boldsymbol{k}+\boldsymbol{q},\alpha} \right) \langle n| \, \eta S^{(\Omega)} \, |m\rangle \,, \tag{B.9}$$

so that

$$\langle n| \, \eta S^{(\Omega)} \, |m\rangle = \mathcal{X}^{(3)} \, \langle n| \, \eta \mathcal{H}_1^{(\Omega)} \, |m\rangle = \frac{-\langle n| \, \eta \mathcal{H}_1^{(\Omega)} \, |m\rangle}{E_{\boldsymbol{k}+\boldsymbol{q},\alpha} - E_{\boldsymbol{k},\alpha'} - \omega_{\boldsymbol{q}\Gamma}} \tag{B.10}$$

Term (4)

Let

$$\langle n| = \langle \boldsymbol{k}, \alpha'; 0| \,,$$
$$|m\rangle = |\boldsymbol{k}+\boldsymbol{q}, \alpha; -\boldsymbol{q}, \Gamma\rangle \,.$$

Then

$$\langle n| \left(\mathcal{H}_0 \eta S^{(\Omega)} - \eta S^{(\Omega)} \mathcal{H}_0\right) |m\rangle = \left(E_{\boldsymbol{k},\alpha'} - E_{\boldsymbol{k}+\boldsymbol{q},\alpha} - \omega_{-\boldsymbol{q}\Gamma}\right) \langle n| \eta S^{(\Omega)} |m\rangle \,, \quad \text{(B.11)}$$

so that

$$\langle n| \eta S^{(\Omega)} |m\rangle = \mathcal{X}^{(4)} \langle n| \eta \mathcal{H}_1^{(\Omega)} |m\rangle = \frac{-\langle n| \eta \mathcal{H}_1^{(\Omega)} |m\rangle}{E_{\boldsymbol{k}+\boldsymbol{q},\alpha} - E_{\boldsymbol{k},\alpha'} + \omega_{\boldsymbol{q}\Gamma}}. \quad \text{(B.12)}$$

We determine the coefficients to be

$$\mathcal{X}^{\alpha\alpha'}_{\boldsymbol{k}\boldsymbol{q}\Gamma} = \mathcal{X}^{(1)} = -\mathcal{X}^{(3)} = \frac{1}{E_{\boldsymbol{k}+\boldsymbol{q},\alpha} - E_{\boldsymbol{k},\alpha'} - \omega_{\Gamma,\boldsymbol{q}}} \quad \text{(B.13)}$$

$$\mathcal{Y}^{\alpha\alpha'}_{\boldsymbol{k}\boldsymbol{q}\Gamma} = \mathcal{X}^{(2)} = -\mathcal{X}^{(4)} = \frac{1}{E_{\boldsymbol{k}+\boldsymbol{q},\alpha} - E_{\boldsymbol{k},\alpha'} + \omega_{\Gamma,\boldsymbol{q}}} \quad \text{(B.14)}$$

B.2 Collinear AFMI enhancement factors

The inverse Bogoliubov transformation for an anti-ferromagnet has the well-known form of Eq. (4.56) which can be expressed as

$$T_{\boldsymbol{q}}^{-1} = \begin{bmatrix} u_{\boldsymbol{q}AA} & u_{\boldsymbol{q}AB} & v_{\boldsymbol{q}AA} & v_{\boldsymbol{q}AB} \\ u_{\boldsymbol{q}BA} & u_{\boldsymbol{q}BB} & v_{\boldsymbol{q}BA} & v_{\boldsymbol{q}BB} \\ v^*_{-\boldsymbol{q}AA} & v^*_{-\boldsymbol{q}AB} & u^*_{-\boldsymbol{q}AA} & u^*_{-\boldsymbol{q}AB} \\ v^*_{-\boldsymbol{q}BA} & u^*_{-\boldsymbol{q}BB} & u^*_{-\boldsymbol{q}BA} & u^*_{-\boldsymbol{q}BB} \end{bmatrix} = \begin{bmatrix} u_{\boldsymbol{q}} & 0 & 0 & v_{\boldsymbol{q}} \\ 0 & u_{\boldsymbol{q}} & v_{\boldsymbol{q}} & 0 \\ 0 & v_{\boldsymbol{q}} & u_{\boldsymbol{q}} & 0 \\ v_{\boldsymbol{q}} & 0 & 0 & u_{\boldsymbol{q}} \end{bmatrix}, \quad \text{(B.15)}$$

in the framework of Colpa [20]. from this matrix we read out the expressions in Eqs. (4.37), (4.38), (4.39) and (4.40) to be

$$\begin{aligned} A_1(\boldsymbol{q}, A, \alpha, \alpha', \beta, \beta') &= \sum_{\Omega\Omega'} \left(g_\Omega^{\beta'\beta} g_{\Omega'}^{\alpha\alpha'} u^*_{\boldsymbol{q}\Omega A} u_{\boldsymbol{q}\Omega' A} + g_\Omega^{\beta'\beta} g_{\Omega'}^{\alpha'\alpha} u^*_{\boldsymbol{q}\Omega A} v^*_{-\boldsymbol{q}\Omega' A} \right) \\ &= g_A^{\beta'\beta} g_A^{\alpha\alpha'} u^2_{\boldsymbol{q}} + g_A^{\beta'\beta} g_B^{\alpha'\alpha} u_{\boldsymbol{q}} v_{\boldsymbol{q}} \end{aligned} \quad \text{(B.16)}$$

$$\begin{aligned} A_1(\boldsymbol{q}, B, \alpha, \alpha', \beta, \beta') &= \sum_{\Omega\Omega'} \left(g_\Omega^{\beta'\beta} g_{\Omega'}^{\alpha\alpha'} u^*_{\boldsymbol{q}\Omega B} u_{\boldsymbol{q}\Omega' B} + g_\Omega^{\beta'\beta} g_{\Omega'}^{\alpha'\alpha} u^*_{\boldsymbol{q}\Omega B} v^*_{-\boldsymbol{q}\Omega' B} \right) \\ &= g_B^{\beta'\beta} g_B^{\alpha\alpha'} u^2_{\boldsymbol{q}} + g_B^{\beta'\beta} g_A^{\alpha'\alpha} u_{\boldsymbol{q}} v_{\boldsymbol{q}} \end{aligned} \quad \text{(B.17)}$$

$$A_2(\boldsymbol{q},A,\alpha,\alpha',\beta,\beta') = \sum_{\Omega\Omega'}\left(g_{\Omega}^{\beta'\beta}g_{\Omega'}^{\alpha\alpha'}v^*_{\boldsymbol{q}\Omega A}v_{\boldsymbol{q}\Omega' A} + g_{\Omega}^{\beta'\beta}g_{\Omega'}^{\alpha'\alpha}v^*_{\boldsymbol{q}\Omega A}u^*_{-\boldsymbol{q}\Omega' A}\right) = g_B^{\beta'\beta}g_B^{\alpha\alpha'}v_{\boldsymbol{q}}^2 + g_B^{\beta'\beta}g_A^{\alpha'\alpha}v_{\boldsymbol{q}}u_{\boldsymbol{q}} \tag{B.18}$$

$$A_2(\boldsymbol{q},B,\alpha,\alpha',\beta,\beta') = \sum_{\Omega\Omega'}\left(g_{\Omega}^{\beta'\beta}g_{\Omega'}^{\alpha\alpha'}v^*_{\boldsymbol{q}\Omega B}v_{\boldsymbol{q}\Omega' B} + g_{\Omega}^{\beta'\beta}g_{\Omega'}^{\alpha'\alpha}v^*_{\boldsymbol{q}\Omega B}u^*_{-\boldsymbol{q}\Omega' B}\right) = g_A^{\beta'\beta}g_A^{\alpha\alpha'}v_{\boldsymbol{q}}^2 + g_A^{\beta'\beta}g_B^{\alpha'\alpha}v_{\boldsymbol{q}}u_{\boldsymbol{q}} \tag{B.19}$$

$$B_1(\boldsymbol{q},A,\alpha,\alpha',\beta,\beta') = \sum_{\Omega\Omega'}\left(g_{\Omega}^{\alpha\alpha'}g_{\Omega'}^{\beta'\beta}u_{\boldsymbol{q}\Omega A}u^*_{\boldsymbol{q}\Omega' A} + g_{\Omega}^{\alpha\alpha'}g_{\Omega'}^{\beta\beta'}u_{\boldsymbol{q}\Omega A}v_{-\boldsymbol{q}\Omega' A}\right) = g_A^{\alpha\alpha'}g_A^{\beta'\beta}u_{\boldsymbol{q}}^2 + g_A^{\alpha\alpha'}g_B^{\beta\beta'}u_{\boldsymbol{q}}v_{\boldsymbol{q}} \tag{B.20}$$

$$B_1(\boldsymbol{q},B,\alpha,\alpha',\beta,\beta') = \sum_{\Omega\Omega'}\left(g_{\Omega}^{\alpha\alpha'}g_{\Omega'}^{\beta'\beta}u_{\boldsymbol{q}\Omega B}u^*_{\boldsymbol{q}\Omega' B} + g_{\Omega}^{\alpha\alpha'}g_{\Omega'}^{\beta\beta'}u_{\boldsymbol{q}\Omega B}v_{-\boldsymbol{q}\Omega' B}\right) = g_B^{\alpha\alpha'}g_B^{\beta'\beta}u_{\boldsymbol{q}}^2 + g_B^{\alpha\alpha'}g_A^{\beta\beta'}u_{\boldsymbol{q}}v_{\boldsymbol{q}} \tag{B.21}$$

$$B_2(\boldsymbol{q},A,\alpha,\alpha',\beta,\beta') = \sum_{\Omega\Omega'}\left(g_{\Omega}^{\alpha\alpha'}g_{\Omega'}^{\beta'\beta}v_{\boldsymbol{q}\Omega A}v^*_{\boldsymbol{q}\Omega' A} + g_{\Omega}^{\alpha\alpha'}g_{\Omega'}^{\beta\beta'}v_{\boldsymbol{q}\Omega A}u_{-\boldsymbol{q}\Omega' A}\right) = g_B^{\alpha\alpha'}g_B^{\beta'\beta}v_{\boldsymbol{q}}^2 + g_B^{\alpha\alpha'}g_A^{\beta\beta'}v_{\boldsymbol{q}}u_{\boldsymbol{q}} \tag{B.22}$$

$$B_2(\boldsymbol{q},B,\alpha,\alpha',\beta,\beta') = \sum_{\Omega\Omega'}\left(g_{\Omega}^{\alpha\alpha'}g_{\Omega'}^{\beta'\beta}v_{\boldsymbol{q}\Omega B}v^*_{\boldsymbol{q}\Omega' B} + g_{\Omega}^{\alpha\alpha'}g_{\Omega'}^{\beta\beta'}v_{\boldsymbol{q}\Omega B}u_{-\boldsymbol{q}\Omega' B}\right) = g_A^{\alpha\alpha'}g_A^{\beta'\beta}v_{\boldsymbol{q}}^2 + g_A^{\alpha\alpha'}g_B^{\beta\beta'}v_{\boldsymbol{q}}u_{\boldsymbol{q}} \tag{B.23}$$

We use that $g_1^{A\uparrow} = g_1^{B\downarrow} = 0$ to show

$$A_\nu(\boldsymbol{q},\Omega,\uparrow,\downarrow,\uparrow,\downarrow) = 0, \qquad B_\nu(\boldsymbol{q},\Omega,\uparrow,\downarrow,\uparrow,\downarrow) = 0 \tag{B.24}$$

$$A_\nu(\boldsymbol{q},\Omega,\downarrow,\uparrow,\downarrow,\uparrow) = 0, \qquad B_\nu(\boldsymbol{q},\Omega,\downarrow,\uparrow,\downarrow,\uparrow) = 0 \tag{B.25}$$

for $\nu \in \{1,2\},\ \Omega \in \{A,B\}$. Furthermore

$$A_1(\boldsymbol{q},A,\uparrow,\downarrow,\downarrow,\uparrow) = A_1(\boldsymbol{q},B,\downarrow,\uparrow,\uparrow,\downarrow) = 0 \tag{B.26}$$

$$A_2(\boldsymbol{q},B,\uparrow,\downarrow,\downarrow,\uparrow) = A_2(\boldsymbol{q},A,\downarrow,\uparrow,\uparrow,\downarrow) = 0 \tag{B.27}$$

$$B_1(\boldsymbol{q},A,\uparrow,\downarrow,\downarrow,\uparrow) = B_1(\boldsymbol{q},B,\downarrow,\uparrow,\uparrow,\downarrow) = 0 \tag{B.28}$$

$$B_2(\boldsymbol{q},B,\uparrow,\downarrow,\downarrow,\uparrow) = B_2(\boldsymbol{q},A,\downarrow,\uparrow,\uparrow,\downarrow) = 0 \tag{B.29}$$

The only non-zero coefficients end up being

$$A_1(\boldsymbol{q},B,\uparrow,\downarrow,\downarrow,\uparrow) = B_1(\boldsymbol{q},B,\uparrow,\downarrow,\downarrow,\uparrow) = g_1^{B\uparrow}g_1^{B\uparrow}u_{\boldsymbol{q}}^2 + g_1^{B\uparrow}g_1^{A\downarrow}u_{\boldsymbol{q}}v_{\boldsymbol{q}} \tag{B.30}$$

$$A_2(\boldsymbol{q},A,\uparrow,\downarrow,\downarrow,\uparrow) = B_2(\boldsymbol{q},A,\uparrow,\downarrow,\downarrow,\uparrow) = g_1^{B\uparrow}g_1^{B\uparrow}v_{\boldsymbol{q}}^2 + g_1^{B\uparrow}g_1^{A\downarrow}v_{\boldsymbol{q}}u_{\boldsymbol{q}} \tag{B.31}$$

$$A_1(\boldsymbol{q},A,\downarrow,\uparrow,\uparrow,\downarrow) = B_1(\boldsymbol{q},A,\downarrow,\uparrow,\uparrow,\downarrow) = g_1^{A\downarrow}g_1^{A\downarrow}u_{\boldsymbol{q}}^2 + g_1^{A\downarrow}g_1^{B\uparrow}u_{\boldsymbol{q}}v_{\boldsymbol{q}} \tag{B.32}$$

$$A_2(\boldsymbol{q},B,\downarrow,\uparrow,\uparrow,\downarrow) = B_2(\boldsymbol{q},B,\downarrow,\uparrow,\uparrow,\downarrow) = g_1^{A\downarrow}g_1^{A\downarrow}v_{\boldsymbol{q}}^2 + g_1^{A\downarrow}g_1^{B\uparrow}v_{\boldsymbol{q}}u_{\boldsymbol{q}} \tag{B.33}$$

Appendix C

BCS theory

C.1 Gap functions

We remind ourselves of the gap function for unpolarised pairs along with the unpolarised spin singlet and triplet superconducting order parameters.

$$\Delta_{\boldsymbol{k}\sigma_1\sigma_2} = -\sum_{\boldsymbol{k'}\sigma_3\sigma_4} \tilde{V}^{\sigma_1\sigma_2\sigma_3\sigma_4}_{\boldsymbol{k}\boldsymbol{k'}} \Delta_{\boldsymbol{k'}\sigma_4\sigma_3} \chi_{\boldsymbol{k}}(T) \tag{C.1}$$

$$\Delta^{O(s)}_{\boldsymbol{k},\uparrow\downarrow} = \Delta_{\boldsymbol{k},\uparrow\downarrow} - \Delta_{\boldsymbol{k},\downarrow\uparrow} \tag{C.2}$$

$$\Delta^{E(s)}_{\boldsymbol{k},\uparrow\downarrow} = \Delta_{\boldsymbol{k},\uparrow\downarrow} + \Delta_{\boldsymbol{k},\downarrow\uparrow} \tag{C.3}$$

We can then show that the even part in k of the unpolarised potential gives us a gap function for the singlet pair

$$\begin{aligned}
\Delta^{O(s)}_{\boldsymbol{k},\uparrow\downarrow} &= -\sum_{\boldsymbol{k'}} \Big[V^{\uparrow\downarrow\downarrow\uparrow}_{\boldsymbol{k}\boldsymbol{k'}} \Delta_{\boldsymbol{k'},\uparrow\downarrow} + V^{\uparrow\downarrow\uparrow\downarrow}_{\boldsymbol{k}\boldsymbol{k'}} \Delta_{\boldsymbol{k'},\downarrow\uparrow} - V^{\downarrow\uparrow\downarrow\uparrow}_{\boldsymbol{k}\boldsymbol{k'}} \Delta_{\boldsymbol{k'},\uparrow\downarrow} - V^{\downarrow\uparrow\uparrow\downarrow}_{\boldsymbol{k}\boldsymbol{k'}} \Delta_{\boldsymbol{k'},\downarrow\uparrow} \Big] \chi_{\boldsymbol{k'}} \\
&= -\sum_{\boldsymbol{k'}} \Big[\underbrace{\left(V^{\uparrow\downarrow\downarrow\uparrow}_{\boldsymbol{k}\boldsymbol{k'}} + V^{\uparrow\downarrow\downarrow\uparrow}_{-\boldsymbol{k}\boldsymbol{k'}} \right)}_{=V^{E(\boldsymbol{k})}_{\boldsymbol{k}\boldsymbol{k'}}} \Delta_{\boldsymbol{k'},\uparrow\downarrow} - \underbrace{\left(V^{\downarrow\uparrow\uparrow\downarrow}_{\boldsymbol{k}\boldsymbol{k'}} + V^{\downarrow\uparrow\uparrow\downarrow}_{-\boldsymbol{k}\boldsymbol{k'}} \right)}_{=V^{E(\boldsymbol{k})}_{\boldsymbol{k}\boldsymbol{k'}}} \Delta_{\boldsymbol{k'},\downarrow\uparrow} \Big] \chi_{\boldsymbol{k'}} \\
&= -\sum_{\boldsymbol{k'}} V^{E(\boldsymbol{k})}_{\boldsymbol{k}\boldsymbol{k'}} \, \Delta^{O(s)}_{\boldsymbol{k'},\uparrow\downarrow} \, \chi_{\boldsymbol{k'}}
\end{aligned} \tag{C.4}$$

while the odd part in k of the unpolarised potential gives us a gap function for the unpolarised triplet pair

$$\begin{aligned}
\Delta^{E(s)}_{\boldsymbol{k},\uparrow\downarrow} &= -\sum_{\boldsymbol{k'}} \Big[V^{\uparrow\downarrow\downarrow\uparrow}_{\boldsymbol{k}\boldsymbol{k'}} \Delta_{\boldsymbol{k'},\uparrow\downarrow} + V^{\uparrow\downarrow\uparrow\downarrow}_{\boldsymbol{k}\boldsymbol{k'}} \Delta_{\boldsymbol{k'},\downarrow\uparrow} + V^{\downarrow\uparrow\downarrow\uparrow}_{\boldsymbol{k}\boldsymbol{k'}} \Delta_{\boldsymbol{k'},\uparrow\downarrow} + V^{\downarrow\uparrow\uparrow\downarrow}_{\boldsymbol{k}\boldsymbol{k'}} \Delta_{\boldsymbol{k'},\downarrow\uparrow} \Big] \chi_{\boldsymbol{k'}} \\
&= -\sum_{\boldsymbol{k'}} \Big[\underbrace{\left(V^{\uparrow\downarrow\downarrow\uparrow}_{\boldsymbol{k}\boldsymbol{k'}} - V^{\uparrow\downarrow\downarrow\uparrow}_{-\boldsymbol{k}\boldsymbol{k'}} \right)}_{=V^{O(\boldsymbol{k})}_{\boldsymbol{k}\boldsymbol{k'}}} \Delta_{\boldsymbol{k'},\uparrow\downarrow} + \underbrace{\left(V^{\downarrow\uparrow\uparrow\downarrow}_{\boldsymbol{k}\boldsymbol{k'}} - V^{\downarrow\uparrow\uparrow\downarrow}_{-\boldsymbol{k}\boldsymbol{k'}} \right)}_{=V^{O(\boldsymbol{k})}_{\boldsymbol{k}\boldsymbol{k'}}} \Delta_{\boldsymbol{k'},\downarrow\uparrow} \Big] \chi_{\boldsymbol{k'}} \\
&= -\sum_{\boldsymbol{k'}} V^{O(\boldsymbol{k})}_{\boldsymbol{k}\boldsymbol{k'}} \, \Delta^{E(s)}_{\boldsymbol{k'},\uparrow\downarrow} \, \chi_{\boldsymbol{k'}}
\end{aligned} \tag{C.5}$$

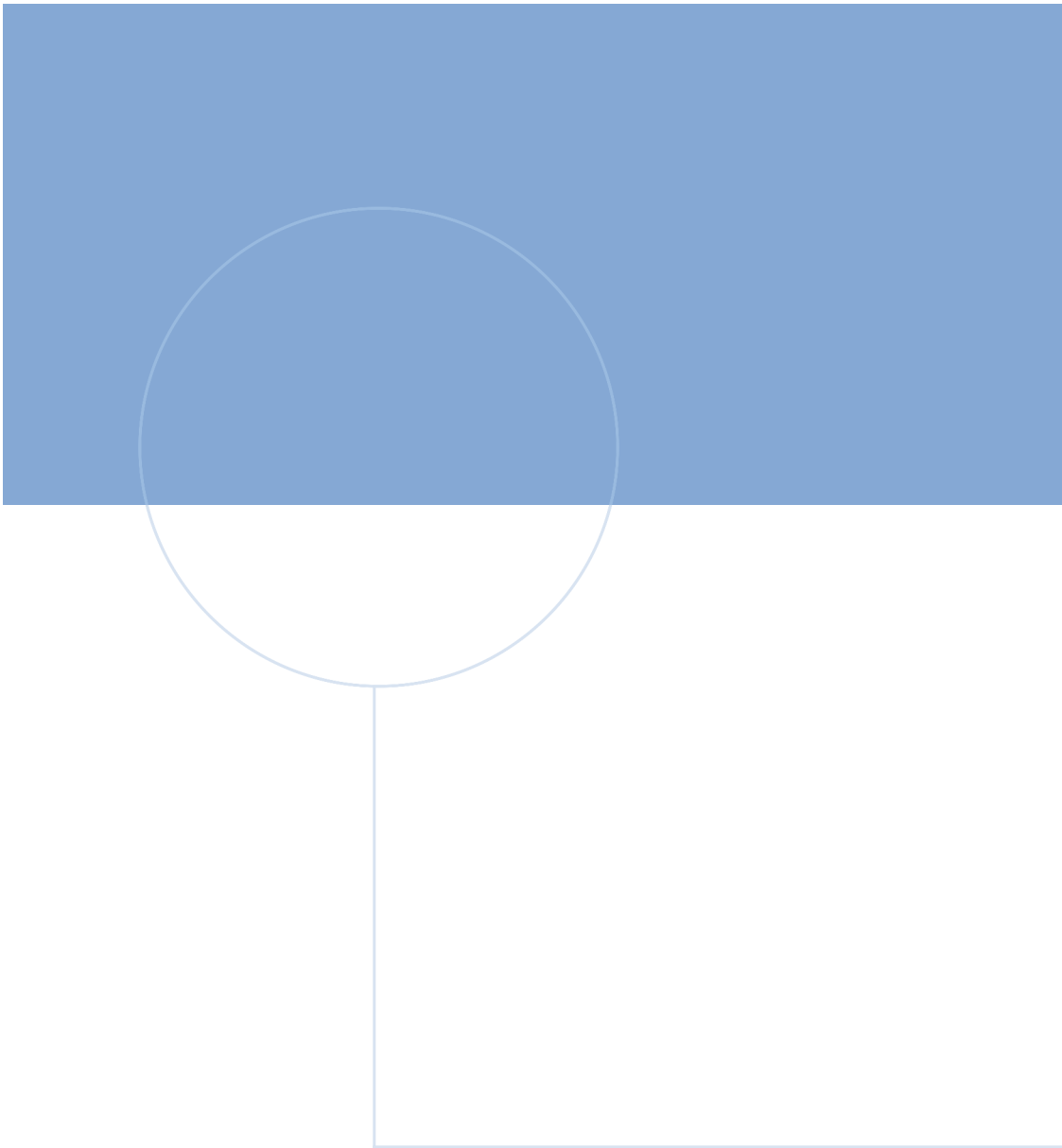

NTNU

Norwegian University of
Science and Technology